Age Dating of Rainfall-runoff Water with Sulfur Hexafluoride and Discharge Processes in a Forested Headwater Catchment

January 2018

Koichi SAKAKIBARA

Age Dating of Rainfall-runoff Water with Sulfur Hexafluoride and Discharge Processes in a Forested Headwater Catchment

A Dissertation Submitted to

the Graduate School of Life and Environmental Sciences,

the University of Tsukuba

in Partial Fulfillment of the Requirements

for the Degree of Doctor of Philosophy in Environmental Studies

(Doctoral Program in Sustainable Environmental Studies)

Koichi SAKAKIBARA

Abstract

The clarification of rainfall–runoff processes in headwater regions has been a distinctive challenge in catchment hydrology linked to sustainable water resource management and flood countermeasures. Time-variant water age in catchments can fundamentally describe catchment function controlling rainfall–runoff generation, groundwater flow pathway, and water storage. Sulfur hexafluoride (SF_6) has been widely applied as a tracer to date young water age in many previous studies. However, although rainstorm events have been recognized as an active phase in catchment hydrology, accurate and precise time variances of water age and related water dynamics during rainfall have not been well clarified yet. Here, to reveal temporal variations of discharge water (spring) age and related hydrological processes in a forested headwater catchment with an area of 4.5 ha during rainstorm events, periodic and intensive field observations were conducted in Yamakiya district (Fukushima, Japan) from May 2015 to May 2017. Discharge volume, groundwater table level, and amount of precipitation were measured at intervals of 10 min. Groundwater, spring water, soil water, and precipitation water samples were collected for determining stable isotopic compositions, inorganic solute concentrations, and dissolved gas concentration (SF_6) in water. To begin, the author developed an apparatus for measuring dissolved SF_6 in water. This apparatus is new in terms of ease of use and suitability for analyzing dissolved SF_6 in water. Therefore, the developed system was used for determining dissolved SF_6 in water samples in this study.

The relation between the age of spring water and spring discharge volume shows opposite trends between rainless periods (light negative correlation between age and discharge) and rainfall periods (positive correlation between age and discharge). This indicates the differences in hydrological processes during rainless and rainfall periods. In terms of water age, the author clearly observed older water ages for the spring (13.6 years at most) during periods of intense rainfall than those observed during rainless periods (1.8–6.8 years). Groundwater age near the

spring discharge point was older (9.2–12.8 years) shortly after a rainstorm than it was during rainless periods (<1–8.5 years). In the case of tracer data, the stable isotopic composition of rainwater observed in rainfall changed largely during rainfall events, whereas that of spring water did not change significantly, indicating that the rainfall component did not contribute significantly to spring water during rainstorms. In addition, chloride ions, sodium ions, and silica concentrations in spring water during rainfall periods changed toward the dominant values of the older groundwater component stored in the catchment. This change in timing corresponds to that of the discharge of older spring water during rainstorms.

All observed data suggest the contribution of the older groundwater component stored in bedrock to spring discharge during rainstorms. Moreover, considering the temporal change in groundwater age, replacement of younger water with older groundwater in the valley due to the bedrock groundwater contribution through abundant bedrock fractures is indicated as a mechanism for the discharge of older water during rainfall events. In addition, although no clear change in the groundwater flow system was observed based on the hydraulic potential distribution, the hydraulic gradient between groundwater near a spring and a discharge point increased by 10% as compared to that before rainfall. Therefore, this 10% increase in the hydraulic gradient is suggested as the driving force behind those phenomena. The main finding is that rainfall affects the groundwater flow system in headwater regions with a thin soil layer and fractured bedrock serves as an important trigger for the discharge of older water components with ages >10 years stored in the catchment.

The author focused on the groundwater component in the rainfall–runoff water to reduce the number of complex factors. As a result, the study inferred results opposite to those of previous studies using stable isotopic compositions; the present study clearly supports the concerns expressed in previous studies with respect to the fact that the dating method based on stable isotopes misses older water components. This study provides new insights into older

water dynamics and responses to rainfall in headwater regions, which are important source regions of discharge water. Future studies can possibly discuss the effects of rainfall (direct or indirect) on the older groundwater to further interpret rainfall–runoff processes based on water age information with high time resolution during rainstorms.

Keywords: rainfall–runoff processes; SF_6; water age; headwater catchment; multi-tracer approach

Table of Contents

List of Tables and Figures

Tables

Figures

CHAPTER 1 INTRODUCTION

1.1 Rainfall–runoff processes in watersheds

Understanding flood generation mechanisms (or rainfall–runoff processes) is important for preventing and predicting natural disasters such as flood, landslide, and mudslide (Jothityangkoon and Sivapalan, 2001; Burguete et al., 2002). Especially, heavy rainfall in headwater regions is directly related to the magnitude of damage downstream because these regions are recognized as the origin of runoff generation. Rainfall–runoff models developed by many researchers are useful for forecasting river flow (Chou, 2007; Lamb et al., 2016). However, these models have sometimes failed to predict water-related disasters in response to extreme rainfall events. Therefore, understanding rainfall–runoff processes in headwater regions remains a crucial challenge not only from the hydrology viewpoint but also from the disaster prevention viewpoint.

Typically, attempts to clarify rainfall–runoff processes have employed component separation techniques. Hewlett and Hibbert (1967) first developed a simple and reliable hydrograph separation method that can separate rainfall–runoff water into quick flow and base flow. They tested 200 rainfall events in 15 forested headwater catchments and found a suitable mathematical rule. This method has been used by many researchers, even in recent years (Katsuyama et al., 2010). These studies improved the "Variable Source Area Concept" proposed by Hewlett and Hibbert (1967), according to which water discharge areas (or sources) depend highly on the magnitude of rainfall.

After the advancement of chemical analysis and water sampling techniques, stable isotopes of oxygen and hydrogen have been applied widely as highly conservative tracers for hydrograph separation (Klaus and McDonnell, 2013). Because stable isotopic compositions in rainwater (new water) and water stored in the catchment before rainfall (old water) are usually different

or vary seasonally, they are useful to demarcate a hydrograph into new and old water. Sklash and Farvolden (1979) and Sklash et al. (1986) mentioned that rainfall–runoff water in headwater catchments mainly consists of old water (as opposed to new water). This is one of the most important findings in catchment hydrology and gives rise to two simple but puzzling questions, namely "where and how do catchments store the water?" and "how do catchments release the old water due to rainfall input?" (Kirchner, 2003; McDonnell, 2003).

Many studies have attempted to answer the above questions during and after the International Hydrologic Decade (1965–1974) and various aspects of rainfall–runoff processes have been conceptualized (Figure 1; McDonnell, 2003; Asano et al., 2005). Whipkey (1965), Sklash et al. (1986), and Marui (1991) suggested that lateral subsurface flow is dominated due to the large hydraulic head gradient caused by a rise in the groundwater table or tentative groundwater ridge near a stream. Onodera (1991) and Cloke et al. (2006) suggested and examined the role of entrapped air and capillary fringes, which raise the hydraulic gradient for water discharge during rainfall events. Then, the saturated surface area near a stream grows and extends, resulting in the generation of saturated surface flow (McDonnell, 2003; Menichino and Hester, 2015). In addition, based on water balance, many studies, including Tanaka et al. (1984), McDonnell (1990), and Meerveld and McDonnell (2006), have indicated the preferential subsurface water flow through pipes created naturally by tree and plant roots. These lead to nonlinear hydrological phenomena, especially during rainfall.

Another important finding of previous studies is the contribution of bedrock groundwater to rainfall‐runoff water during rainstorms. Previously, the bedrock–soil interface was treated as an impermeable boundary and the rainfall–runoff model did not suitably consider groundwater flow in the bedrock. However, Anderson et al. (1997) and Montgomery et al. (1997) indicated the important influence of bedrock groundwater on runoff generation during rainstorms. Onda et al. (2001 and 2006) performed runoff analyses based on hydrometric observations in the

region underlain by various bedrocks such as granite and shale. They concluded that the delayed peak runoff in regions with underlying sedimentary rock was caused by the contribution of bedrock groundwater. In addition, Kosugi et al. (2006) calculated the annual bedrock infiltration rate to be 35–55% of the total annual precipitation, which is stored as groundwater in the bedrock.

Recently, Iwagami et al. (2010) quantified the contribution of bedrock groundwater to discharge water at the hillslope scale by performing end-member mixing analysis by using stable oxygen/hydrogen isotopes and silica. Suarez et al. (2015), too, employed end-member mixing analysis to clarify the contribution of deeper groundwater to river discharge at the watershed scale in Africa. Additionally, Gabrielli et al. (2012) applied a new portable bedrock drilling system to explore bedrock groundwater dynamics and highlighted the importance of fractures in the bedrock as conduits for rapid lateral flow of water to the stream. This suggests that traditional hydrometric data alone do not represent bedrock groundwater flow processes accurately; therefore, new techniques for measuring bedrock groundwater flow or new tracers representing bedrock groundwater dynamics are necessary for understanding the role of bedrock groundwater during rainfall.

As mentioned above, many studies have attempted to model rainfall–runoff processes through conceptualization and quantification of rainfall–runoff phenomena (Figure 1). As a result, many aspects of rainfall–runoff processes in terms of spatial variability and quantity of contributing component on rainfall–runoff water have been clarified. However, few studies have attempted to incorporate time information in rainfall–runoff processes. For reliable and concrete modeling of rainfall–runoff processes, time information such as “when and how the discharge water has been stored in the subsurface area after rainfall input” is necessary.

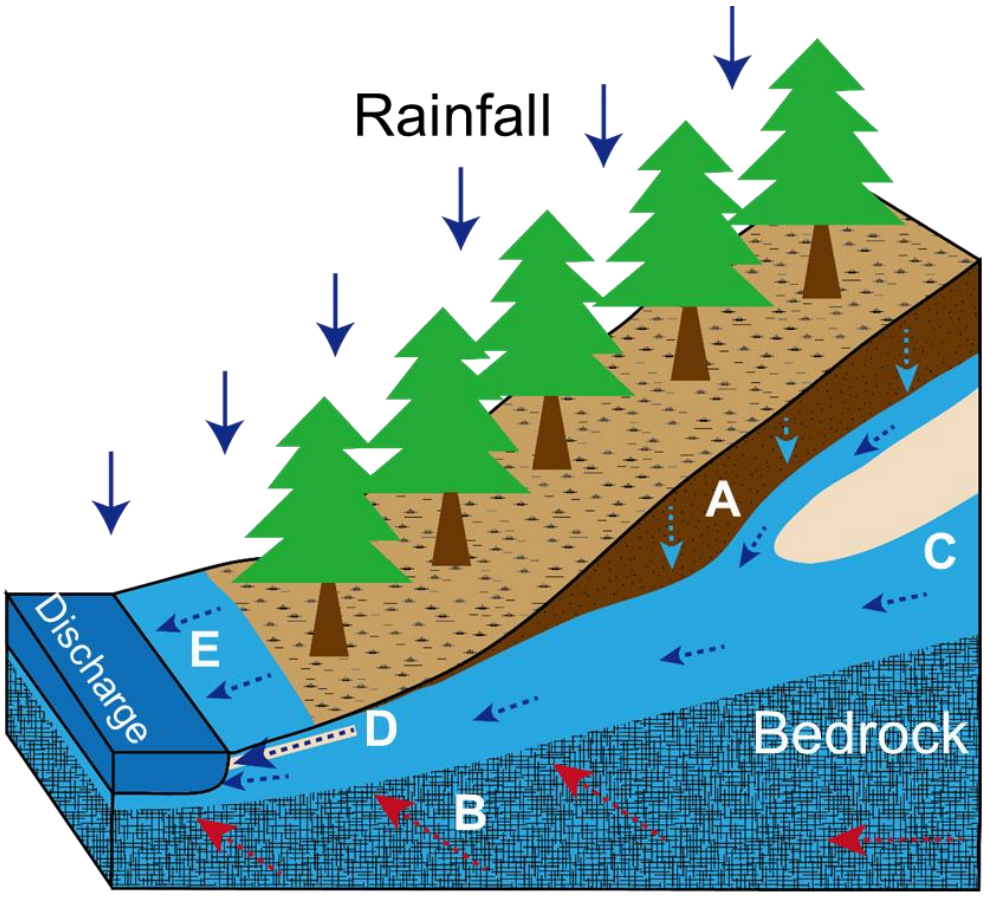

Figure 1. Conceptual model of rainfall–runoff processes according to previous studies. The figure shows A: groundwater ridge, B: bedrock groundwater contribution, C: role of entrapped air, D: preferential flow via pipe, and E: growth of saturated area and saturated surface water flow.

1.2 Age of rainfall–runoff water

The time-variant residence time of water (water age) in catchments can fundamentally describe the catchment function controlling rainfall–runoff generation, groundwater flow pathways, and water storage (McGuire and McDonnell, 2006; McDonnell et al., 2010). This information has contributed significantly to hydrology owing to its focus not only on catchment scale but also on the large-scale watershed with respect to rainfall–runoff processes, flood generation processes, effects of climate change on the watershed, and sustainable water resource management (Uhlenbrook et al., 2002; Botter et al., 2010; Manning et al., 2012; Klaus et al., 2015; Danesh-Yazdi et al., 2016; Ma and Yamanaka, 2016). Therefore, obtaining water age information and its temporal variance is very important for both hydrological sciences and social sciences from the viewpoint of efficient use of water resources.

The broad interest in "how we estimate water age" has been elevated, leading to the development of various dating methods (McGuire and McDonnell, 2006; Hrachowitz et al., 2009; Gusyev et al., 2013; Yager et al., 2013; Beyer et al., 2014; Busenberg and Plummer, 2014; Haase et al., 2014). Although the determination of water age remains considerably challenging, the convolution integral method using stable isotopic compositions (Maloszewski and Zuber, 1982; McGuire and McDonnell, 2006) and the environmental dating tracer method (e.g., ^{3}H, CFCs, and SF_6) (Reilly et al., 1994; Leibundgut et al., 2009) have been recognized as the main tools to date young water.

The convolution integral method using stable isotopes is a traditional approach for determining the age of water (McGuire and McDonnell, 2006). The method employs long-term records of conservative tracers (stable isotopic compositions) of both precipitation and discharge water with transfer functions that determine the distribution of water age (McGuire and McDonnell, 2006; Klaus et al., 2015). Many studies employing the convolution integral method using stable isotopes have indicated the preferential contribution of young water

components to discharge water during rainstorms, leading to younger ages in rainfall–runoff water (Tetzlaff et al., 2014; Klaus et al., 2015; Soulsby et al., 2015). However, the dating range of the convolution integral method using stable isotopes is limited because continuous long-term tracer observation in precipitation and discharge water is usually difficult (Stewart et al., 2010; Frisbee et al., 2013). This is why the results of most studies using stable isotopes indicate younger water ages ranging between several days and several years.

In contrast, tritium (^{3}H), chlorofluorocarbons (CFCs), and sulfur hexafluoride (SF_6) have been frequently used as environmental tracers to date young water (Busenberg and Plummer, 1992; Busenberg and Plummer, 2000; Morgenstern et al., 2010; Darling et al., 2012; Kashiwaya et al., 2014; Kelly and Glenn, 2015). Useful tracers for dating water include ^{3}H, CFCs, and SF_6, as shown in Figure 2 (based on Mahara, 2009; Suckow, 2014). Many useful dating tracers have been identified. However, tracers other than stable isotopic compositions of oxygen and hydrogen, such as ^{3}H, CFCs, and SF_6, are difficult to quantify owing to the difficulties associated with sampling and analysis processes. The age of water can be estimated based on the well-known tracer chronicles of the atmospheric mixing ratio and radioactive decay constant (^{3}H) or solubility (CFCs, SF_6) in water (Leibundgut et al., 2009). The dating range obtained from these tracers is wider (approximately 1 to 60 years) than that obtained using stable isotope tracers, whereas age dating with a time resolution of days or months is difficult to achieve owing to the spatiotemporal variety of tracer concentrations in the environment.

SF_6 is one of the most effective tracers for estimating the age of water with a 1-year time resolution because of its chemical stability and the continuous increase in SF_6 mixing ratio of more than 8% per year in the Northern Hemisphere (Figure 3; Maiss and Levin, 1994; Solomon et al., 2015). Manning et al. (2012), Busenberg and Plummer (2014), and Kamtchueng et al. (2015) periodically observed the SF_6 concentration in spring water in mountainous areas and found that the apparent SF_6 age of a spring differs seasonally over several years. The authors

indicated that these seasonal changes, especially the younger water age in the rainy season or warm days after heavy snowfall periods, can be ascribed to preferential groundwater recharge by intense rainfall and snowmelt (Manning et al., 2012; Kamtchueng et al., 2015). The results obtained using the SF_6 tracer method seem to be similar to those obtained using the method of stable isotopes.

However, recent studies have focused on the lack of water components with long residence times when the convolution integral method using stable isotopes is employed (Stewart et al., 2010; Frisbee et al., 2011; Gardner et al., 2011; Frisbee et al., 2013). Previously, studies using stable isotopes as tracers reported only very young water ages from days to several years (McGuire and McDonnell, 2006; Klaus et al., 2015), whereas older water components (more than 20 years) were frequently observed when using other environmental tracers such as SF_6 (Koh et al., 2007; Gourcy et al., 2009; Ako et al., 2013; Hiyama et al., 2013; Kamtchueng et al., 2015). Stewart et al. (2010) and Frisbee et al. (2013) clearly indicated the inconsistent spring water ages obtained using stable isotope tracers and other tracer signatures, and inferred that the necessary information about the deeper groundwater system based on stable isotope tracers is lacking. However, this concern about rainfall–runoff processes has been ignored thus far because the dating methods using stable isotopes and other tracers such as SF_6 seemed to show consistent results, as described in previous paragraphs. The age of water decreases owing to the contribution of new water (precipitation) during rainfall or in the rainy season.

Nevertheless, based on the traditional hydrograph separation method (reviewed in detail in Klaus and McDonnell, 2013), it is assumed that water discharge from deeper aquifers is induced by intense rainfall events, especially in headwater catchments. Especially, the aquifer underlying fracture bedrock in headwater areas markedly releases bedrock groundwater with potentially older water ages during rainstorms (Kosugi et al., 2006; Kosugi et al., 2008; Iwagami et al., 2010; Gabrielli et al., 2012; Suarez et al., 2015). This finding clearly disagrees

with those of previous studies in which stable isotopes were used. The tracer studies using SF_6 show consistent results with those of the method of stable isotopes during the wet season because these studies focused only on the steady state (rainless time) during rainy seasons or high flow seasons. In other words, there are no studies on the variation in discharge water age during certain rainstorms that employ tracer data such as SF_6. Another problem is that the SF_6 analytical procedure and the associated water age estimation method have been developed mostly in the United States or European countries. Unfortunately, there are few SF_6 analytical systems in Japan. Therefore, there is a need to develop the SF_6 analytical system in Japan, and such a system would contribute to international activities related to water resource management and disaster prevention.

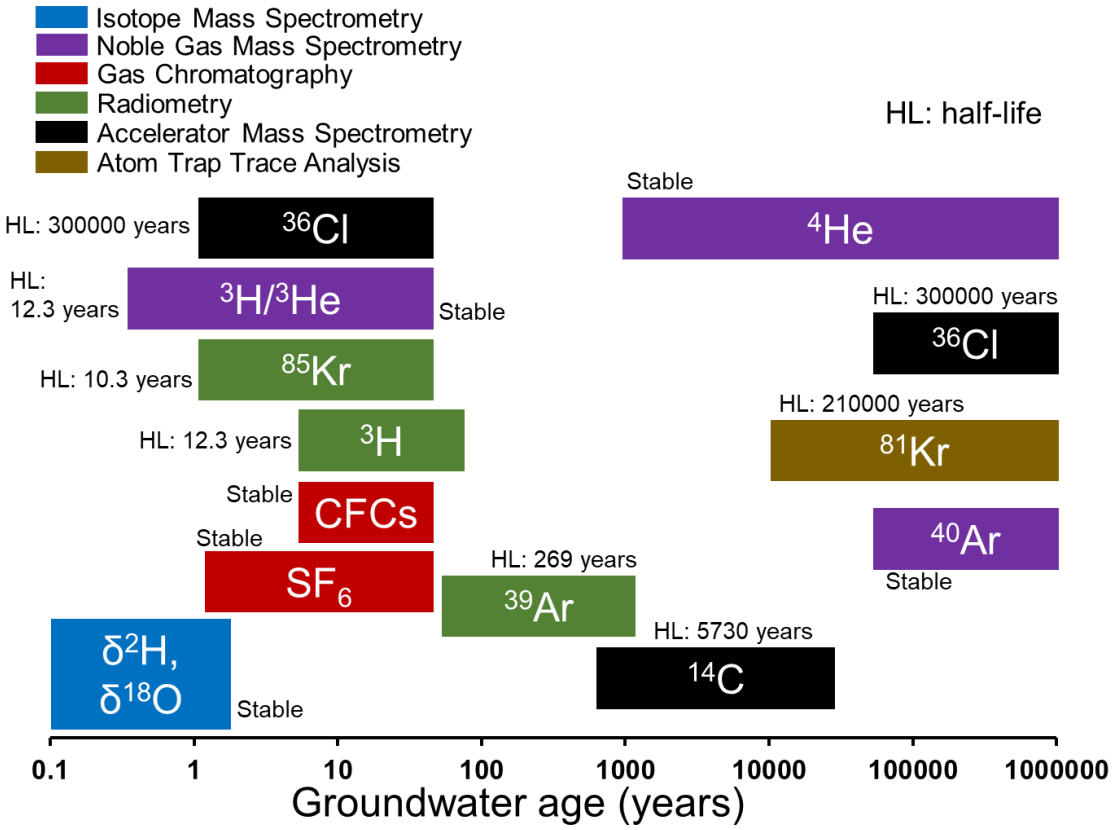

Figure 2. Useful tracers for dating water with possible dating range and analysis method (Modified Mahara (2009) and Suckow (2014)).

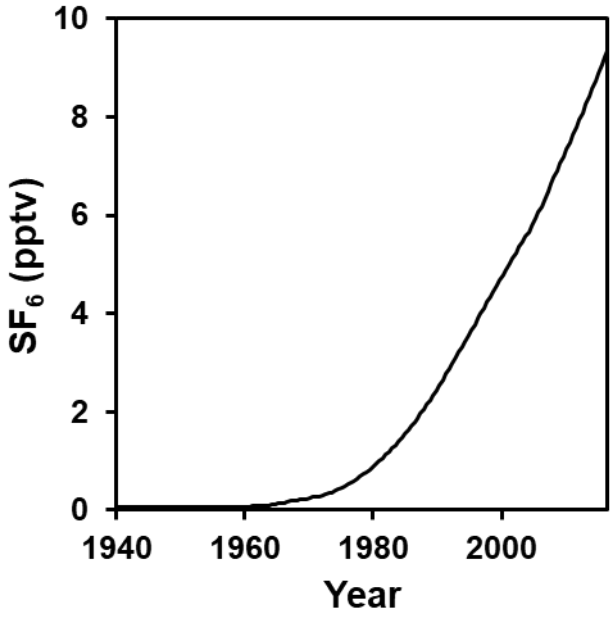

Figure 3. Atmospheric SF_6 mixing ratio recorded in Northern Hemisphere-air (NH-air). Data were obtained from the USGS (The Reston Groundwater Dating Laboratory: http://water.usgs.gov/lab/; last accessed on May 10, 2016).

1.3 Differences among water dating methods

Many studies have used stable isotopic compositions and SF_6 as the main tracers for dating young water (Pearce et al., 1986; Busenberg and Plummer, 2000; Kabeya et al., 2007; Kamtchueng et al., 2015). The basic concept of dating methods using stable isotopic compositions and SF_6 is shown in Figure 4. Tracer compositions and concentrations of input water to the catchment, such as that of precipitation, show clear temporal variations before being a part of the hydrological system. On the way of flowing toward the discharge from the hydrological system, these tracer chronicles are affected by water-mixing processes. As a result, temporal variations of tracer compositions and concentrations in input water are damped, as shown in Figure 4. These temporal variations of tracers in discharge water serve as references for dating water. Thus, water age can be determined by comparing the determined tracer composition or concentration in water samples with the tracer chronicle in discharge water (dating reference of water).

There are several differences between dating methods using stable isotopic compositions and those using SF_6 (Figure 5). Stable isotopes of oxygen and hydrogen are parts of water molecules, and their compositions in input water depend on rainfall. In other words, stable isotopic compositions in rainfall show clear seasonal variations that can be generally approximated by a sine curve (Kawaraya et al., 2000). Stable isotopic compositions only change through mixing with other water stored in the catchment (e.g., soil water and groundwater) (Nakaya et al., 2007). Therefore, in the case of water dating methods using stable isotopic compositions, temporal variation in stable isotopic compositions in precipitation can be used as input tracer information, and the calculated water age should reflect the time elapsed between the rainfall input to the catchment and water discharged from the catchment (McGuire and McDonnell, 2006). However, there is one limitation: if the evaporation effect, which causes isotopic enrichment (Barnes and Allison, 1988), is strong in the catchment, it would be difficult

to estimate the water age using stable isotopic compositions of oxygen and hydrogen.

In contrast, SF_6 is a gas and exists in the atmosphere. The SF_6 in rainwater, surface water, and soil water, which face the atmosphere, enters an equilibrium with atmospheric SF_6 concentration during flow, which is an important precondition in this water dating method (Busenberg and Plummer, 2000). Once these waters recharge the groundwater, the SF_6 dissolved in water is conserved (IAEA, 2006). Therefore, in the case of water dating methods using SF_6, the temporal variation in SF_6 present in the atmosphere can be used as the input tracer information and the calculated water age is expected to reflect the time elapsed between groundwater recharge and groundwater discharge from the saturated subsurface area. The SF_6 tracer method has limitations such as effects on local SF_6 contamination and excess air (EA) in water samples, which results in underestimation of water age (e.g., Busenberg and Plummer, 2000; Koh et al., 2007).

Figure 6 shows ideal cases of references for water dating under the assumptions of piston flow (no mixing), exponential flow (completely mixing), and exponential piston flow based on the probability density function shown in Figure 7. The temporal variations of stable isotopic composition in precipitation generally show seasonal characteristics, whereas the SF_6 present in the atmosphere increases monotonically owing to the expansion of human activities in the world (Rigby et al., 2010); these trends reflect the references under the assumption of piston flow in Figure 6.

In the case of water dating methods using stable isotopic compositions, there are clear differences in stable isotopic compositions of the references within a year; however, if the mixing process for longer than years-scale is considered, the time resolution of stable isotopic compositions in the reference curve becomes unclear. In contrast, the SF_6 references considering both no mixing and exponential mixing have clear gradients on the yearly scale; however, it is difficult to perceive variations within scales of days or months. Therefore, the

water age dating method using stable isotopic compositions is suitable for application to very young water with age less than several years, whereas the water age dating method using SF_6 is suitable for application to young water of ages between 1 year and 60 years with a 1-year time resolution. Generally, groundwater shows longer residence time than other natural water such as soil water and river water. For example, Tsuchihara et al. (2014) clarified that the age of groundwater in Japan is more than 4 years, Koh et al. (2007) clarified that the age of groundwater in Korea is more than 1 year, and Gooddy et al. (2006) clarified that the age of groundwater in the United Kingdom is more than 16 years. Thus, the SF_6 tracer is more suitable for water dating, especially dating the groundwater component, than stable isotopic composition tracers because of the wide variety of groundwater ages.

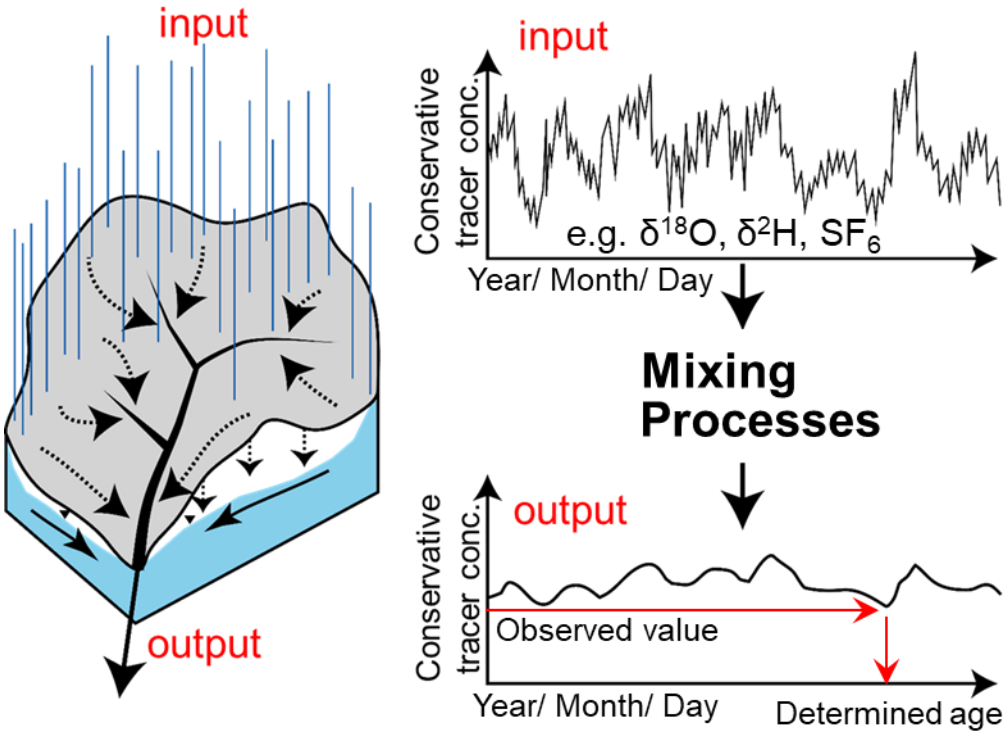

Figure 4. Basic concept of dating method using long-term stable isotopic compositions and SF_6 (according to McGuire and McDonnell, 2006).

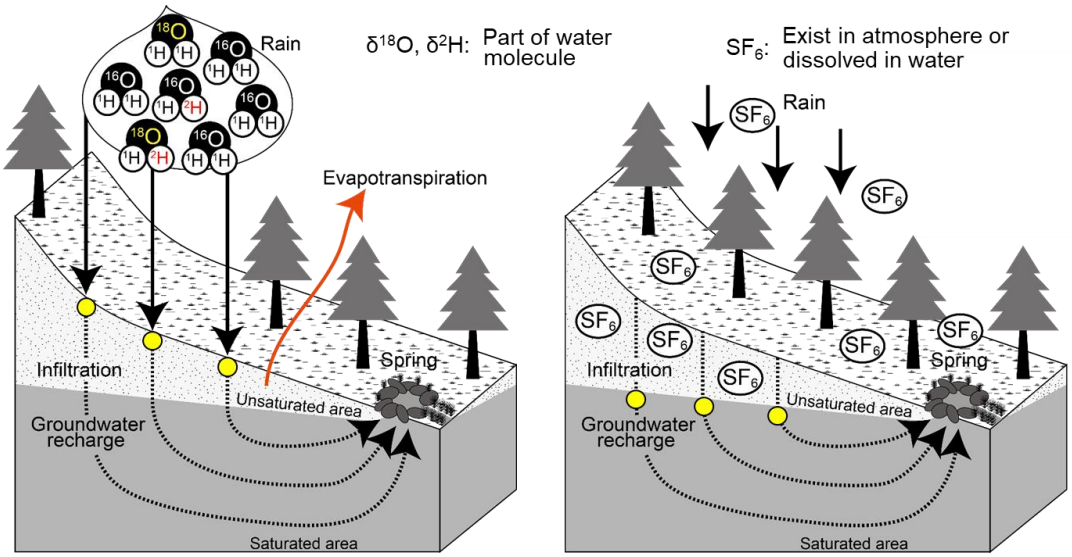

Residence time of water by stable isotopes: The elapsed time between the time of rainfall input to the catchment and the time of water discharge from the catchment.

Residence time of water by SF_6: The elapsed time between the time of groundwater recharge and the time of groundwater discharge from the saturated subsurface area.

Figure 5. Differences between dating method using long-term stable isotopic compositions and SF_6.

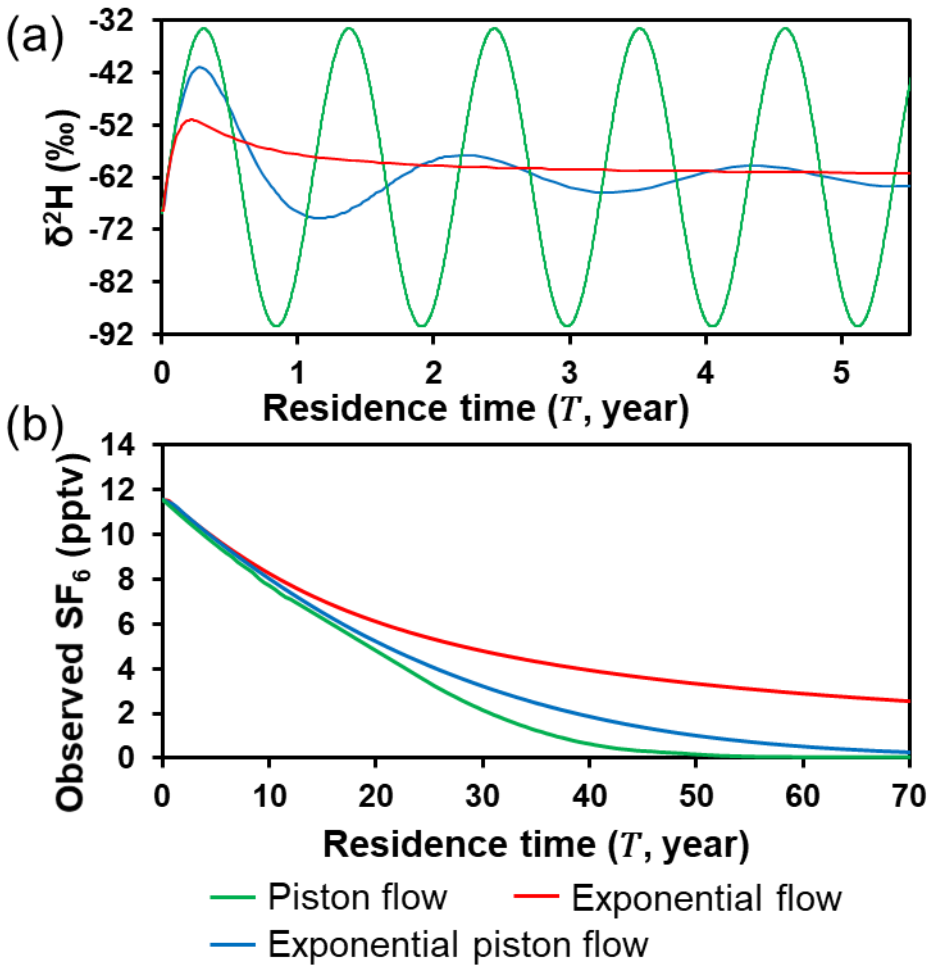

Figure 6. Differences in references for dating water using (a) stable hydrogen isotope and (b) SF_6 under assumptions of piston flow, exponential flow, and exponential piston flow. The figure highlights that stable isotopes are useful tracers for dating water of age less than a few years, whereas SF_6 is a useful tracer for dating water characterized by a wider age range.

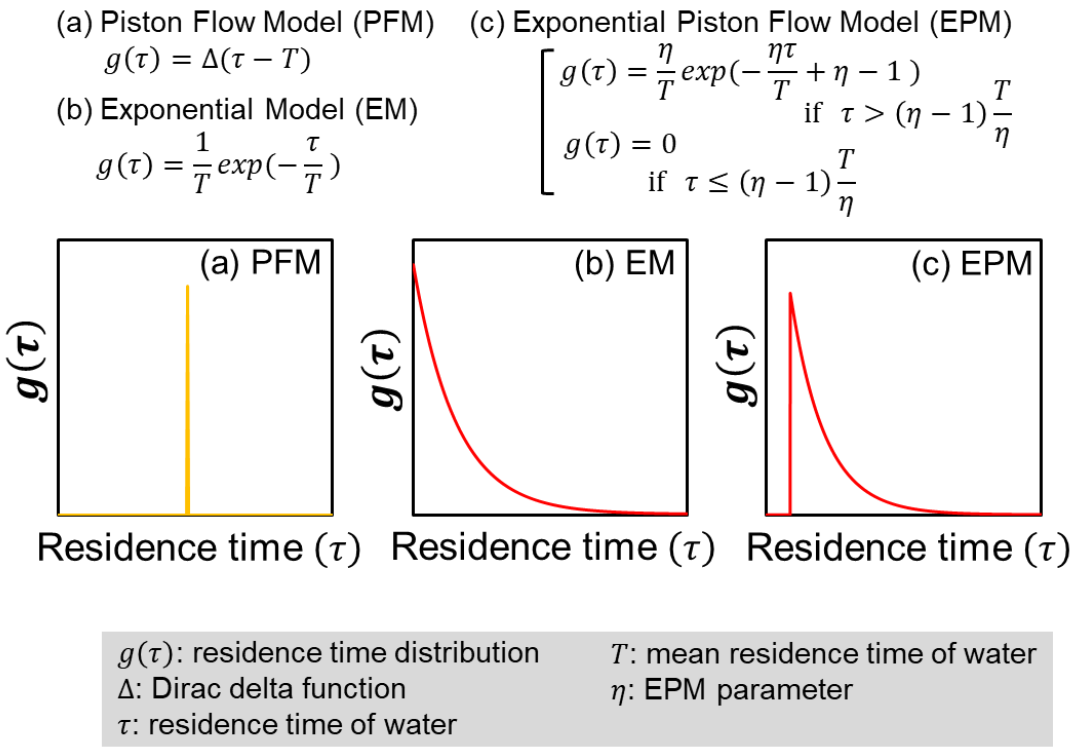

Figure 7. Probability density function (residence time distribution) of each groundwater model (a, piston flow model; b, exponential model; c, exponential piston flow model).

1.4 Development of analysis procedure of dissolved SF_6 in water

SF_6 is an ideal tracer for dating young groundwater because of its highly conservative characteristics in the environment, little microbial degradation/absorption, and little natural background/contamination (Maiss and Brenninkmeijer, 1998; Busenberg and Plummer, 2000; Koh et al., 2007). Since a SF_6 analytical system and the associated dating procedure have been developed and reported by Busenberg and Plummer (2000), many studies of hydrology have employed SF_6 as a tracer. Thus, Busenberg and Plummer (2000) are recognized as pioneers of this field of study. Most related studies were conducted in European countries or in the United States (Busenberg and Plummer, 2000; Gooddy et al., 2006); however, there are very few studies that have used SF_6 in hydrology in Japan (Asai et al., 2011; Kashiwaya et al., 2014).

Traditionally, SF_6 has been applied as a tracer in the oceanic circulation discipline in Japan. Magi and Shitashima (2002) and Tokieda et al. (2007) developed an apparatus with a complex control system for analyzing the concentration of SF_6 dissolved in seawater. The systems developed by Busenberg and Plummer (2000) for determining the concentration of SF_6 in groundwater and those developed by Magi and Shitashima (2002) and Tokieda et al. (2007) for determining the concentration of SF_6 in seawater are fundamentally similar. However, there are also several differences: The former analytical system is equipped with a vacuum system for striping SF_6 dissolved in groundwater, which makes it very difficult for novice users to manage. In contrast, the latter analytical system stripes the SF_6 gas dissolved in seawater through a bubbling system that employs ultra-pure nitrogen gas (degree of purity > 99.99995%), which is easy for novice users to control. Unfortunately, all parameters such as valve change timing and flow rate of carrier gas in the latter system are regulated automatically by the complex control system, which means that the installation cost is extremely high. Therefore, we need to develop a highly versatile SF_6 analytical system. Otherwise, it would be difficult for researchers all over the world to extend SF_6 applications to hydrology in the future.

Recently, efforts to develop a global standard of analytical reliability of dissolved SF_6 concentration in water have been accelerated across laboratories in developed countries. High analytical accuracy is important for obtaining the results in hydrology given the very low concentration of dissolved SF_6 in water (order of parts per trillion: ppt). Therefore, small uncertainties in SF_6 analysis may lead to large errors in the results and their interpretation. Labasque et al. (2014) reported the analytical reliability of techniques to determine the concentration of dissolved SF_6 in groundwater used in 13 different laboratories in countries such as the United States, Germany, United Kingdom, and Korea. The study mentioned that even if each analytical system in each laboratory has acceptable accuracy, the error in water dating is more than 3 years across the laboratories. However, there are few reports on the analytical accuracy of techniques for determining the concentration of SF_6 dissolved in groundwater in Japan. To close this gap, a SF_6 analytical system must be installed and the application of SF_6 tracer in hydrology in Japan should be widened, which would lead to better international cooperation in hydrology.

1.5 Objectives

Considering the lack of time information about rainfall–runoff processes (section 1.1), few applications of the SF_6 tracer method for dating water during heavy rainfall (section 1.2), advantage of the SF_6 tracer method for dating young water (section 1.3), the small number of available SF_6 analytical systems in Japan, and necessity for international cooperation in water dating studies (section 1.4), the author of the present study set the following four main objectives:

1) Install a unique analytical system for determining the dissolved SF_6 concentration in water and evaluate its analytical precision

2) Investigate temporal changes in discharge water age during rainfall

3) Clarify why the age of discharge water changes during rainfall

4) Clarify rainfall–runoff processes in terms of variations in water age

CHAPTER 2 STUDY AREA

The present study was carried out in a small headwater catchment (Seto Catchment: 37°35′N, 140°42′E) with an area of 0.045 km^2, located in Yamakiya district in Fukushima Prefecture, Japan (Figure 8), which is a typical landscape (forested headwater catchment) in Japan. There are two streams in the catchment—the main stream and its tributary—which originate from perennial springs (Figure 8). The streams finally join the Abukuma River, which is one of the longest rivers in Japan. Its water is used for both industrial and domestic purposes. Therefore, the study catchment, which is upstream of the Abukuma River, is important from the viewpoints of water resource management and prevention of water-related natural disasters.

The maximum, minimum, and average elevations are ~700, 550, and 600 m, respectively. The catchment is fully covered with forest (29% conifer, 71% broad-leaf), and the forest floor is covered with considerable undergrowth, except in the winter season. The mean annual air temperature and gross rainfall observed from 1995 to 2014 are 10.3°C and 1350 mm (AMeDAS, at Iitate with an elevation of 460 m, 10 km away from the study area), respectively. The mean annual potential evapotranspiration from 1995 to 2014 is 1010 mm (MeteoCrop database, at Fukushima with an elevation of 70 m, 30 km away from the study area, Japan National Institute for Agro-Environmental Sciences). Seven boreholes were installed in the catchment; Table 1 presents detailed information about these boreholes, including their geological information and pumping test results. Data from borehole drilling suggest that the main basement rock in the study area is granite, which contains a crack-containing layer and a weathered sedimentary layer, formed ~100 million years ago (Cretaceous). According to the pumping test results, the hydraulic conductivity of the layer at a depth of 10 m below the ground surface in the study area is of the order of 10^{-3} to 10^{-4} cm/s. Figure 9 shows the observed porosity, degree of saturation, and saturated hydraulic conductivity of the soil layer at borehole locations WL and

WM in February 2017. The porosity, degree of saturation, and saturated hydraulic conductivity in the soil layer lie between 65% and 84%, 45% and 98%, and order of 10^{-2} and 10^{-5} cm/s, respectively.

In addition, this catchment is located only ~35 km northwest of the Fukushima Dai-ichi Nuclear Power Plant (NDNPP). Therefore, the region received heavy local fallout (300–1000 kBq/m^2 of ^{137}Cs) after the FDNPP accident (March 2011) (MEXT, 2011). A significant part of this contamination remains in the forest and in the upper layer of soil in this region (Takahashi et al., 2015; Kato et al., 2017). According to Iwagami et al. (2017), although dissolved radionuclide concentrations in stream water and groundwater have decreased continuously, they remain detectable, especially during rainstorm events. However, intrusion and discharge processes of radionuclide in water have not been clarified yet (Iwagami et al., 2017). Therefore, studies pertaining to water discharge processes, including groundwater flow systems, should be undertaken in this area (Seto Catchment).

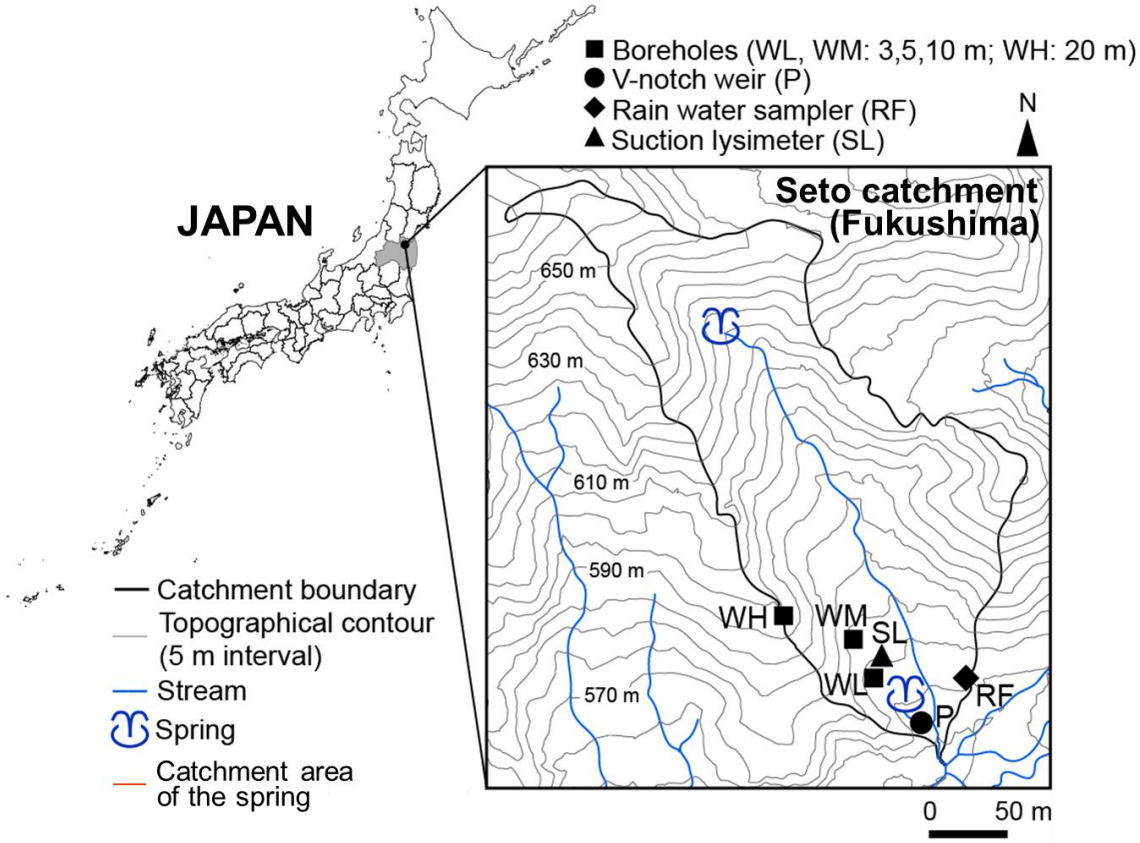

Figure 8. Study area.

Table 1. Detailed borehole information, including geological information and pumping test results.

Observation well	Well depth	Screen depth	Geology at screem	Hydraulic conductivity
WL	3 m	2–3 m	Weathered granite	$2.0*10^{-4}$–$6.0*10^{-4}$ cm/s
	5 m	4–5 m	Weathered granite	$1.1*10^{-4}$–$3.5*10^{-4}$ cm/s
	10 m	8–10 m	Fractured granite	$7.4*10^{-5}$–$1.9*10^{-4}$ cm/s
WM	3 m	2–3 m	Weathered granite	$3.4*10^{-3}$–$1.8*10^{-2}$ cm/s
	5 m	4–5 m	Weathered granite	$2.1*10^{-3}$–$9.4*10^{-3}$ cm/s
	10 m	8–10 m	Fractured granite	$1.6*10^{-4}$–$6.0*10^{-4}$ cm/s
WH	20 m	10–20 m	Fractured granite	$1.1*10^{-3}$–$3.8*10^{-3}$ cm/s

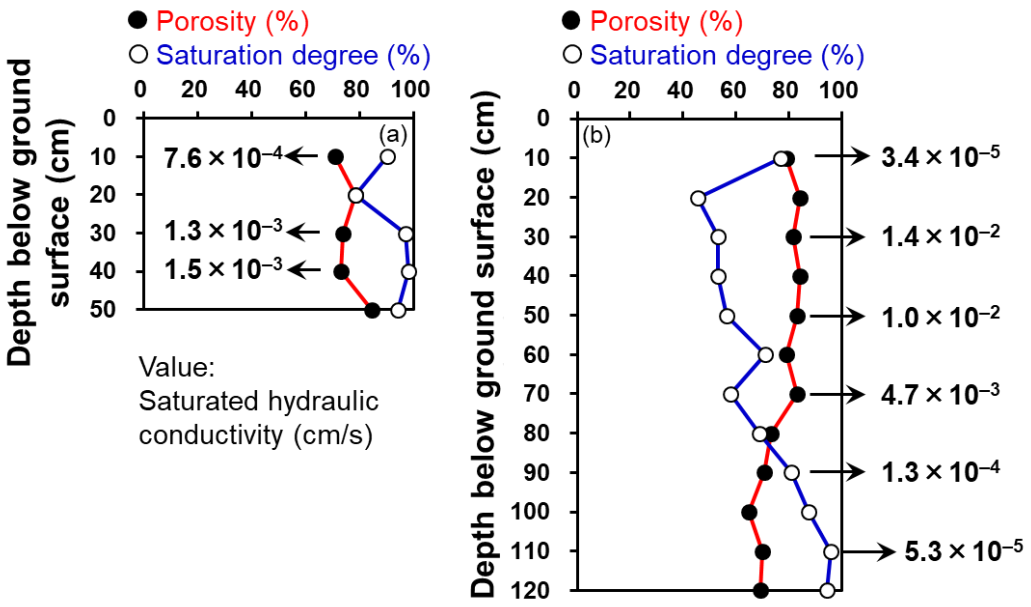

Figure 9. Observed profile of porosity, degree of saturation, and saturated hydraulic conductivity of soil layer at borehole locations WL (a) and WM (b) in February 2017.

CHAPTER 3 METHODS

3.1 Installation of SF_6 analytical system

3.1.1 Apparatus installation and SF_6 measurement

Figure 10 shows a schematic of the apparatus developed in this study for measuring the SF_6 dissolved in water. The system was developed based on the explanations and ideas of Busenberg and Plummer (2000) and Tokieda et al. (2007). Nevertheless, the installed apparatus is novel in terms of ease of use and suitability for analyzing the SF_6 dissolved in groundwater.

The apparatus consists of a 700-mL glass bubbler, various columns, various valves, and a detector connected to the integrator. The 700-mL bubbling system can extract dissolved SF_6 from a 500-mL water sample at most. The columns include an analytical column with MS-5A, a separation column (pre-column) with MS-5A, dummy columns with MS-5A, trap columns with Porapak-Q, and H_2O- and CO_2-removing columns with anhydrone and ascarite, respectively. Dummy columns in the constant-temperature oven of the gas chromatograph employed in the apparatus are not used directly in the analysis processes. However, these columns buffer the pressure shocks caused by valve operations. The valves can control the flows of gas and water. A gas chromatograph with an electron capture detector (Shimadzu GC-8AIE) and integrator (Shimadzu C-R8A) were used for the analytical system in the apparatus.

Pressure regulators and flow meters were installed in the system for adjusting and regulating the appropriate carrier gas and bubbling gas flow rate. Ultra-pure nitrogen (N_2 > 99.99995%) was used as both the carrier gas and bubbling gas. Gas filters were connected immediately after the ultra-pure nitrogen tank. These filters are very important for certifying the analytical result and maintaining the system, including the various columns and detectors.

The differences between the apparatus developed in this study and that developed by Busenberg and Plummer (2000) are shown in Figure 11 in the form of simplified schematics.

System 1 (Busenberg and Plummer, 2000) includes a vacuum system for striping the SF_6 dissolved in groundwater, whereas system 2 (present study) uses a bubbling system for extracting SF_6 from water. The vacuum system is very rapid in striping the dissolved gasses from a water sample. However, most novice users find it difficult to control the vacuum system. In contrast, the bubbling system is user-friendly, although its extraction time is longer than that of the vacuum system. In the present study, the bubbling system was selected because of its high versatility compared to that of the vacuum system.

For quantifying the concentration of SF_6 dissolved in water, the calibration curve method was applied. Therefore, it was necessary to generate a calibration curve by using standard SF_6 gases and constant-volume tubes before analyzing the concentration of dissolved SF_6 in water. In each analytical run, this apparatus was calibrated using standard gases (5 and 50 pptv) and constant-volume tubes (0.5 and 1.0 cm^3). The standard gas was injected into the system from V1 in Figure 10 after being quantified using a constant-volume tube (loop 1: 1.0 cm^3, loop 2: 0.5 cm^3). Then, it was trapped in a small trap column with Porapak-Q at a temperature of −80°C. The trapped standard gas was injected into the analytical column by placing the trap column into water at 85°C. For analyzing the gas samples, including standard gas, the large trap connected to V3 was not used. This is because the trapping time was short (1 min 45 s) and a longer trap column was not necessary for the analysis. A chromatogram of the analyzed SF_6 standard gas is shown in Figure 12, where a sharp and clear SF_6 peak can be seen on the stable baseline. Figure 13 shows the calibration line between the quantity of SF_6 and the detected SF_6 area. The calibration line is clearly linear with the determination coefficient (R^2) of more than 0.999. These two figures indicate that the developed apparatus can be calibrated reliably.

For extracting the SF_6 dissolved in water, the apparatus used a bubbling system. A water sample (~320 mL) was pulled into the bubbler from the water inlet connected to a three-way valve by increasing the pressure inside the sample bottle by using ultra-pure nitrogen gas. This

procedure can avoid SF_6 contamination from the atmosphere. Bubbling of ultra-pure nitrogen gas at a rate of 250 mL/min was initiated by turning on valve 6. The extracted gases, including SF_6, were trapped in Porapak-Q in the large trap connected to V3 after water vapor was removed by the anhydrone in the H_2O trap between V6 and V3. The trapping temperature was −80°C, which is lower than the melting/boiling point of SF_6. Then, the trapped gases were moved to a small trap by placing the large trap column into 85°C water after removing CO_2 and H_2O by using the CO_2 and H_2O traps. This process allowed for the detection of SF_6 with a sharp peak, which means that the analytical error of the system was reduced. Finally, the trapped gases, including SF_6, were injected into the analytical column by immersing the small trap column in 85°C water. Then, the gases were analyzed using GC-8AIE. The obtained SF_6 area in the SF_6 chromatogram was converted to SF_6 concentration based on the calibration line and the volume of water sample analyzed.

Each parameter (sample volume, bubbling duration, column and detector temperature, and gas flow rate) was optimized by trial-and-error. The list of optimized parameters is presented in Table 2. Figure 14 shows the test results of optimal bubbling duration to extract the SF_6 dissolved in water samples. We used the same water samples, which had the same SF_6 concentration, and changed only the bubbling time from 5 to 25 min in each analysis run. Then, each analyzed SF_6 concentration was plotted on a figure showing the relation between bubbling duration (min) and SF_6 concentration (fmol/L). In the case of 9−20 min bubbling, the analyzed SF_6 concentrations in water were almost the same (2.37 fmol/L on average), despite the different bubbling durations. However, the detected SF_6 concentrations were much lower when the bubbling duration was less than 7 min or more than 25 min. When the bubbling duration was short, the dissolved SF_6 in a water sample was not extracted completely. In contrast, when the bubbling duration was long, the trap column could not retain the gases including SF_6. Therefore, bubbling durations of 9−20 min are suitable for SF_6 analysis, and we set 13 min as the optimal

bubbling duration in the developed analytical system (Table 2).

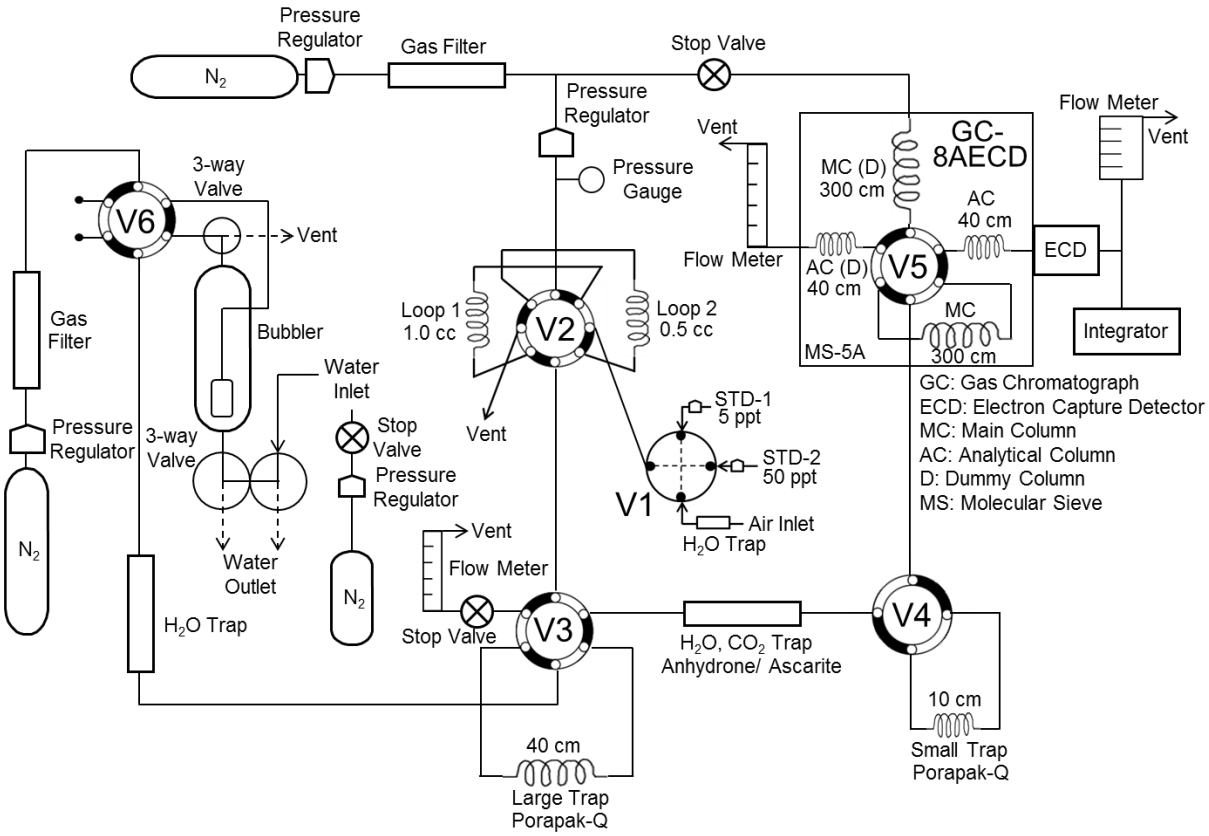

Figure 10. Schematic of apparatus developed in this study for measuring dissolved SF_6 in water.

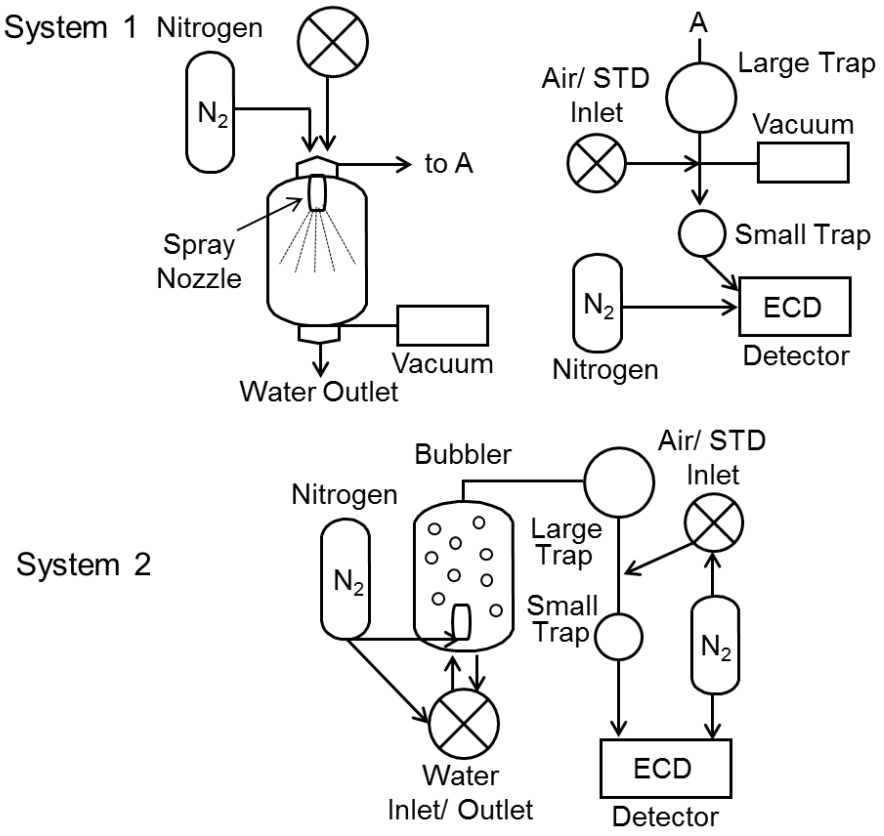

Figure 11. Simplified schematics of apparatus for measuring dissolved SF_6 in water showing differences between the apparatus developed in the present study and that developed by Busenberg and Plummer (2000).

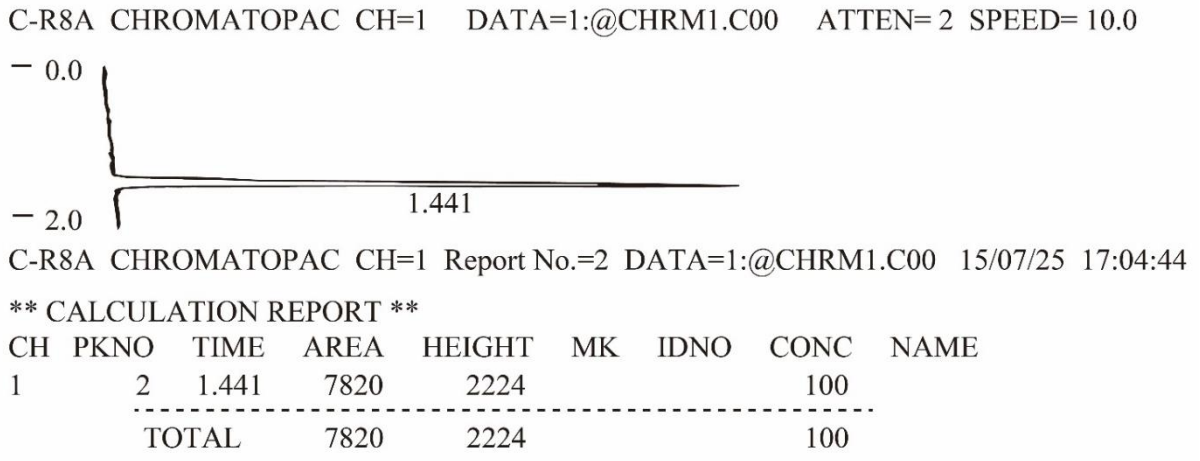

Figure 12. SF_6 chromatogram obtained using the analytical system developed in the present study.

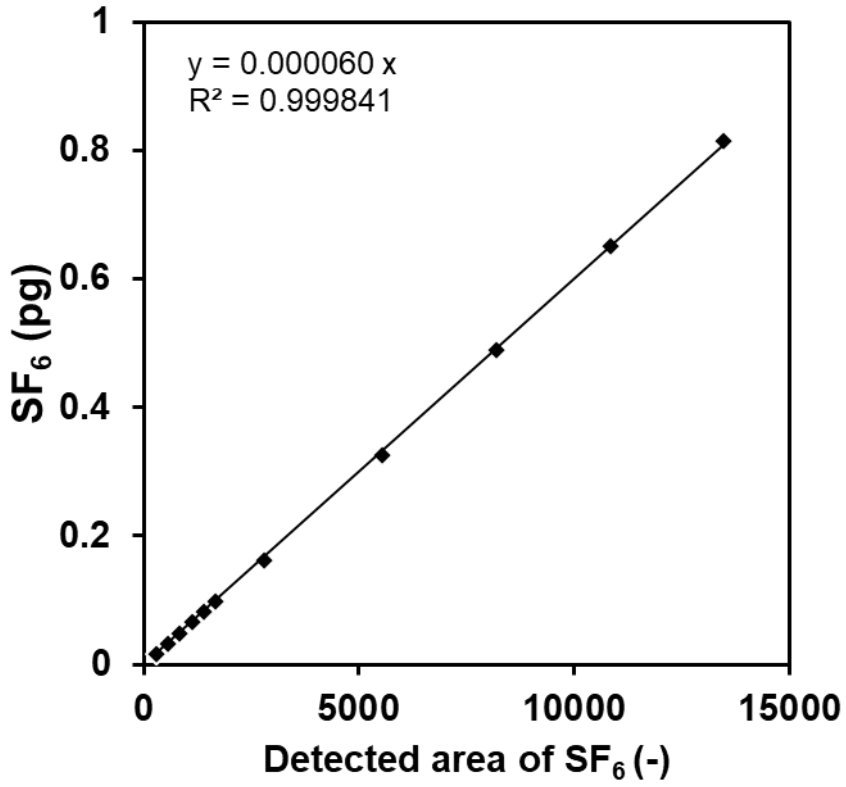

Figure 13. Calibration line between quantity of SF_6 and detected SF_6 area by using SF_6 analytical system developed in the present study.

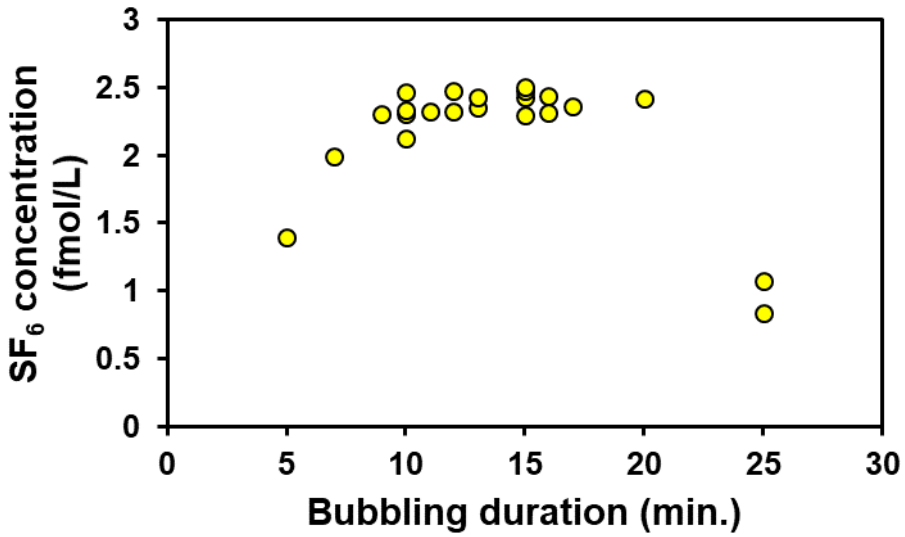

Figure 14. Test result of optimal bubbling duration to extract dissolved SF_6 from water samples. This figure indicates that the suitable bubbling duration is between 9 and 20 min.

Table 2. Optimized analytical conditions for determining dissolved SF_6 in water by using GC-8AIE.

Water sample volume	~320 mL
Air sample volume	1 mL
Bubbling time	13 min.
Bubbling gas flow rate	250 mL
Cooling temperature of the trap	-80℃
Heating temperature of the trap	80℃
GC oven temperature	70℃
ECD temperature	210℃
Carrier gas flow rate	40 mL

3.1.2 Analytical accuracy and detection limit

To determine the analytical accuracy, repeat analyses were conducted using two standard gases (5 and 50 pptv) with a constant-volume tube (0.5 and 1.0 cm^3) and water samples collected under the same conditions. Figure 15(a) shows the 20-times repeated analysis results of standard gases with three different concentrations of SF_6. In cases 1, 2, and 3, the 50-pptv standard gas with a 0.5- cm^3 tube, 5-pptv standard gas with a 1.0- cm^3 tube, and 5-pptv standard gas with a 0.5- cm^3 tube, respectively, were used. The standard deviation in each case was 0.02 fmol (case 1), 0.01 fmol (case 2), and 0.01 fmol (case 3), respectively. In addition, the coefficient of variation (CV = standard deviation/average) in each case was 1.5% (case 1), 8.1% (case 2), and 5.8% (case 3). Therefore, the analytical accuracy of this system was between $\pm$ 0.01 and $\pm$0.02 fmol. The CVs in cases 2 and 3 were higher than 5% because of the very small quantity of SF_6 in the analytical target. Figure 15(b) shows the 16-times repeated analysis results using water samples, which reflects the analytical accuracy of determination of dissolved SF_6 concentration in water. The standard deviation and coefficient of variation were 0.07 fmol/L and 2.9%, respectively. The detection limit of this analytical system was 0.1 fmol. This was in the case of using the 5-pptv standard gas and 0.5-cc constant-volume tube, which is the minimum quantity of SF_6 that we can inject into the analytical column by using the prepared standard gases and constant-volume tubes. However, considering that a distinct peak appeared in the chromatogram of 0.1 fmol, the SF_6 detection limit of the developed system should be lower than 0.1 fmol.

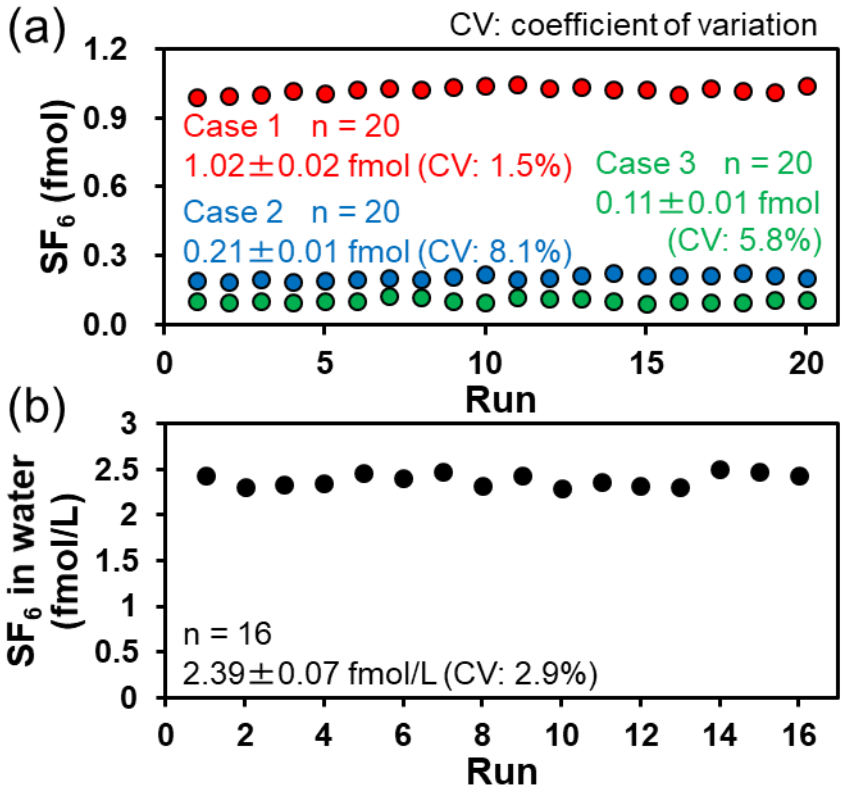

Figure 15. (a) 20-times repeated analysis results of standard gases with three SF_6 quantities. Cases 1, 2, and 3 employ the 50-pptv standard with 0.5-cm^3 tube, 5-pptv standard with 1.0-cm^3 tube, and 5-pptv standard with 0.5-cm^3 tube, respectively. (b) 16-times repeated analysis results using water sample, which reflects the analytical accuracy of dissolved SF_6 concentration in water.

3.1.3 Problems and improvement work

The author has attempted to remove and reduce any difficulties and errors associated with the developed system through maintenance and parts replacement. However, several problems persist, which are described in this section. The author hopes that users will make the system more user-friendly in the future in terms of allowing for more accurate analysis.

First, we should determine the exact SF_6 detection limit of the system. Unfortunately, the developed system has no standard gas and constant-volume tube for concentrations lower than 5 pptv and volumes smaller than 0.5 cc, respectively. For determining the exact SF_6 detection limit of the system, a new constant-volume tube or new standard gases are necessary. The detection limit and analysis accuracy information are related directly to the reliability of the research results when water or gas samples with very low SF_6 concentration are analyzed. Therefore, an exact SF_6 detection limit along with its accuracy should be determined in the future.

Second, the back-flush system does not work perfectly in the developed analytical system. It flushes unnecessary gases (e.g., O_2, H_2, and CO) out of the system before they flow into the analytical column. If the back-flush system works perfectly, only SF_6 (analysis target) is injected into the analytical column. In other words, contamination of the analytical column by unnecessary gasses can be prevented by the back-flush system. Therefore, the back-flush system can shorten the duration of each analysis run. The back-flush system does not work well mainly because of a problem in the 300-cm main column shown in Figure 10. The extracted gases, including SF_6, must flow in the 300-cm main column, regardless of whether valve 5 is the right or left position. Thus, when the back-flushing starts, the unnecessary gasses must be flushed out of the system before they flow into the 300-cm main column. This problem can be solved by adding a new six-way valve before V5 in the system and repositioning the 300-cm main column before the new valve. The new valve allows only SF_6 gas to be injected into the

analytical column and facilitates the flushing of unnecessary gasses out of the system.

Third, the purge housing system does not work effectively. This problem originates from the line design step. The purge housing system can eliminate any possible diffusion from the atmosphere into the valve, and works by filling an ultra-pure carrier gas (N_2) into the purge housing chamber of each valve. The developed system has a purge housing line placed just before the carrier gas outlet. The system works better with the purge housing than without it. However, the purge housing chamber should be filled with the ultra-pure carrier gas (N_2); therefore, the purge housing line should be connected directly to the ultra-pure N_2 tank.

These three problems or possible improvements constitute the scope of future work of this study. If all problems associated with the SF_6 analytical system developed in this study are solved, SF_6 analysis would become more accurate and faster than it is now, which can contribute positively to future hydrological studies using the SF_6 tracer.

3.2 Hydrometric recording and chemical analysis

Hydrological data (rainfall, discharge, and groundwater table level) were recorded in the designed experimental catchment from May 2015 to May 2017 (~2 years in total). All equipment was installed in the tributary area of Seto Catchment (Figure 8). Figure 16 shows the locations of the equipment on a cross section of the tributary area with geological information. The spring downstream was the main target of rainfall–runoff water in this study; therefore, discharge volume was monitored downstream of the discharge point at intervals of 10 min by using a V-notch weir and a water table recorder (TruTrack, WT-HR500; Figure 17). Additionally, seven boreholes were drilled in the catchment to facilitate the evaluation of groundwater flow dynamics in relation to rainfall–runoff processes. The WL-3 m, 5 m, 10 m; WM-3 m, 5 m, 10 m; and WH-20 m boreholes with a diameter of 0.065 m were located near the spring of the valley, at the boundary between the hillslope and valley, and in the ridge area, respectively (Figure 18). The screen depths of the 3-m, 5-m, 10-m, and 20-m boreholes were 2–3 m, 4–5 m, 8–10 m, and 10–20 m below the ground surface, respectively (Table 1). A water level recorder (HOBO CO-U20-001-01, Tempcon instrumentation Ltd., UK) was installed in each borehole by using a wire rope to monitor the groundwater table at intervals of 10 min. Rainfall was measured in increments of 0.2 mm by using a tipping-bucket rain gauge (Davis #7852M, CA, USA) installed along the ridge (RF in Figure 8; Figure 19). In addition, the recorded discharge height and groundwater table levels were calibrated against discharge and groundwater table levels measured manually during both rainless and rainfall periods.

Water sampling campaigns were conducted periodically under rainless conditions and intensively during four rainstorms (July 15th–17th, 2015; August 22nd–24th, 2016; August 29th–31st, 2016; and September 20th–22nd, 2016) to determine the stable isotopic compositions, inorganic solute concentrations, and SF_6 contents of water. Groundwater was sampled four times both during rainless periods and just after heavy rainfall (May 3rd, 2016; August 31st,

2016; November 22nd, 2016; and February 20th, 2017). Detailed sampling and analysis information is given in Tables 3 and 4, respectively. The sampling and analysis procedures for SF_6 are explained in the next section. The spring water was sampled manually during the daytime and automatically during night time by using an automated water sampler (Sigma SD900, HACH, Loveland, CO, USA) at the spring discharge point. Groundwater was collected from each borehole by using a pump run by compressed air (GEO-pump-BENNETT-1400) after sufficiently purging the water pooled in the boreholes. Approximately three times the volume of pooled groundwater was flushed before groundwater sampling. Rainwater was collected from the ridge area (RF in Figure 8; Figure 19) by using a 30-L plastic container for periodical rainfall sampling and a 0.5-L conical flask for intensive rainwater sampling during rainstorms. Evaporation of rainwater from the container or flask was avoided using a handmade system comprising a plastic funnel and a ping-pong ball. Soil water from depths of 10, 30, and 50 cm below the ground surface near the WL borehole (SL in Figure 8; Figure 20) was sampled using suction lysimeters. The numbers of collected samples of each water type during the observation period are listed in Table 5.

The dissolved inorganic contents and oxygen/hydrogen stable isotopic compositions of all water samples were analyzed. The Cl^-, NO_3^-, and SO_4^{2-} concentrations were determined using an ion chromatograph (SHIMADZU, HIC-10A super) after filtering the samples with a 0.20-μm cellulose ester filter. The Na^+, K^+, Ca^{2+}, Mg^{2+}, and SiO_2 concentrations were analyzed after filtering the samples by using an inductively coupled plasma mass spectrometry optical emission spectrometer (PERKIN ELMER, Optima 7300DV). The HCO_3^- concentration was deduced by titration with 0.005 M sulfuric acid. The stable isotopic compositions of hydrogen and oxygen were measured using an isotopic water analyzer (Picarro, L2120-i). The measured stable isotopic compositions were expressed using conventional δ-notations as permil deviations from the Vienna Standard Mean Ocean Water (V-SMOW). The analytical accuracies

of the stable isotopic compositions of ^{18}O and ^{2}H were ± 0.1‰ and ± 0.5‰, respectively.

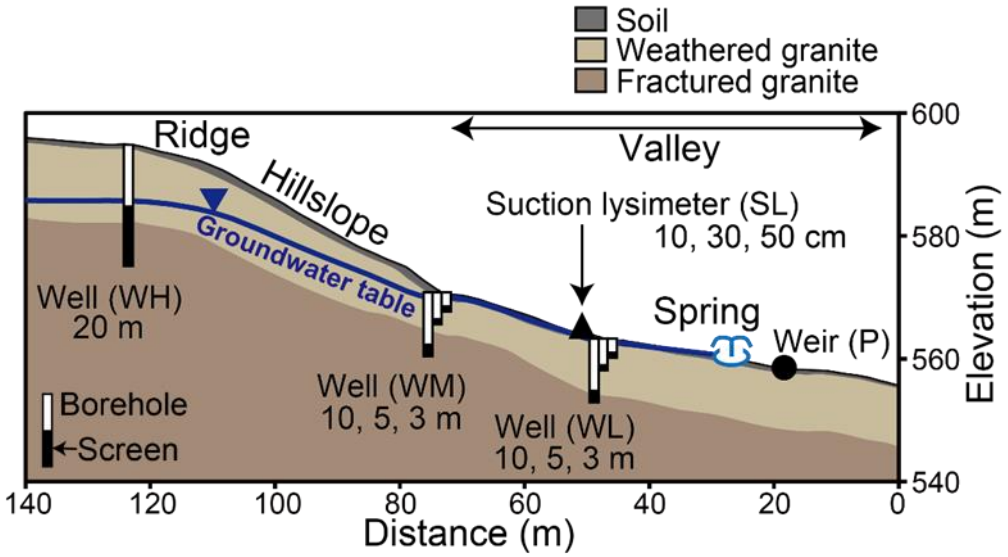

Figure 16. Detailed locations of equipment and geological information on a cross section along the valley of the tributary area in Figure 8.

Figure 17. Installed V-notch weir and water table recorder for monitoring water discharge (P in Figure 8).

Figure 18. Installed boreholes at the boundary between the hillslope and valley (WM).

Figure 19. Installed rainfall monitoring system and rainfall collectors (RF in Figure 8).

Figure 20. Installed suction lysimeters for collecting soil water (SL in Figure 8).

Table 3. Sampling and analysis information.

Observation period	May, 2015–May, 2017
Observed rainfall event	Jul-15–17, 2015; Aug-22–24, 2016; Aug-29–31, 2016; Sep-20–22, 2016
Groundwater sampling	May-3, 2016; Aug-31, 2016; Nov-22, 2016; Feb-20, 2017
Hydrological observation	1. Spring discharge at P [10 minutes interval]
	2. Groundwater table level at WL, WM, and WH [10 minutes interval]
	3. Rainfall at RF [5 minutes interval]
Sampled water	1. Spring water at discharge point
	2. Groundwater at WL, WM, and WH
	3. Soil water at SL
	4. Rainfall at RF
Analyzed items	$\delta^{18}O/\delta^{2}H/Cl^{-}/NO_3^{-}/SO_4^{2-}/HCO_3^{-}/Na^{+}/K^{+}/Ca^{2+}/Mg^{2+}/SiO_2/SF_6$

Table 4. Timetable of field observations and water sampling.

* number: the number of conducted surveys within a month

Year	2015								2016												2017				
Month	May	Jun	Jul	Aug	Sep	Oct	Nov	Dec	Jan	Feb	Mar	Apr	May	Jun	Jul	Aug	Sep	Oct	Nov	Dec	Jan	Feb	Mar	Apr	May	Total
Sampling	1		3	1	1		1	1		1	1		2	1	1	2	1	1	1	1		1		1	1	23
→ SF_6 in spring	1		1				1	1		1	1		1	1	1	2	1	1	1	1		1		1	1	18
→ SF_6 in GW													1			1			1			1				4
Rain event			1													2	1									4

Table 5. List of total number of collected samples during observation period.

Water	n*	n_{SF6}**
Rain	41	0
Soil water 10 cm	22	0
Soil water 30 cm	22	0
Soil water 50 cm	20	0
Groundwater WL3 m	15	4
Groundwater WL5 m	19	4
Groundwater WL10 m	13	4
Groundwater WM3 m	15	4
Groundwater WM5 m	15	4
Groundwater WM10 m	14	4
Groundwater WH20 m	7	4
Spring	74	37

* The number of samples for isotopic and ion analyses

**The number of samples for SF_6 analyses

3.3 Water dating method using SF_6

Spring water and groundwater were sampled in 450-mL amber glass bottles sealed with screw caps and butyl tape to determine the dissolved SF_6 concentration. The samples were collected in duplicate or triplicate to reduce any measurement error. A nylon tube connected to an appropriate pump (Geo-pump-CFC-a, GEO-pump-BENNETT-1400) was placed at the bottom of the bottle to replace air-contaminated water with pure groundwater or spring water. After overflowing at least 2 L of the samples, the tube was slowly removed. Thus, contamination of the sampled water with air was avoided. Figures 21 and 22 show examples of collection of spring water and groundwater for SF_6 analysis.

The dissolved SF_6 was analyzed using a purge-and-trap gas chromatography procedure (Busenberg and Plummer, 2000) and a Shimadzu GC-8A gas chromatograph equipped with an electron capture detector (ECD) at the University of Tsukuba, Japan (Figure 10). The SF_6 in the water samples was striped using ultra-pure N_2 gas at 250 mL/min (bubbling system) and then trapped in the Porapak-Q column at –80°C. Finally, the trapped SF_6 was injected into an ECD gas chromatograph by placing the trap column into 85°C water. It was confirmed that only SF_6-free materials were used to build all experimental equipment, including stainless steel, copper, glass, nylon, and grease-less material. The analytical accuracy of the gas samples, such as the standard gas and air samples, was less than 1.5% and that of the SF_6 in dissolved water was less than 3%.

The dissolved SF_6 concentrations of the groundwater and spring water were converted to the atmospheric mixing ratio according to Henry's law and based on several parameters (recharge temperature, recharge elevation, and EA; Busenberg and Plummer, 2000; IAEA, 2006). Manning et al. (2012) defined each parameter as follows: the recharge temperature is the temperature at the groundwater table when water recharges the groundwater; the recharge elevation is the ground surface elevation at which water recharges the groundwater; and EA is

the gas contained in groundwater that has more than equilibrium solubility with the atmosphere (IAEA, 2006). In this study, the 20-year average air temperature (10.4°C [1997–2017]; AMeDAS) in Iitate village (10 km away from the study area) and average elevation of the region (601.2 m) were set as the recharge temperature and recharge elevation (Gooddy et al., 2006) because the present study area is a small catchment, which means that the dating error originating from these two parameters is limited (Manning et al., 2012).

EA is one of the parameters leading to the underestimation of water age owing to poor water solubility of SF_6 (Gooddy et al., 2006). Generally, the amount of EA in collected water can be determined based on the concentration of noble gases such as Ar, N_2, or Ne (Plummer et al., 2001; Zuber et al., 2005; Koh et al., 2007; Young et al., 2013). If 1 cm^3/L EA is contained in the water samples, the age determined by SF_6 is underestimated by 1–2 years. The effects of EA on the estimation of water age by using SF_6 are presented in Figure 23. In addition, Hall et al. (2012) investigated the behavior of noble gases in subsurface areas during rainfall and indicated that the effect of EA on groundwater during rainfall is stronger. In this study, although no EA determination was implemented because of the difficulty of its measurement in Japan, 1.4 cm^3/L was set as the average EA in granite geology for correcting the observed raw SF_6 concentration in sampled water based on Wilson and McNeill (1997) and Morikawa (2004) (Figure 24). Lapworth et al. (2013) and Kamtchueng et al. (2015), who did not perform EA measurement for dating water using a SF_6 tracer, too referred to Wilson and McNeill (1997). In the present study, we added EA information of fractured granite geology (referred to from [Morikawa, 2004]) into Wilson and McNeill's model (Figure 24). Zuber et al. (2005), Salle et al. (2012), and Young et al. (2013) reported that EA in spring water and groundwater is less than 4 cm^3/L, whereas others such as Bohlke et al. (2007) and Jaunat et al. (2012) observed more than 10 cm^3/L EA in some water samples. This topic is very important to verify the results of the present study; therefore, EA in water and its effect on the results of this study are

discussed in the Discussion chapter.

In this study, the SF_6 age of water was determined under the assumption of the piston flow model, which corresponds to the apparent water age. The piston flow model is described in detail in Gooddy et al. (2006) analogously to water flow through a pipe from the point of recharge to the point of discharge, without mixing during transit. The piston flow assumption is simple and the most probable groundwater flow model when focusing on springs, borehole water, and water in the headwater region (Gooddy et al., 2006; Long and Putnam, 2006; Kamtchueng et al., 2015). It is available without any other parameters related to complex mixing flow models. Therefore, the piston flow model age, which corresponds to the apparent water age, was mainly used in this study as the SF_6 age.

Trial practice was implemented for grasping age differences among the following groundwater mixing models: piston flow model, exponential model, and exponential-piston flow model. Figure 7 shows the probability density functions (transit time distributions: TTDs) of each groundwater model. By using the TTDs, each modeled reference curve was constructed, and are shown in Figure 6(b). This figure indicates slight differences among the reference curves of various groundwater flow models, and the mean residence time ranges from 0 to 20 years. However, gaps among these reference curves increase as the mean residence time increases (Figure 6(b)). Therefore, when focusing on young water aged less than 20 years, the possible error in estimated water age depending on different mixing assumptions is less than several years. In contrast, when focusing on older water with age of more than 20 years, large differences in the dating references lead to large uncertainties in estimates of water age. This study area is part of the headwater catchment; therefore, the mean residence time may be short and possible errors originating from differences in the mixing assumptions may be small as well.

The natural background of SF_6 concentration in air is known to be <0.04 pptv (Maiss and

Brenninkmeijer, 1998), which can be neglected considering the recent rapid and monotonic increase in SF_6 in the atmosphere. The release of SF_6 into air by anthropogenic activity (mainly industrial purposes) started in 1953; currently (2016), the SF_6 mixing ratio in the Northern Hemisphere atmosphere is, on average, more than 8.9 pptv. The well-known SF_6 chronicle of the Northern Hemisphere, where the study area is located, is available at the following website: https://water.usgs.gov/lab/ (USGS, The Reston Groundwater Dating Laboratory) (Figure 3). Various studies have applied these SF_6 air curve data to date water (Busenberg and Plummer, 2000; Koh et al., 2007; Busenberg and Plummer, 2014). Additionally, the atmospheric SF_6 concentration observed by Japan's National Institute for Environmental Studies (NIES, https://www.nies.go.jp/) from 2006 to 2013 in Hokkaido and Okinawa, which are the northernmost and southernmost prefectures in Japan, shows a trend similar to the averaged Northern Hemisphere SF_6 chronicle, with a difference of only several percent. However, Asai et al. (2011 and 2017) and Friedrich et al. (2013) indicated that the SF_6 atmospheric mixing ratios in populated and industrialized regions are not always but often higher owing to human-activity-induced SF_6 loading, leading to significant errors in the estimated age of water. Therefore, the atmospheric SF_6 mixing ratio was observed in the study area during the investigation period (Figure 25-a). Most of observed atmospheric SF_6 mixing ratio was between 9 pptv and 10 pptv. The rainfall effects on the atmospheric SF_6 mixing ratio were also analyzed: there is unclear relation between rainfall and atmospheric SF_6 mixing ratio as shown in Figures 25(b) and 25(c). Figure 26 shows the atmospheric SF_6 concentration in Hokkaido (obtained from NIES database) and the historical SF_6 records of the Northern Hemisphere (obtained from the USGS database). The average observed SF_6 concentration in the study area with the corresponding standard deviation data are also shown in Figure 26. According to the figure, the atmospheric SF_6 concentration in the study area is 27% higher than that in the Northern Hemisphere. Therefore, the SF_6 chronicle in air (piston flow model reference curve) in the study

area was corrected using a 27% offset to the historical SF_6 records of the Northern Hemisphere, as shown by the gray line in Figure 26.

Figure 21. Picture of spring water sampling for SF_6 analysis with an appropriate pump that can prevent air contamination of sampled water.

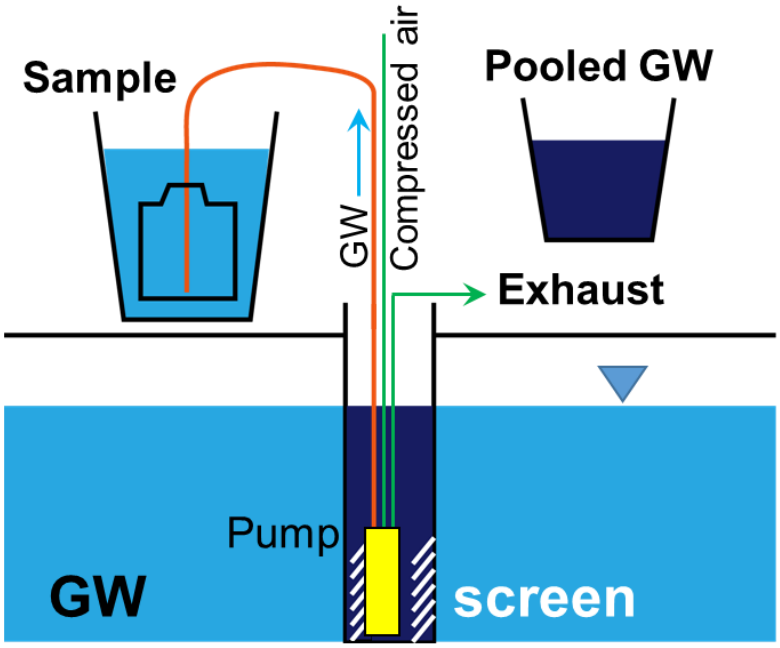

Figure 22. Schematic of groundwater sampling for SF_6 analysis with an appropriate pump that can avoid air contamination of sampled water.

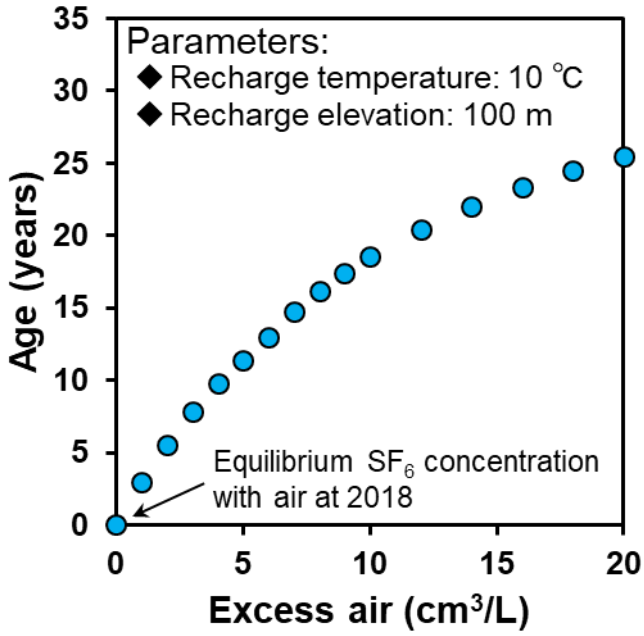

Figure 23. Effects of excess air on water age estimated using SF_6 tracer.

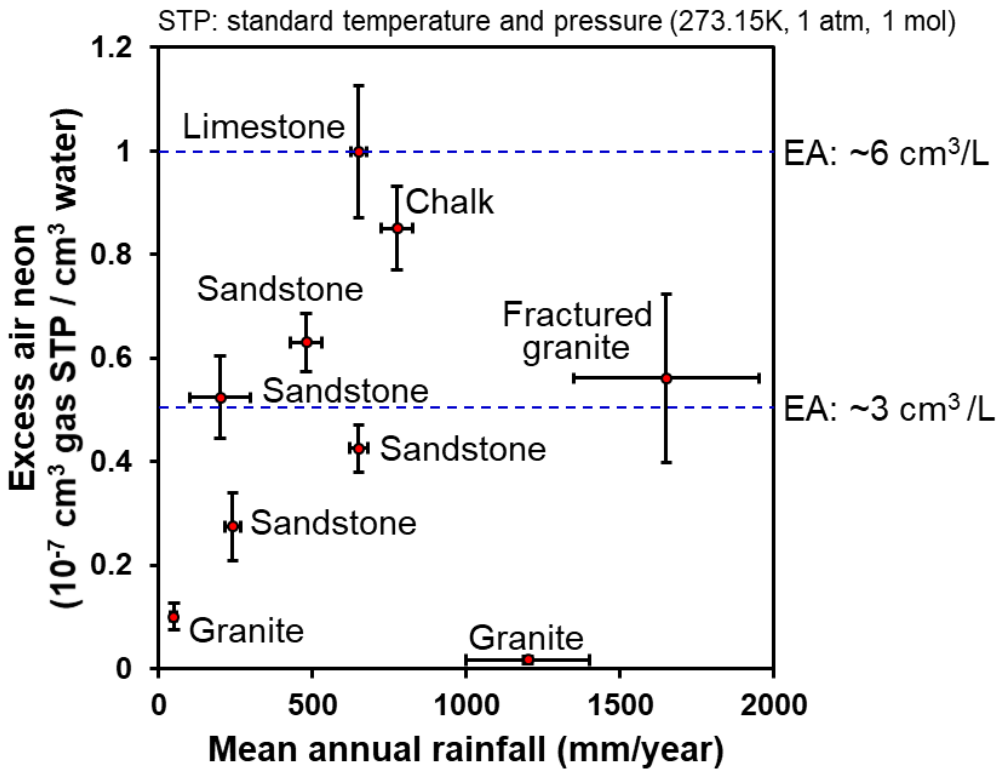

Figure 24. Relations among excess air (EA) in water, mean annual precipitation, and geology (Fractured granite: referred from Morikawa (2004); other geology: referred from Wilson and McNeill (1997)). The higher excess air neon means larger volume of EA in water. The error bars for excess air neon represent the standard error and those for mean annual rainfall represent the standard deviation.

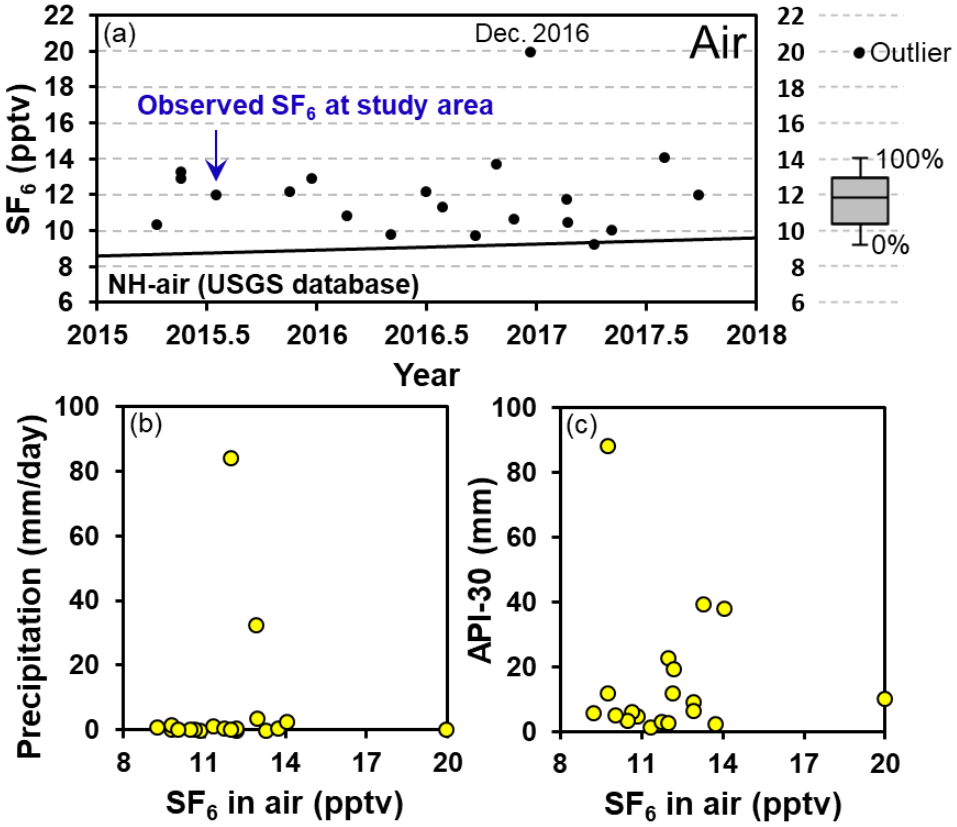

Figure 25. (a) Observed atmospheric SF_6 mixing ratio in the study area during investigation period with the Northern Hemisphere curve. The observed SF_6 concentration in air at December 2016 is an outlier due to statistical consideration. (b) The relation between observed atmospheric SF_6 mixing ratio and precipitation amount at the day of sampling. (c) The relation between observed atmospheric SF_6 mixing ratio and the antecedent precipitation (API 30) at the day of sampling. API: Antecedent Precipitation Index.

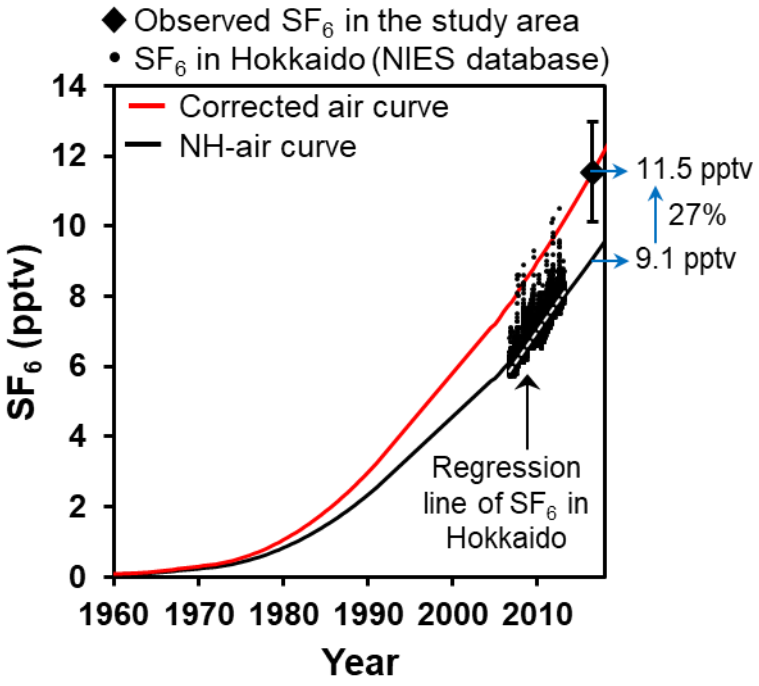

Figure 26. Atmospheric SF_6 mixing ratio recorded in NH-air and air in Japan (Hokkaido: Ochiishi Cape). The average observed SF_6 concentration with the standard deviation in air in the study area are presented as well. Data were obtained from USGS (The Reston Groundwater Dating Laboratory: http://water.usgs.gov/lab/; last accessed on May 10, 2016) and NIES Global Environmental Database (http://db.cger.nies.go.jp/portal/geds/atmosphericAndOceanicMonitoring/; last accessed on March 25, 2016). The dashed line indicates the regression line of SF_6 in Hokkaido, and the red line indicates the corrected air curve in the study area using a 27% offset to the NH-air values.

3.4 End-member mixing analysis

The end-member mixing analysis (EMMA) has been applied widely as a simple and effective method to quantify the contribution of different sources to stream water and groundwater (Hooper et al., 1990; Christophersen and Hooper, 1992; Burns et al., 2001; Liu and Yamanaka, 2012; Tubau et al., 2014; Xing et al., 2015; Yang et al., 2015). EMMA uses the chemical signature of water originating from potential end-members within a catchment to determine the contribution (percent) of each source to the final mixture (Gracz et al., 2015). It can therefore provide concrete and variable information regarding water sources and their contributions. The contributions are calculated as follows:

$$R_x + R_y + R_z = 1 \quad (1)$$

$$C_x R_x + C_y R_y + C_z R_z = C_{final\ mixture} \quad (2)$$

$$D_x R_x + C_y R_y + C_z R_z = D_{final\ mixture} \quad (3)$$

where R is the contribution quantity of the final mixture; C and D are the conservative tracer concentrations; and subscripts x, y, and z represent the end-members of the final mixture. Details of the method and procedures of EMMA are described in Hooper et al. (1990) and Christophersen and Hooper (1992).

Four preconditions are required for applying EMMA: (1) the mixing process of the fixed components should be linear, (2) no concentration change should be generated during the analysis, (3) no chemical change should occur via mixing, and (4) there should be significant differences among the end-members (Sklash and Farvolden, 1979; Barthold et al., 2011).

CHAPTER 4 RESULTS

4.1 Long-term hydrological data and tracer characteristics

Figure 27 shows the hydro-hyetograph (RF and P in Figure 8) and groundwater table level variations (WL, WM, and WH in Figure 8) from May 2015 to May 2017. The spring has water throughout the year. The minimum discharge, corresponding to the base flow, is less than 0.2 L/s during the winter season, and the maximum spring discharge is 3.3 L/s during an intense rainfall event caused by a typhoon. Heavy rainfall exceeding 50 mm/day occurs occasionally, especially from July to November, owing to typhoons in the region. The spring discharge responds strongly to rainfall. In other words, the spring discharge increases promptly during a rainstorm and decreases rapidly after a rainstorm. The calculated discharge rate at discharge point P throughout 2016 was 30% of the total precipitation (1220 mm/year 2016) in the study area. Given that the total amount of reference evapotranspiration at Iitate village was 510 mm in 2016 (MeteoCrop database at Iitate with an elevation of 460 m, 10 km away from the study area, Japan National Institute for Agro-Environmental Sciences), 340 mm of rainwater must percolate toward the deeper subsurface layer (bedrock media).

The groundwater table levels in the valley (WL), ridge area (WH), and its boundary section (WM), too, clearly respond to rainfall, similar to the variation in spring discharge. The weathered and fractured bedrock media seem to allow this clear and prompt groundwater table response to rainfall input. However, the rate of decrease in the ridge groundwater table level after a rainfall event is slower than that in the valley groundwater table level.

In terms of hydraulic potential distribution, shallower groundwater has a higher hydraulic potential than deeper groundwater at WL near the spring point throughout the year. In contrast, groundwater at depths of 3, 5, and 10 m at WM has similar hydraulic potential throughout the year. Therefore, vertical groundwater flow is dominant in the region near the spring (WL),

whereas lateral groundwater flow is dominant at the boundary between the hillslope and the valley (WM). In addition, long-term groundwater table level records indicate no obvious change in the groundwater flow system in the subsurface area at depths of 3–10 m during the observation period, even during heavy rainstorms; alternatively, increases in the hydraulic gradient between groundwater at each borehole and spring discharge point are indicated.

Long-term variations in air and water temperature are monitored and shown in Figure 28. Air temperature and groundwater temperature in each borehole are observed automatically at intervals of 10 min, whereas spring temperature is observed manually during each field survey in rainless periods. This is why the quantity of spring temperature data is lower than that of air and groundwater data. Air temperature varies from –11.3 to 30.7°C throughout the year with seasonal variation; July to August is the hottest season and January to February is the coolest season. Spring water and groundwater temperature variations are clearly damped compared to air temperature variation. In addition, the temperature of deeper groundwater is almost stable throughout the year; for example, the differences between the maximum and minimum water temperature in WL-10 m, WM-10 m, and WH-20 m are 1.0°C, 0.4°C, and 0.4°C, respectively. The average temperature of spring water and groundwater is 10.5–11.0°C, which is quite similar to the 20-year average air temperature in Iitate village, meaning that the defined groundwater recharge temperature (10.4°C) in this study is adequate. Moreover, the maximum and minimum temperatures of shallower groundwater (e.g., WL-3 m and WM-3 m) occur in October and March, respectively. The seasonal variation tendency of groundwater temperature is delayed by almost 2 months compared to that of air temperature variation.

Temporal variations in stable isotopic compositions ($\delta^{18}O$, $\delta^{2}H$) of oxygen and hydrogen in rainwater and spring water collected from May 2015 to May 2017 are shown in Figure 29, while those of groundwater collected four times during the observation period are shown in Figure 30. The stable isotopic compositions of oxygen ($\delta^{18}O$) and hydrogen ($\delta^{2}H$) in rain and spring

water vary from −15.0‰ to −3.7‰ and −109‰ to −21‰ and from −10.3‰ to −7.8‰ and −67‰ to −53‰, respectively, throughout the observation period. The $\delta^{18}O$ and $\delta^{2}H$ variation ranges of rainwater are considerably wider than those of spring water. The stable isotopic compositions of oxygen ($\delta^{18}O$) and hydrogen ($\delta^{2}H$) in groundwater do not vary significantly throughout the observation period compared to those in rainwater and spring water; the range of variation is within 0.6‰ for $\delta^{18}O$ and 3‰ for $\delta^{2}H$ in groundwater samples.

Figure 31 shows the relation between $\delta^{18}O$ and $\delta^{2}H$ for all collected rain and spring water samples. The average $\delta^{18}O$ and $\delta^{2}H$ of soil water and groundwater along with their standard deviations are shown in Figure 31. The local meteoric water line (LMWL) is drawn based on the observed stable isotopic compositions in rainwater sampled during the observation period. Spring water, soil water, and groundwater can mostly be plotted on the LMWL; therefore, the amounts of spring water, soil water, and groundwater that can be ascribed to the effects of precipitation and evaporation on water are limited. In addition, all plotted points of the spring water are surrounded by rainfall points and the variation in the stable isotopic compositions in the spring water appears to be damped compared to that in the rainwater.

Temporal variations in the concentrations of inorganic ions (Cl^{-}, NO_3^{-}, SO_4^{2-}, HCO_3^{-}, Na^{+}, K^{+}, Ca^{2+}, and Mg^{2+}) and silica (SiO_2) in rainwater and spring water collected from May 2015 to May 2017 are shown in Figures 32 and 33, while those in the groundwater collected four times during the observation period are shown in Figures 34–36. All solute tracers show different values between spring water and rainwater, even though the values of SO_4^{2-} in spring water and rainwater are quite similar throughout the observation period. Most solute tracers in spring water during rainfall events show larger variations than in the rainless period. Moreover, most solute tracers (e.g., HCO_3^{-} and Na^{+}) in spring water change toward the rainwater-dominant values during rainstorms; however, Cl^{-} in spring water changes toward the opposite direction of the rainwater-dominant values. Additionally, NO_3^{-} in spring water during

rainstorms has different characteristics from other tracers; NO_3^- in some spring water samples decreases toward rainwater-dominant values, but that in other spring water samples increases toward the opposite direction of the rainwater-dominant values. These findings indicate that spring water during rainfall is simply not affected by rainwater, and mixes with rainwater. This is because if spring water is diluted by rainwater, all solute tracers in spring water during rainfall should change toward the rainwater-dominant values. Solute tracer concentrations in groundwater are mostly stable, regardless of rain conditions, except for the concentrations of sulfate ion and nitrate ion. The concentration of sulfate in valley groundwater (WL-3 m and WL-5 m) in May 2016 (~3 mg/L) is much higher than that in the other groundwater samples (~1 mg/L). However, the sulfate concentration decreases to around 1 mg/L in August 2016. In addition, nitrate concentration in groundwater decreases slightly toward the deeper-groundwater-dominant value (WH-20 m) just after the rainstorm (August 2016).

Figure 37 shows boxplots of the stable isotopic compositions and solute concentrations for all water samples (rainwater, soil water, groundwater, and spring water) collected during the study period. The stable isotopic compositions (‰), Cl^-, Na^+, and SiO_2 concentrations (mg/L), are especially focused on in this study because of their characteristics described in the following parts. Each water type shows a wide variety of tracer concentrations. Especially, the Cl^-, Na^+, and SiO_2 concentrations in rainwater are considerably lower than those in the other water types. Those in spring water (Cl^-, 2.5 mg/L; Na^+, 3.8 mg/L; and SiO_2, 18.2 mg/L) are between those in soil water (or rainwater) and groundwater. In addition, the median value of Cl^- concentration in groundwater ranges from 2.2 to 2.4 mg/L, except for the concentration in ridge groundwater (WH-20 m). Although the 10-cm soil water has a slightly lower Cl^- concentration with a median value of 2.5 mg/L, the 30- and 50-cm soil waters have higher Cl^- concentrations than the other water types; the median Cl^- concentrations in the 30- and 50-cm soil water are 3.1 and 2.9 mg/L, respectively. The median values of Na^+ and SiO_2 in groundwater range from 4.7 to 6.6 mg/L

and from 17.3 to 22.2 mg/L, respectively, except in ridge groundwater (WH-20 m), and these values are notably higher than those in soil water and rainwater.

In the case of ridge groundwater, the median Cl^- concentration (2.7 mg/L) is slightly higher than that in other groundwater types and the median Na^+ and SiO_2 concentrations (Na^+: 4.4 mg/L, SiO_2: 19.9 mg/L) are slightly lower than those in the other groundwater types; however, these values are lower (for Cl^-) and higher (for Na^+ and SiO_2) than the median Cl^-, Na^+, and SiO_2 concentrations in soil water and rainwater. Therefore, the Cl^- accumulated in soil water and the Na^+ and SiO_2 accumulated in groundwater are useful tracers characterizing the behaviors of soil water and groundwater in the study area.

In the case of stable isotopic compositions, the $\delta^{18}O$ and $\delta^{2}H$ in rainwater show large variations with lower median values (−8.7‰ for $\delta^{18}O$ and −57‰ for $\delta^{2}H$) than those in other water types. Shallow soil water has slightly high stable isotopic compositions of both oxygen and hydrogen. The isotopic compositions of oxygen and hydrogen in groundwater are almost similar to each other, regardless of groundwater depth. Therefore, stable isotopic compositions can possibly be used to characterize the effect of rainfall on the groundwater flow system in the study area.

Figure 38 shows a tri-linear diagram of all collected water samples during the observation period. Four categories, including rainwater, soil water, spring water, and groundwater, are plotted in Figure 38. Rainwater and soil water are plotted in many locations, whereas groundwater and spring water are plotted in each cluster in Figure 38. As a trend, spring water is plotted between the soil water and rainwater cluster and groundwater cluster. This suggests that spring water mainly consists of soil water, rainwater, and groundwater as a result of mixing.

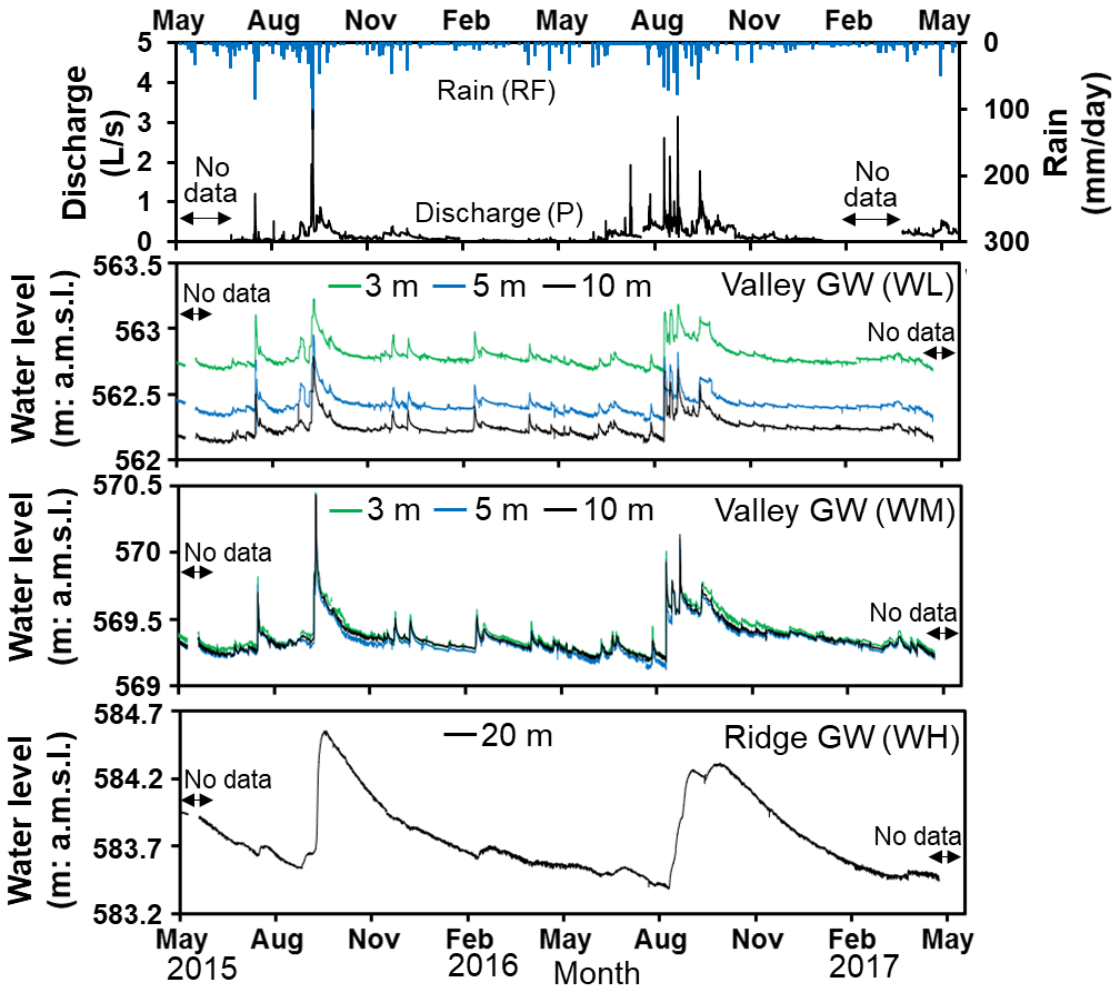

Figure 27. Spring hydrograph at point P in Figure 8, rainfall hyetograph at RF in Figure 8, and variations in groundwater table level at each borehole.

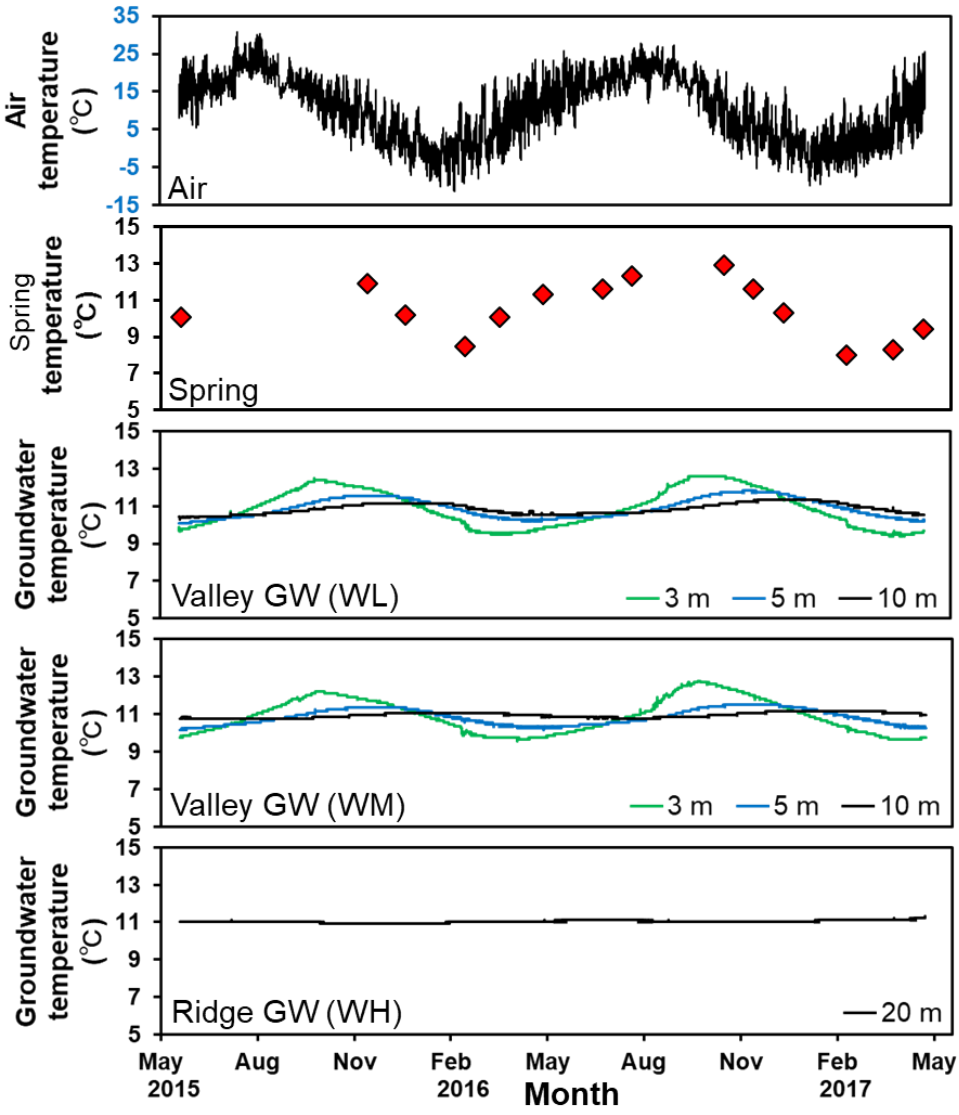

Figure 28. Long-term variation in air, spring water, and groundwater temperature. Air and groundwater temperature were monitored automatically at intervals of 10 min. Spring water temperature was monitored manually at each sampling time.

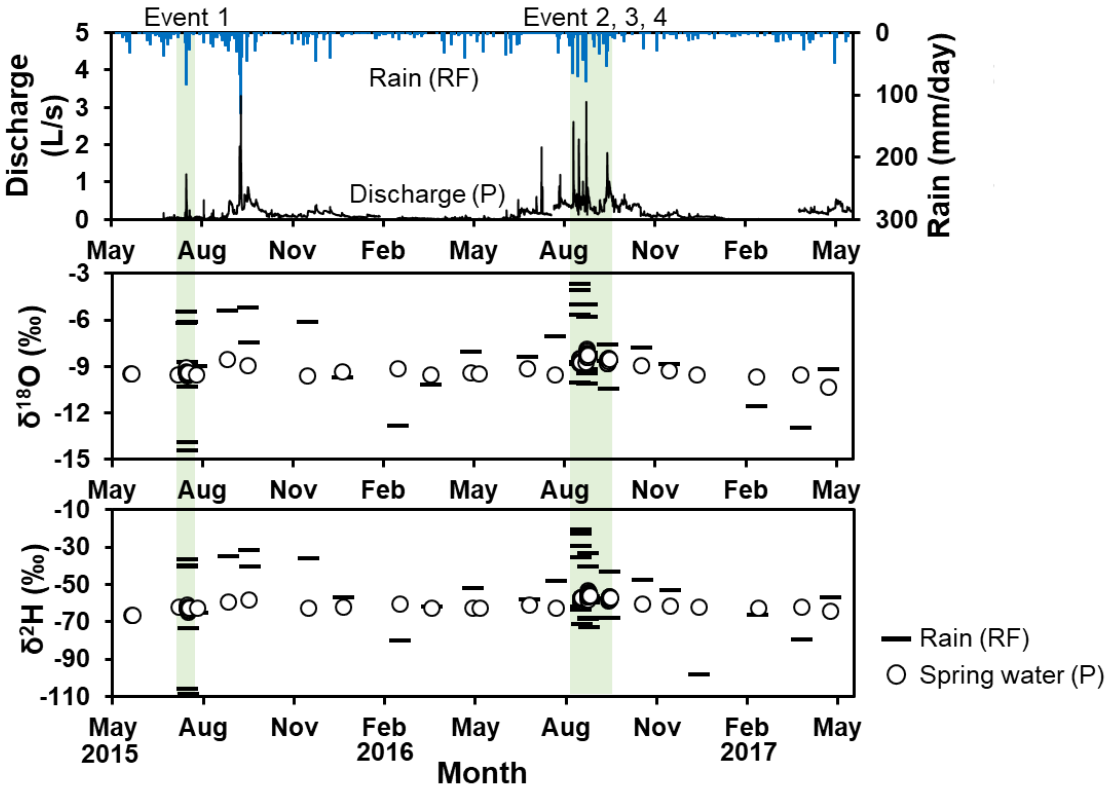

Figure 29. Temporal variations in stable isotopic compositions of oxygen and hydrogen ($\delta^{18}O$, $\delta^{2}H$) in rainwater and spring water collected from May 2015 to May 2017.

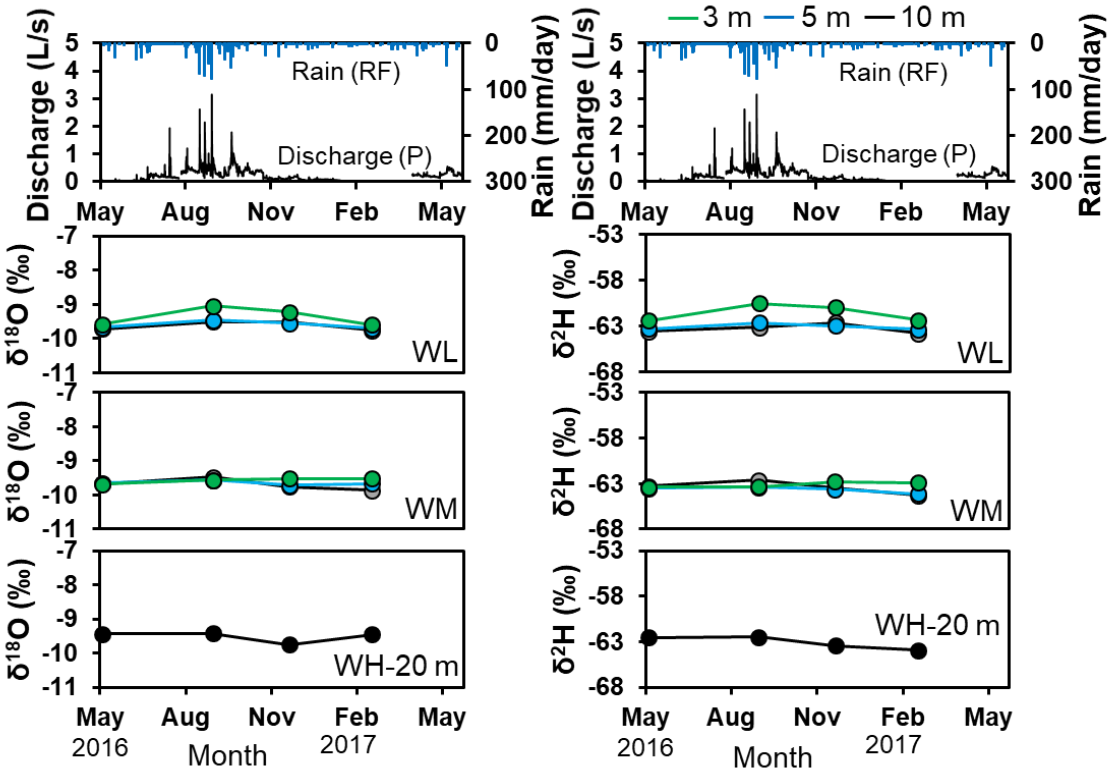

Figure 30. Temporal variations in stable isotopic compositions of oxygen and hydrogen ($\delta^{18}O$, $\delta^{2}H$) in groundwater collected from each borehole.

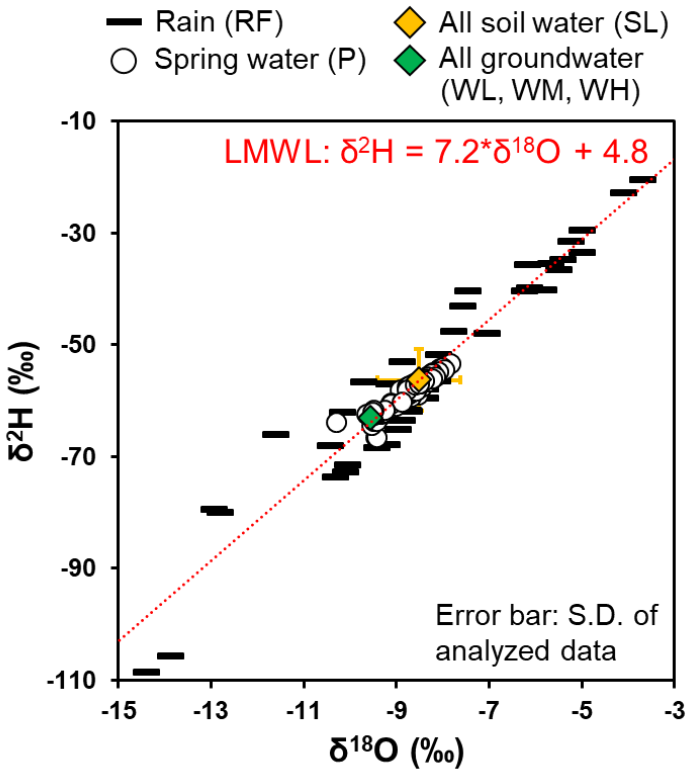

Figure 31. Relation between $\delta^{18}O$ and $\delta^{2}H$ for all collected rain and spring water samples. The average $\delta^{18}O$ and $\delta^{2}H$ of all soil water and groundwater samples with their standard deviations are presented as well. The dotted lines represent the LMWL based on the observed stable isotopic compositions in rainwater during the observation period.

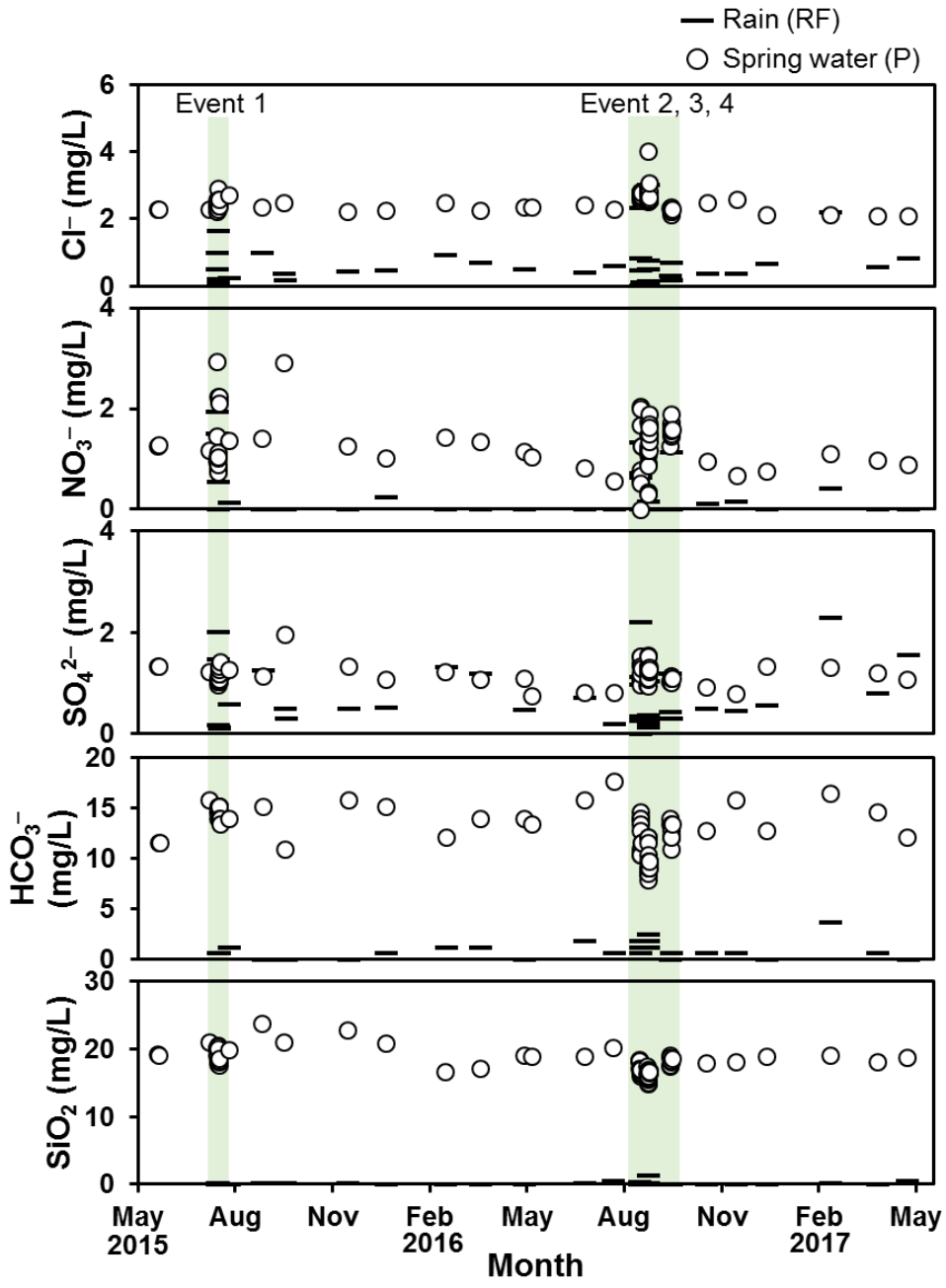

Figure 32. Temporal variations in concentrations of inorganic ions (Cl^-, NO_3^-, SO_4^{2-}, and HCO_3^-) and SiO_2 in rainwater and spring water collected from May 2015 to May 2017.

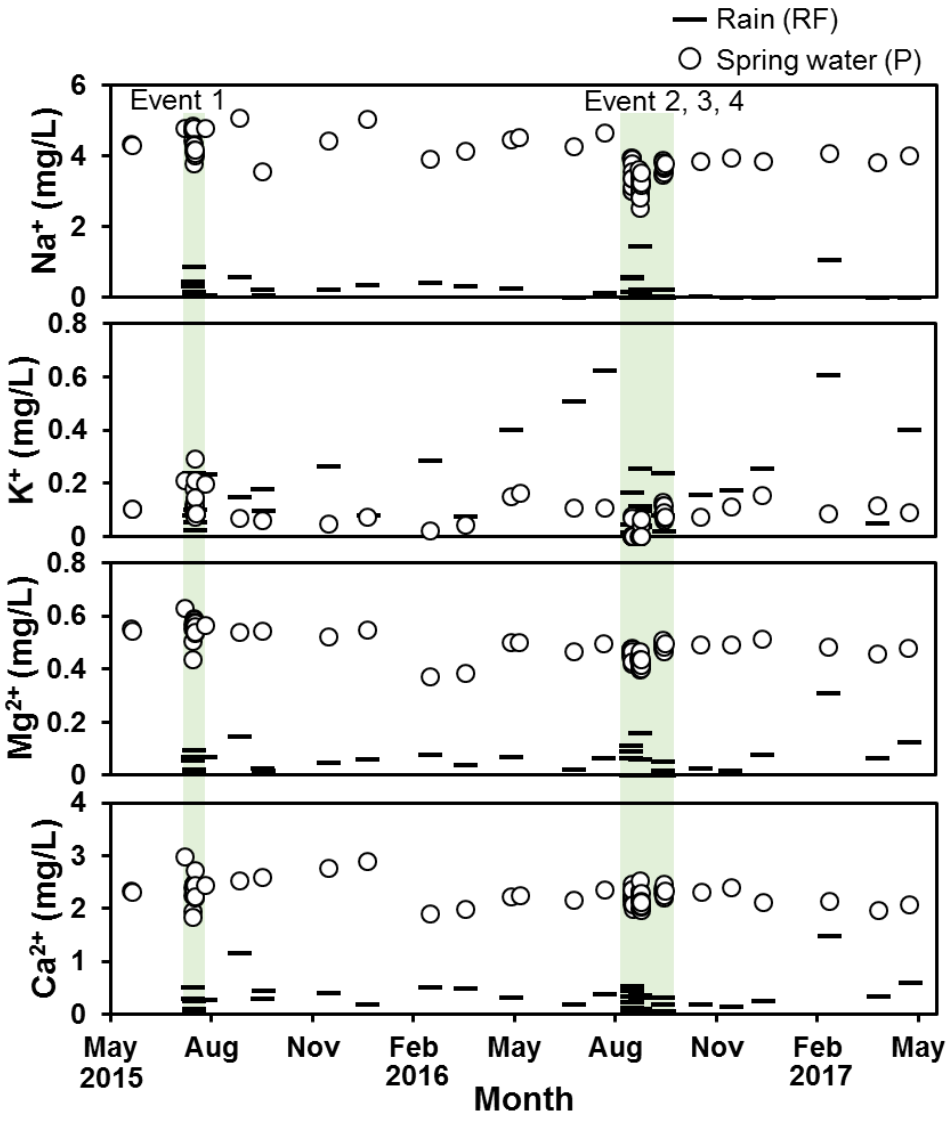

Figure 33. Temporal variations in concentrations of inorganic ions (Na^+, K^+, Mg^{2+}, and Ca^{2+}) in rainwater and spring water collected from May 2015 to May 2017.

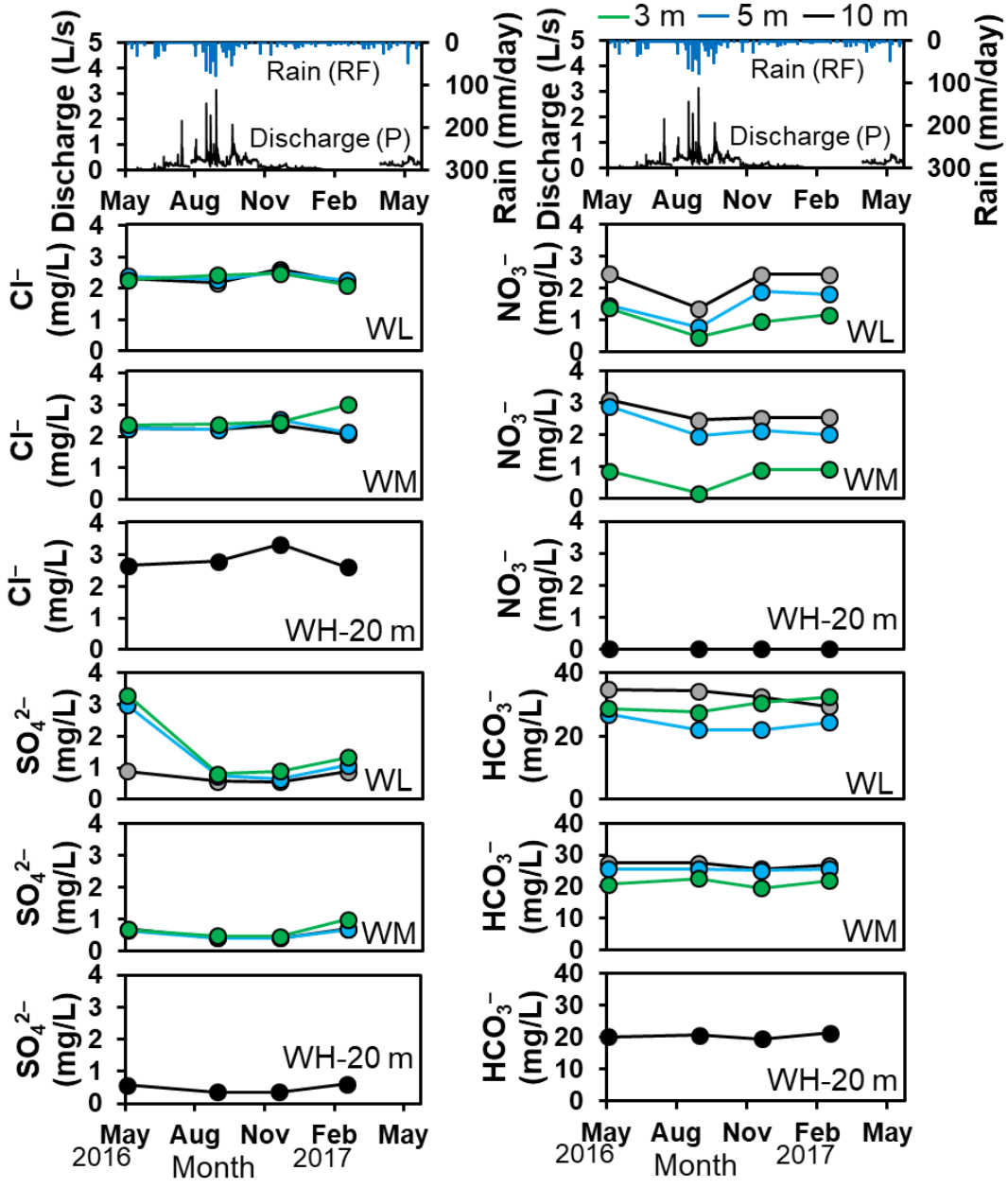

Figure 34. Temporal variations in concentrations of inorganic ions (Cl^-, NO_3^-, SO_4^{2-}, and HCO_3^-) in groundwater collected from each borehole.

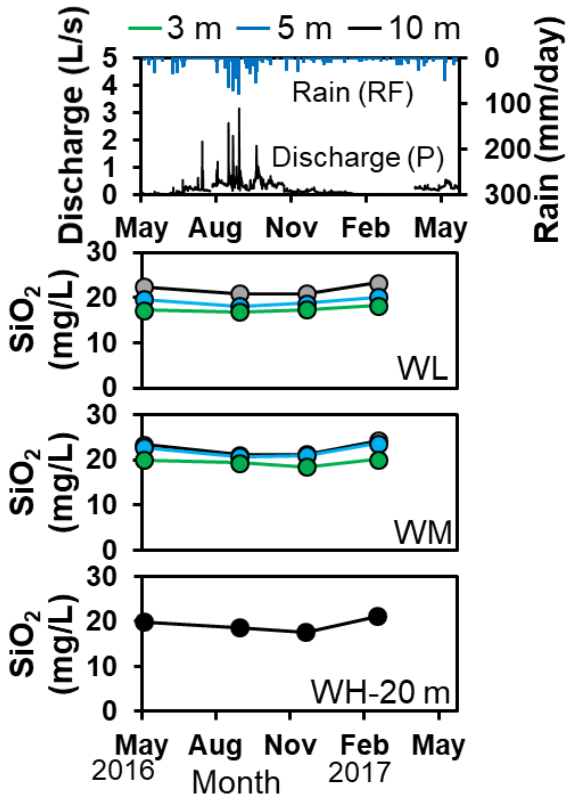

Figure 35. Temporal variations in SiO_2 concentration in groundwater collected from each borehole.

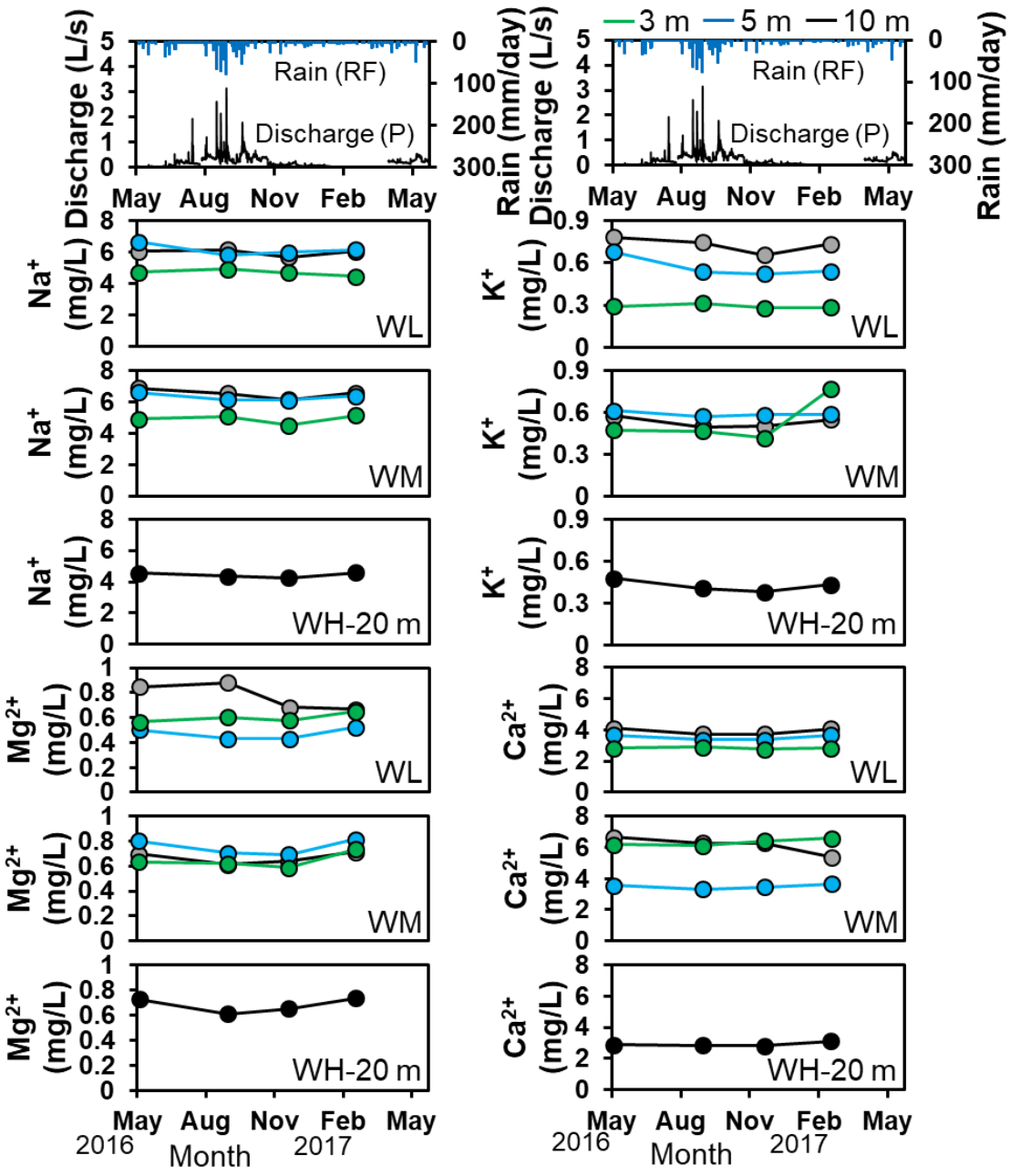

Figure 36. Temporal variations in concentrations of inorganic ions (Na^+, K^+, Mg^{2+}, and Ca^{2+}) in groundwater collected from each borehole.

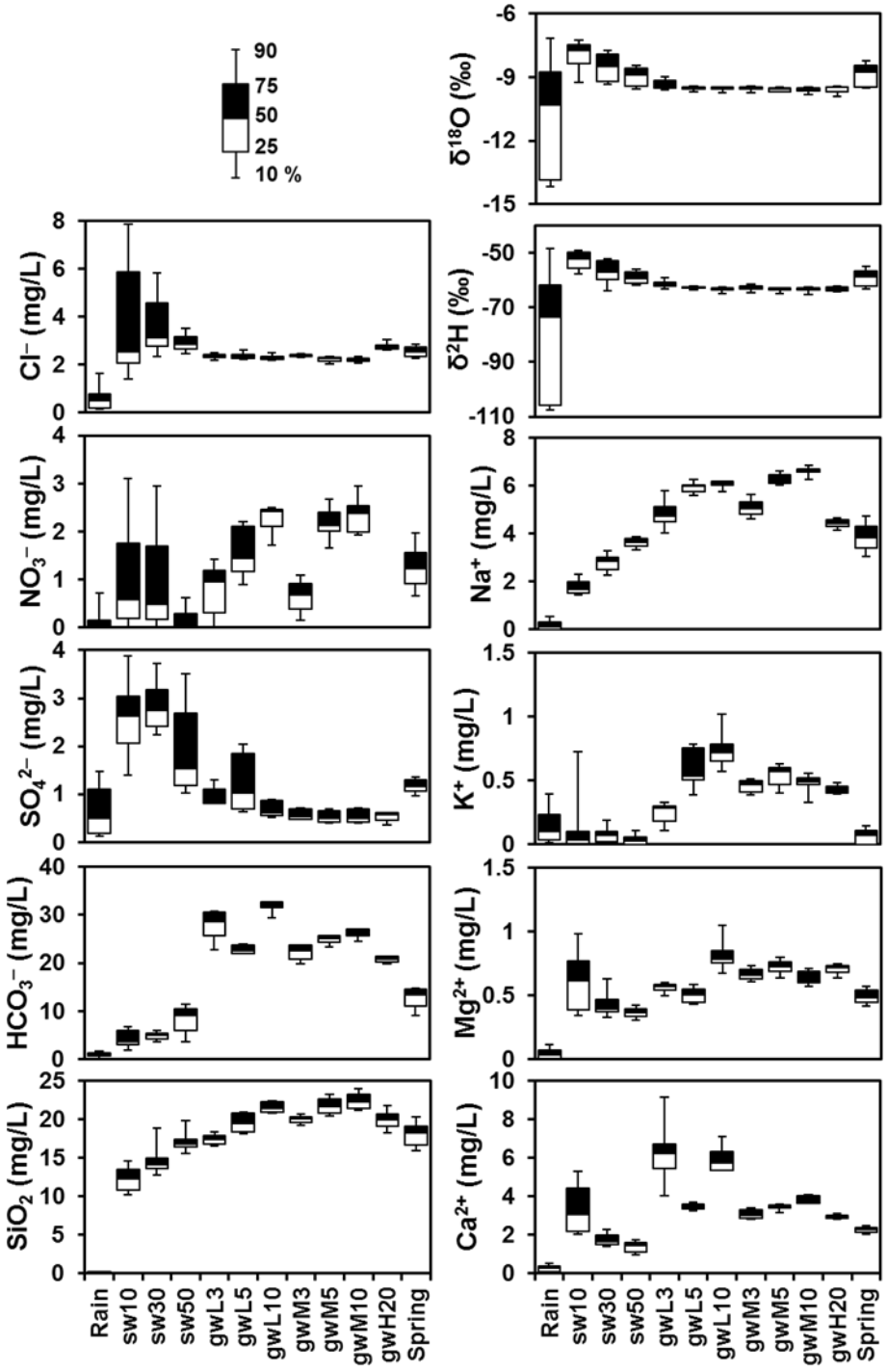

Figure 37. Boxplots of stable isotopic compositions and solute concentrations in all water samples (rainwater, soil water: sw, groundwater: gw, and spring water) collected during the study period.

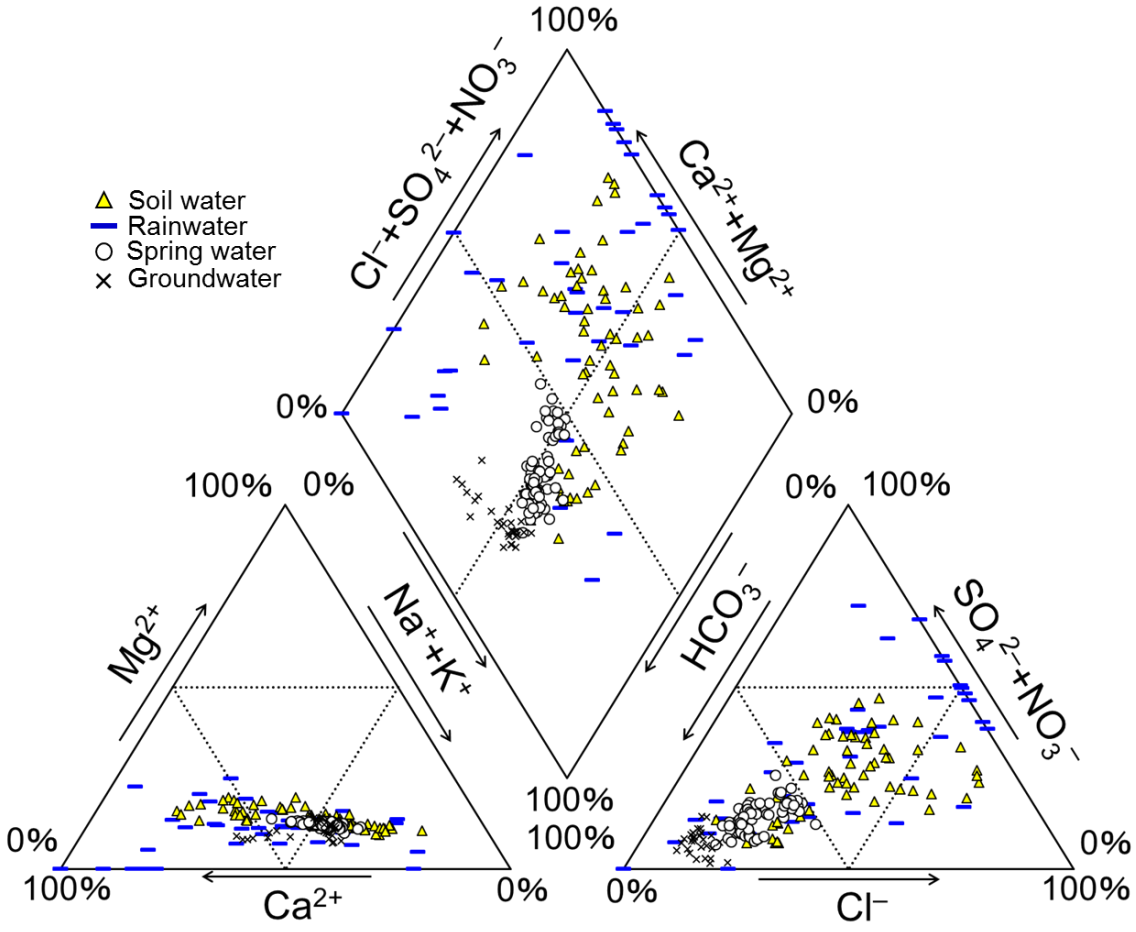

Figure 38. Tri-linear diagram of all water samples collected during the observation period.

4.2 Spatiotemporal variations in water age

Figure 39 shows the temporal variations in observed dissolved SF_6 concentration in spring water under both rainless condition and during rainfall events. The apparent SF_6 age of spring water, which was converted from the dissolved SF_6 concentration in spring water based on the piston flow model, is also presented in the figure. The error bars in Figure 39 reflect the maximum and minimum results using duplicate or triplicate samples.

The observed dissolved SF_6 concentration in spring water under the rainless condition ranges from 3.5–4.6 fmol/L, corresponding to a SF_6 age of 1.8–6.8 years. In contrast, large variations in dissolved SF_6 concentrations in spring water are found in a short period of rainfall. For instance, the SF_6 age of spring water changes from 1.3 to 12.3 years, 9.1 to 11.9 years, and 9.6 to 13.6 years during rainfall events 1, 2, and 3, respectively. In the case of rainfall event 4, the variation in the SF_6 age of spring water is smaller than that during other rainfall events because data from periods only shortly before and after the main rainfall event are available.

The SF_6 concentrations in the groundwater at each borehole are determined four times during the study period: May 2016, August 2016, November 2016, and February 2017. The field observation in August 2016 is carried out shortly after heavy rainfall of 170 mm over five days before the day of sampling. The other field observations are conducted during rainless periods with less than 10 mm of rainfall over five days before the day of sampling. The determined SF_6 concentration with error bars in the groundwater (WL-3 m, 5 m, and 10 m; WM-3 m, 5 m, and 10 m; and WH-20 m) under the rainless condition and shortly after heavy rainfall are shown in Figure 40.

Figure 41 shows the temporal variations in the SF_6 age of groundwater and spring water, while Figure 42 shows the spatial distributions of groundwater and spring water ages determined based on the SF_6 concentration in each field observation with equivalent hydraulic potential lines based on the observed groundwater table level at each borehole. The SF_6 age of

groundwater ranges from <1 year to 8.5 years at WL (valley area), 5.3 years to 13.1 years at WM (boundary between the hill slope and the valley), and 11.1 years to 28.8 years at WH (the ridge area) during the rainless period. Younger groundwater seems to exist in the shallow subsurface area and near the spring discharge point. The groundwater 10 m below the ground surface at the boundary between the hillslope and the valley (WM-10 m) has an older SF_6 age (8.4–13.1 years) compared to the other groundwater samples from the valley. In addition, ridge groundwater from the WH-20 m borehole shows the oldest SF_6 age (11.1–28.8 years) with the lowest SF_6 concentration (1.1–3.1 fmol/L) during the rainless period.

Conversely, the SF_6 age of groundwater varies from 9.2 years to 12.9 years shortly after a heavy rainfall event. The groundwater ages of WM-10 m and WH-20 m are within the range of the groundwater age in the rainless periods, whereas the other groundwater samples (WL-3 m, 5 m, and 10 m; and WM-3 m and 5 m) become older (e.g., groundwater ages at WL-3 m and WM-3 m change to 9.2 and 11.7 years from <1–3.8 years and 5.3–8.1 years, respectively).

The groundwater table levels above the mean sea level at the WL-3 m, WM-3 m, and WH-20 m boreholes are also shown in Figure 42. The red lines in the figure represent the equivalent groundwater age lines with ages of 4, 7, 10, and 13 years. The ridge groundwater samples (WH-20 m) obtained in November 2016 (28.8 years) and February 2017 (26.3 years) show significantly older water ages than any other groundwater samples at those sampling times and in other seasons. Considering the lack of a clear change in the groundwater table level of the WH-20 m groundwater between seasons, it is difficult to explain why the groundwater from the ridge area shows a considerably older age in November 2016 and February 2017. To conveniently explain the variance in ridge groundwater age, additional data, such as spatially dense hydraulic head data of the ridge area, are necessary. Therefore, this topic is part of crucial future work in the study area.

The highlight of Figure 42 is that younger groundwater aged less than 10 years exists in the

shallow subsurface area in the valley region (WL and WM) during rainless periods; however, this groundwater becomes clearly older shortly after heavy rainfall events, where the equivalent groundwater age lines of 4, 7, and 10 years rise to near the ground surface. The variance in the age of spring water in these four observation periods appears to follow that in the age of groundwater. When the valley groundwater near the spring discharge point (e.g., WL-3 m) is young during a rainless period, the spring water is young (2.5–4.9 years) as well. Conversely, when the valley groundwater is older shortly after a heavy rainfall, the spring water, too, is older (9.6 years).

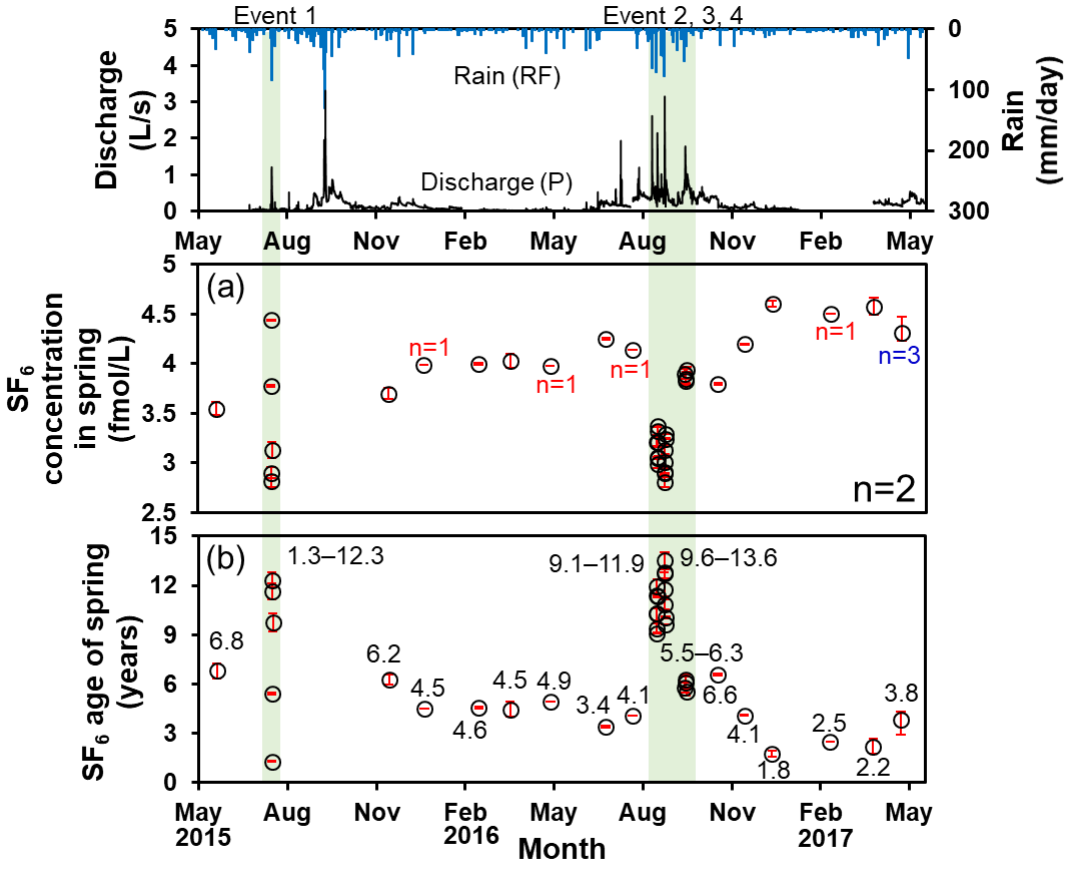

Figure 39. Temporal variations in dissolved SF_6 concentration in spring (a) and apparent SF_6 age of spring (b) both under rainless conditions and during rainfall. The error bars reflect the maximum and minimum results using duplicate or triplicate water samples.

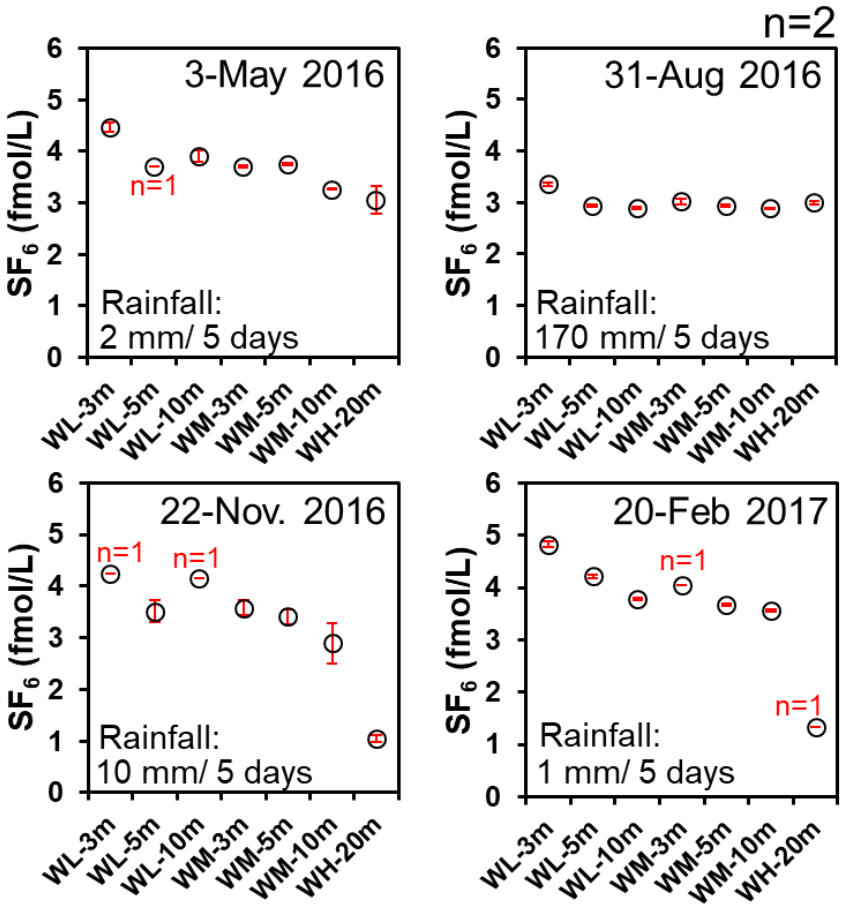

Figure 40. Determined SF_6 concentration with error bars of groundwater (WL-3 m, 5 m, and 10 m; WM-3 m, 5 m, and 10 m; and WH-20 m) under rainless condition and shortly after heavy rainfall. The error bars reflect the maximum and minimum results obtained using duplicate water samples.

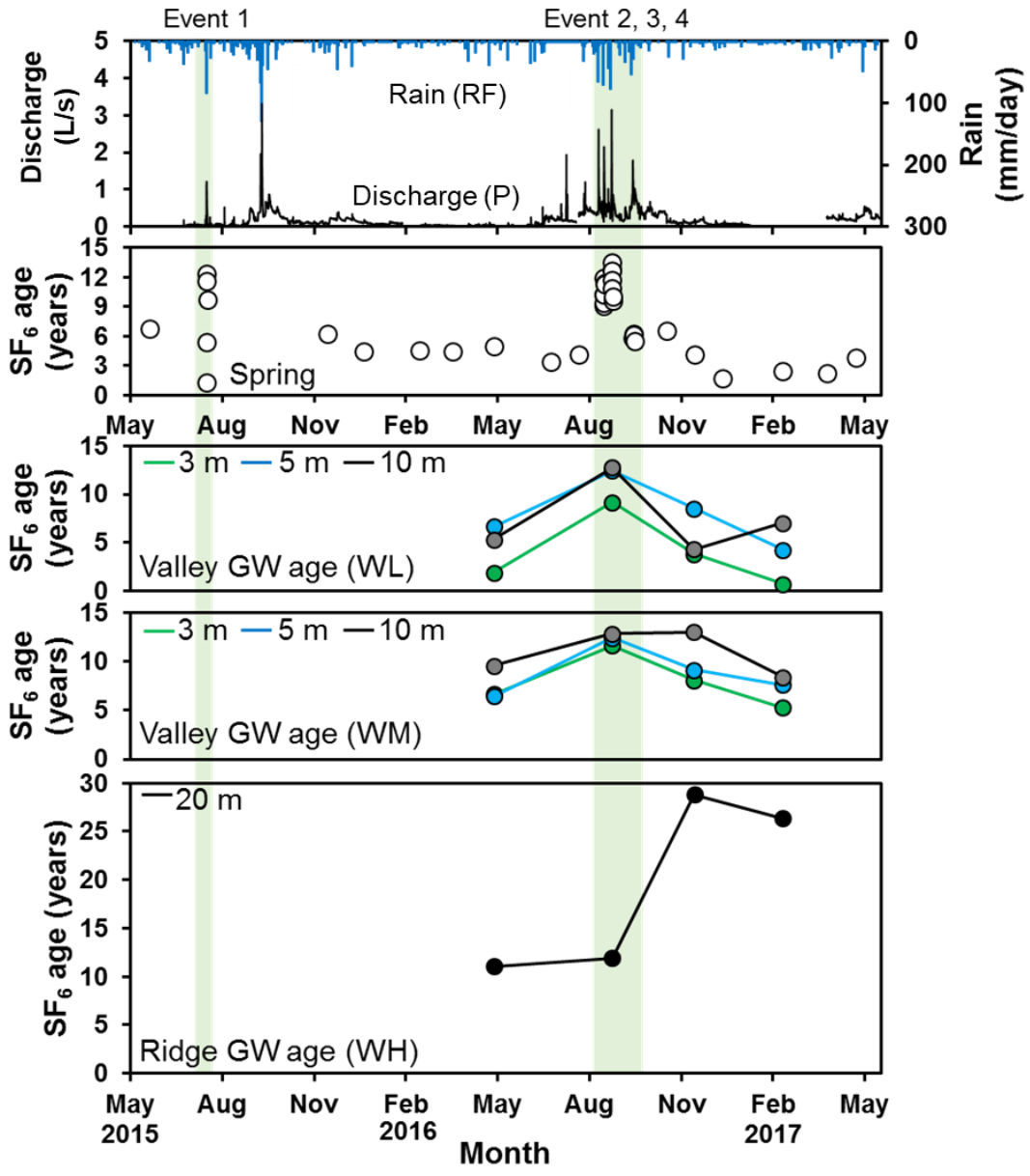

Figure 41. Temporal variation in SF_6 age of groundwater and spring water.

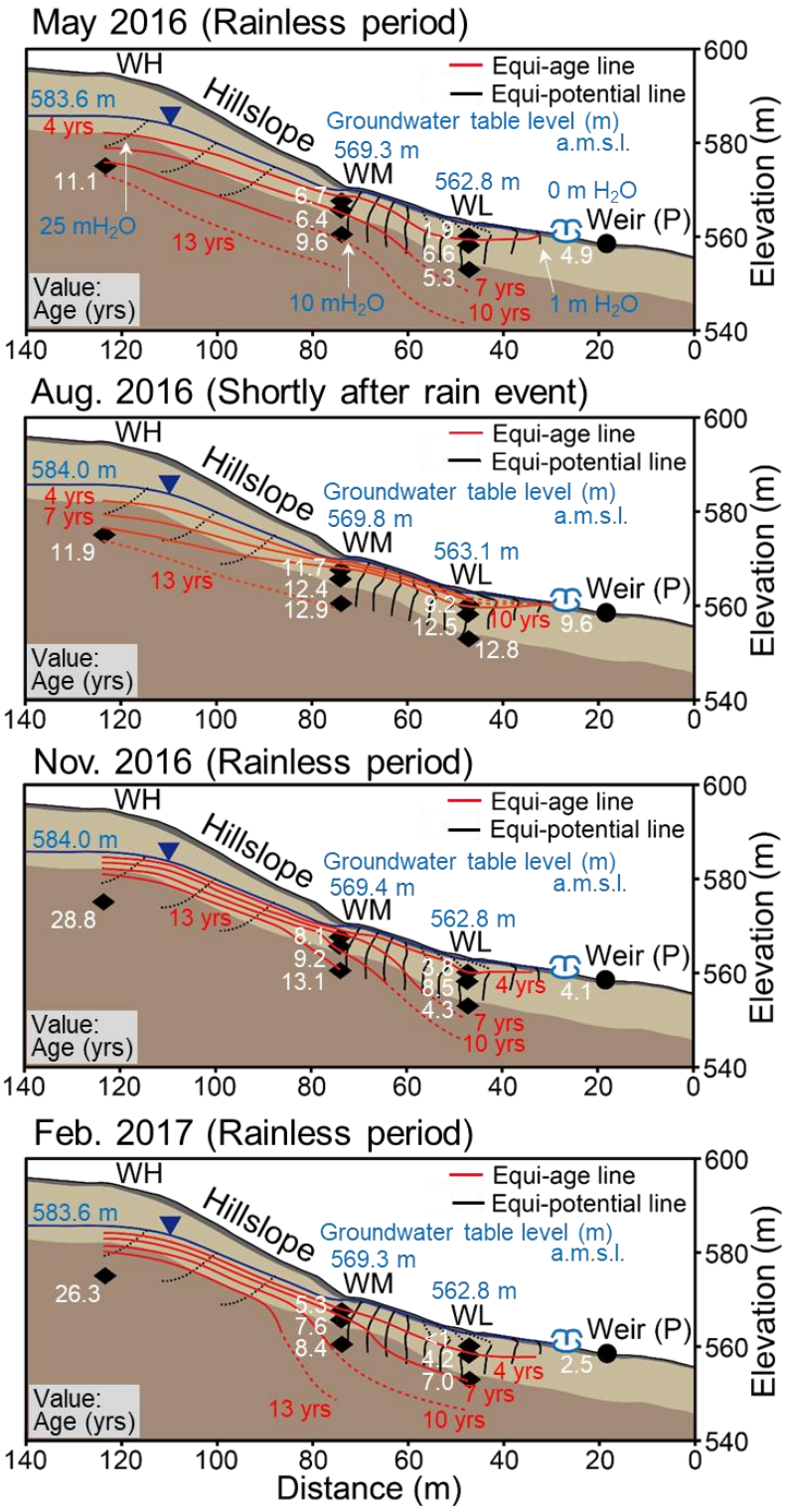

Figure 42. Spatial distribution of SF_6 age of spring water and groundwater at each borehole with equivalent age lines of 4, 7, 10, and 13 years for rainless periods (May 2016, November 2016, and February 2016) and after heavy rainfall (August 2016).

4.3 Hydrological characteristics and water age variations during rainstorm

Figure 43 plots the events with rainfall exceeding 10 mm/day and indicates the relation between the rain conditions and peak spring discharge. The rain conditions are given as an index: the sum of an antecedent precipitation index over 30 days, which is API (30), and the total rainfall until peak discharge for each rainfall event. API (30) is defined as follows:

$$\text{API (30)} = \sum_{i=1}^{30} \frac{P_i}{i} \tag{4}$$

where i is the day count and P_i is the daily precipitation on i days (Iwagami et al., 2010).

The peak spring discharge clearly increases with the rain condition index. However, rainfall events with an index reflecting less than 70 mm of rainfall cause low peak discharge, which means that the rainfall events do not contribute to the high-rate spring discharge phenomenon. The four observed rainfall events are also shown in Figure 43. They are characterized by a large peak discharge volume of more than 1 L/s, although most rainfall events cause small peak discharge of less than 0.5 L/s. Therefore, the four observed rainfall events are characteristic events in the study area.

Figures 44 and 45 show variations in the discharge volume, SF_6 age of the spring, and groundwater table level (WL, WM, and WH) for the following three rainfall events: event 1, July 15–17, 2015; event 2, August 22–24, 2016; and event 3, August 29–31, 2016. SF_6 data on spring water during the peak discharge phase in another rainfall event are inadequate; hence, they have been eliminated from further analysis in this study. The age of spring water ranges from 1.3 to 12.3 years for event 1, from 9.1 to 11.9 years for event 2, and from 9.6 to 13.6 years for event 3. The youngest SF_6 age of the spring (1.3 years) is observed before the rainfall and discharge peaks during rainfall event 1, but it is not observed before the rainfall and discharge peaks during rainfall events 2 and 3. The oldest SF_6 age of the spring (12.3 years for event 1, 11.9 years for event 2, and 13.6 years for event 3) is detected at the rainfall peak and shortly

before the discharge peak in the three rainfall events. Additionally, the spring water maintains an older SF_6 age (~10 years), which is several years older than the SF_6 age of the spring water under rainless conditions during the hydrograph recession phase of rainfall events.

The groundwater table level (WL-3 m, 5 m, and 10 m; WM-3 m, 5 m, and 10 m) along the valley line clearly increases with the discharge volume, as shown in Figure 45. The groundwater table level of each borehole decreases gradually after the peak discharge, although the rates of decrease in the groundwater table level differ across boreholes and events. Additionally, the groundwater table level of the ridge groundwater (WH-20 m) increases slowly during rainfall and after rainfall, which is clearly different from the responses of other observation wells to rainfall input. The initial groundwater table levels of the observation wells during rainfall events 2 and 3 are higher than those during rainfall event 1 (e.g., WL-3 m and WH-20 m; the initial groundwater table level during rainfall event 3 is ~0.3 m higher than that during rainfall event 1; Figure 45). This seems to be due to the difference in the antecedent precipitation amount; the total 7-day antecedent rainfall for events 1, 2, and 3 is 10 mm/7 days, 97 mm/7 days, and 121 mm/7 days, respectively.

Figures 46–48 show temporal variations in the stable isotopic compositions of ($\delta^{18}O$, $\delta^{2}H$) and solute concentrations (Cl^-, NO_3^-, SO_4^{2-}, HCO_3^-, Na^+, K^+, Ca^{2+}, Mg^{2+}, and SiO_2) in rainwater and spring water during the three observed rainfall events. Figures 49–51 present the hydro-hyetograph of the spring, including SF_6 age and selected tracer variations ($\delta^{2}H$, Cl^-, Na^+, and SiO_2) in the spring water and rainwater, in the three rainstorm events (events 1, 2, and 3). The boxplots of the selected tracers ($\delta^{2}H$, Cl^-, Na^+, and SiO_2) based on the tracer data of all collected water samples are also shown in Figures 49–51. The $\delta^{2}H$ of rainwater ranges from –109‰ to –40‰ for event 1,–71‰ to –21‰ for event 2, and–73‰ to –34‰ for event 3. However, that of spring water does not change much, ranging –64‰ to –62‰ for event 1, –59‰ to –57‰ for event 2, and –57‰ to –53‰ for event 3. The Cl^- concentration in spring

water is mostly between 2.2 and 2.6 mg/L during event 1 and between 2.5 and 3.1 mg/L during event 3, while that in spring water sharply increases at the rainfall peak and before the hydrograph peak (2.9 mg/L for event 1 and 4.0 mg/L for event 3). The Cl^- concentration in spring water during event 2 remains almost stable throughout the event, ranging between 2.5 and 2.8 mg/L. The Na^+ and SiO_2 concentrations in rainwater are lower than those in soil and spring water in events 1, 2, and 3. The Na^+ and SiO_2 levels in the spring water decrease by 0.5 and 1.5 mg/L, respectively, under peak rainfall and before the hydrograph peak, almost concurrent to the detection of high Cl^- concentrations in spring water. During the hydrograph peak and recession phases, the spring water maintains lower levels of Na^+ and SiO_2.

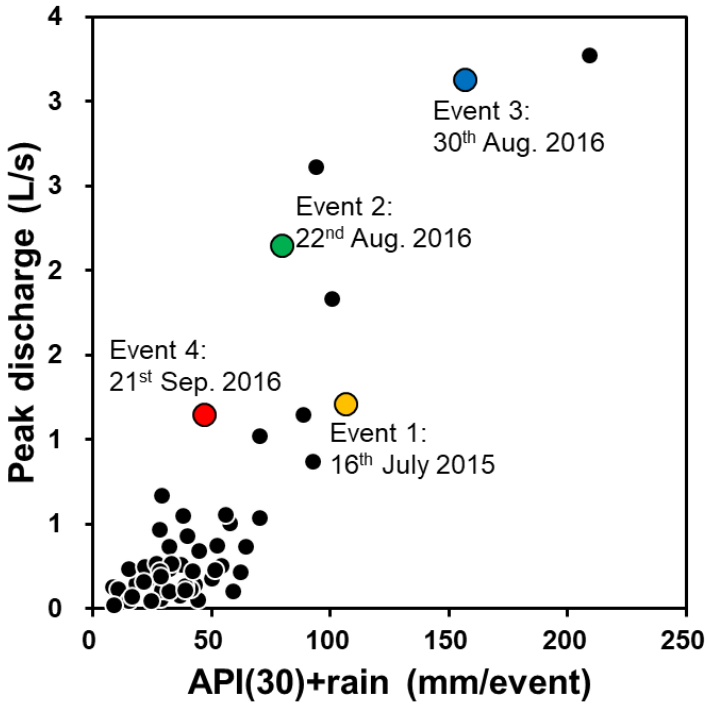

Figure 43. Relation between peak spring discharge for each rainfall event and rain condition. The rain condition is given by the total rainfall amount before the peak spring discharge and the antecedent precipitation (API 30). API: Antecedent Precipitation Index.

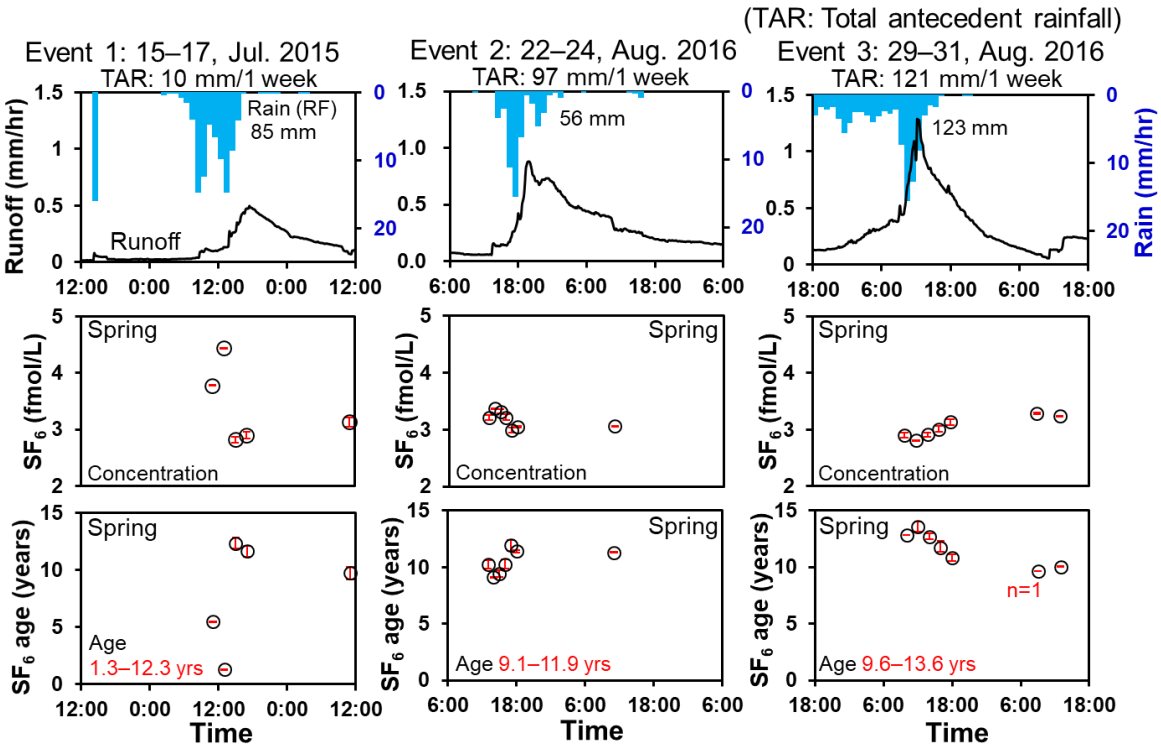

Figure 44. Temporal variations in dissolved SF_6 concentration in spring water and SF_6 age of spring water with hydro-hyetograph during rainfall events: event 1, July 15–17, 2015; event 2, August 22–24, 2016; and event 3, August 29–31, 2016. The error bars reflect the maximum and minimum results using duplicate water samples.

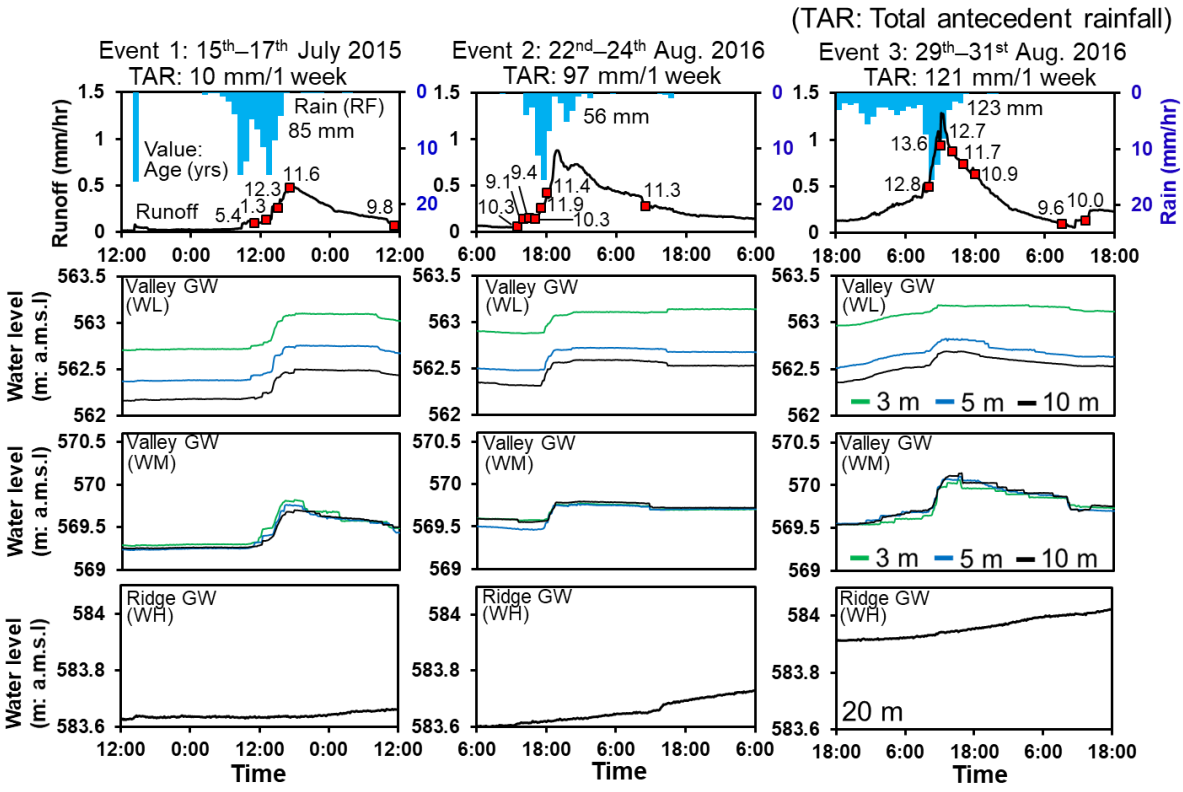

Figure 45. Temporal variations in spring discharge, SF_6 age of spring, and groundwater table level (WL, WM, and WH) during rainfall events: event 1, July 15–17, 2015; event 2, August 22–24, 2016; and event 3, August 29–31, 2016.

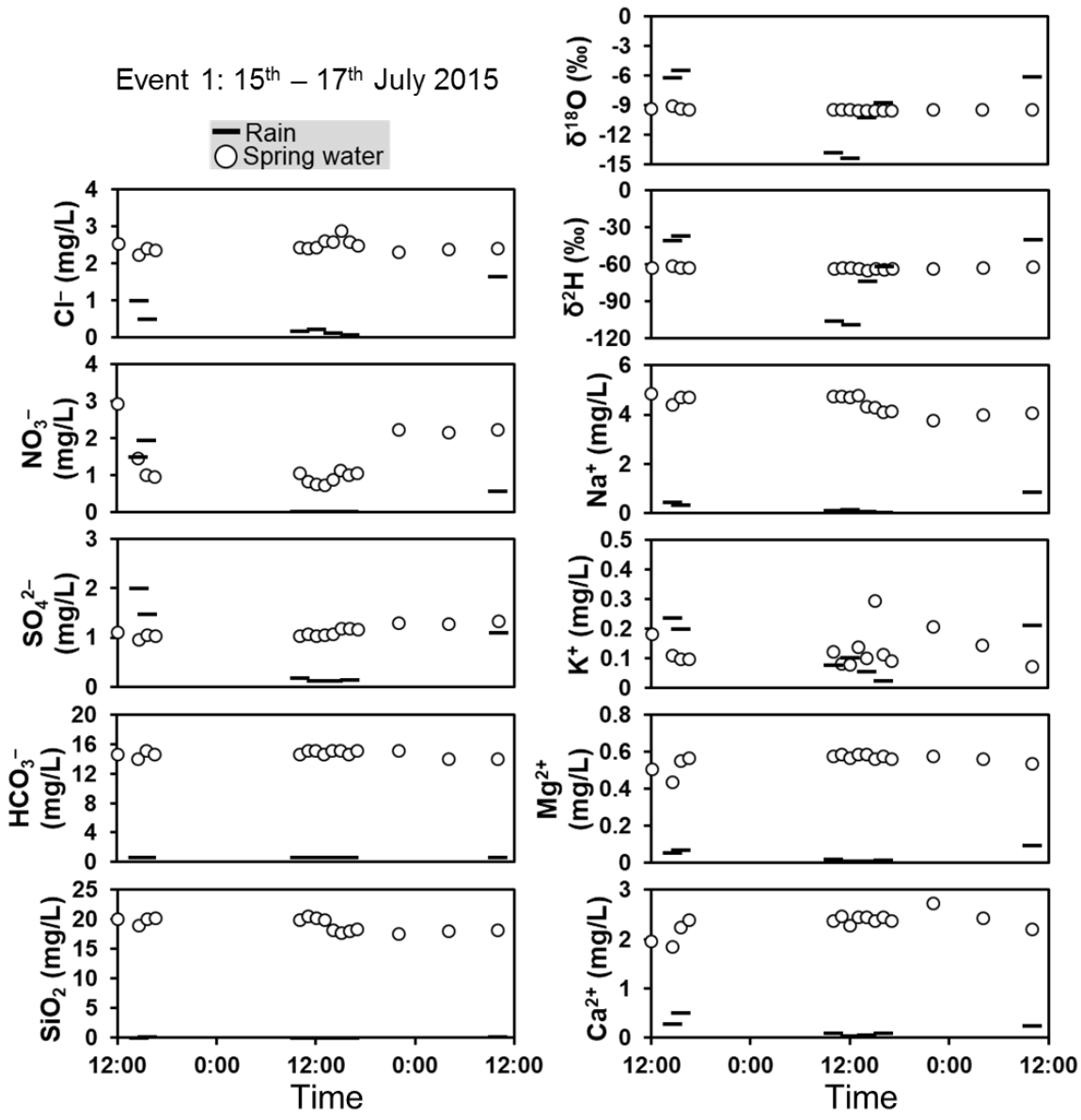

Figure 46. Temporal variations in stable isotopic compositions ($\delta^{18}O$ and $\delta^{2}H$) and solute concentrations (Cl^-, NO_3^-, SO_4^{2-}, HCO_3^-, Na^+, K^+, Mg^{2+}, Ca^{2+}, and SiO_2) in rainwater and spring water during rainfall event 1 (July 15–17, 2015).

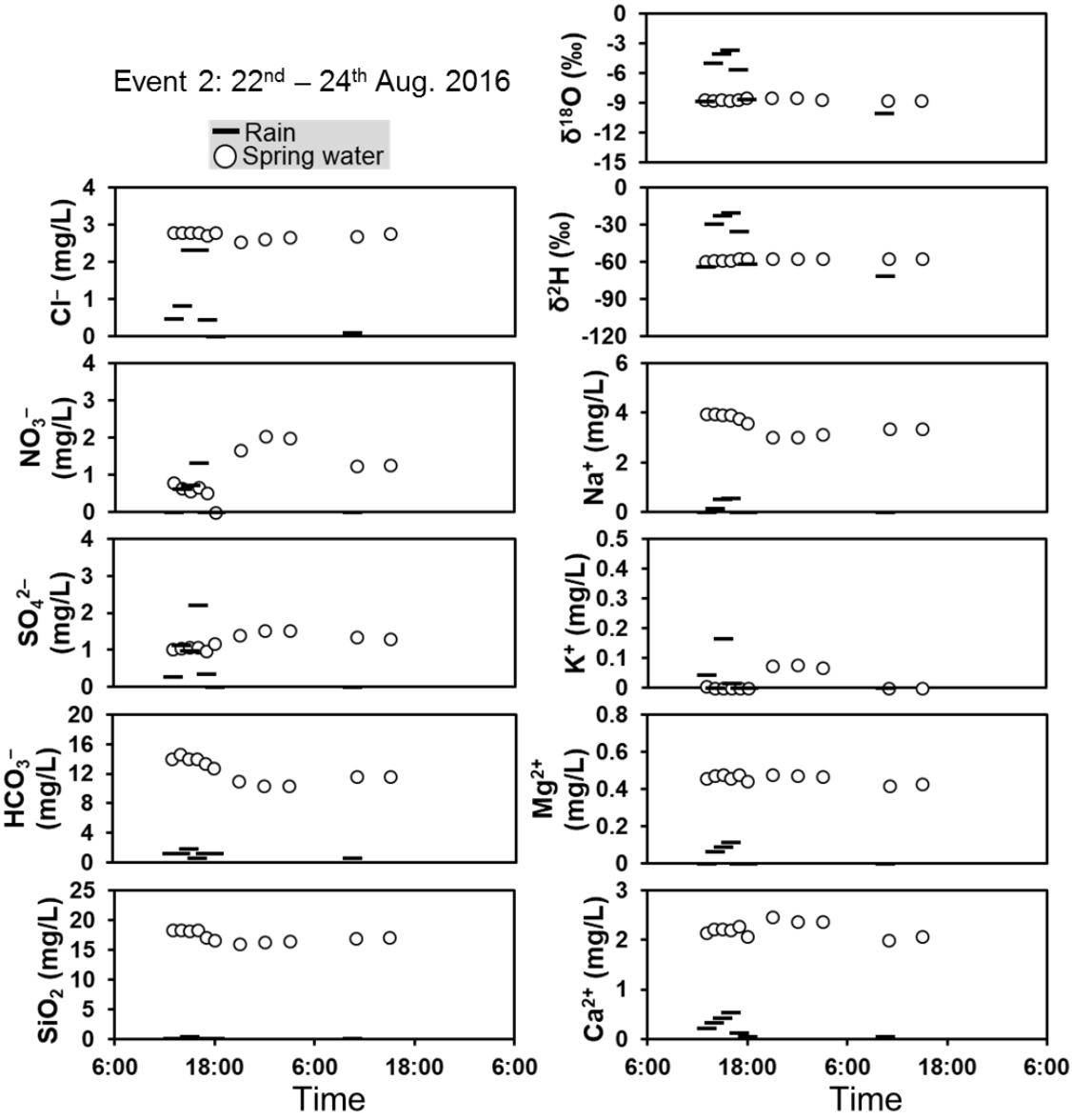

Figure 47. Temporal variations in stable isotopic compositions ($\delta^{18}O$ and $\delta^{2}H$) and solute concentrations (Cl^-, NO_3^-, SO_4^{2-}, HCO_3^-, Na^+, K^+, Mg^{2+}, Ca^{2+}, and SiO_2) in rainwater and spring water during rainfall event 2 (August 22–24, 2016).

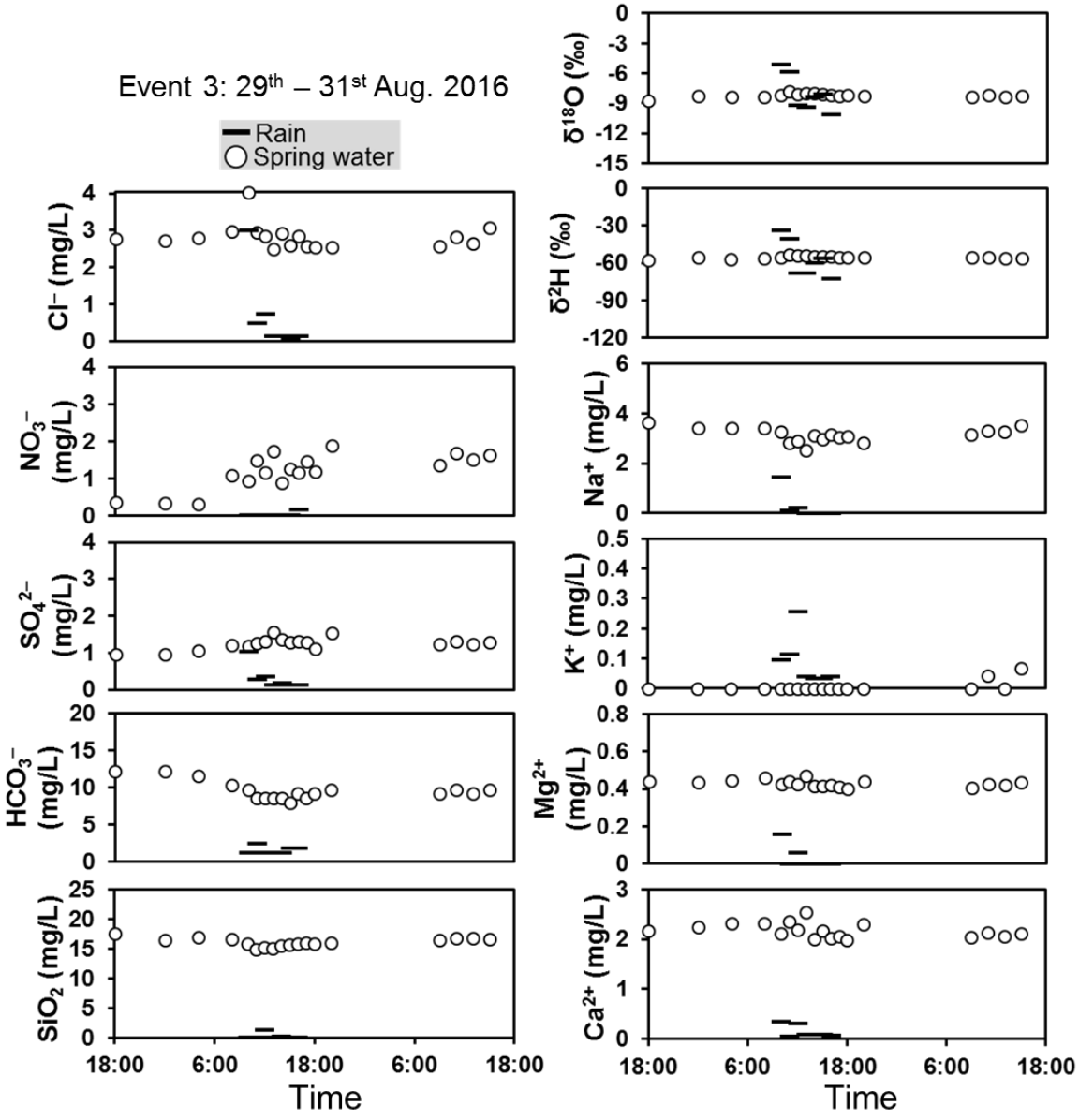

Figure 48. Temporal variations in stable isotopic compositions ($\delta^{18}O$, $\delta^{2}H$) and solute concentrations (Cl^-, NO_3^-, SO_4^{2-}, HCO_3^-, Na^+, K^+, Mg^{2+}, Ca^{2+}, and SiO_2) in rainwater and spring water during rainfall event 3 (August 29–31, 2016).

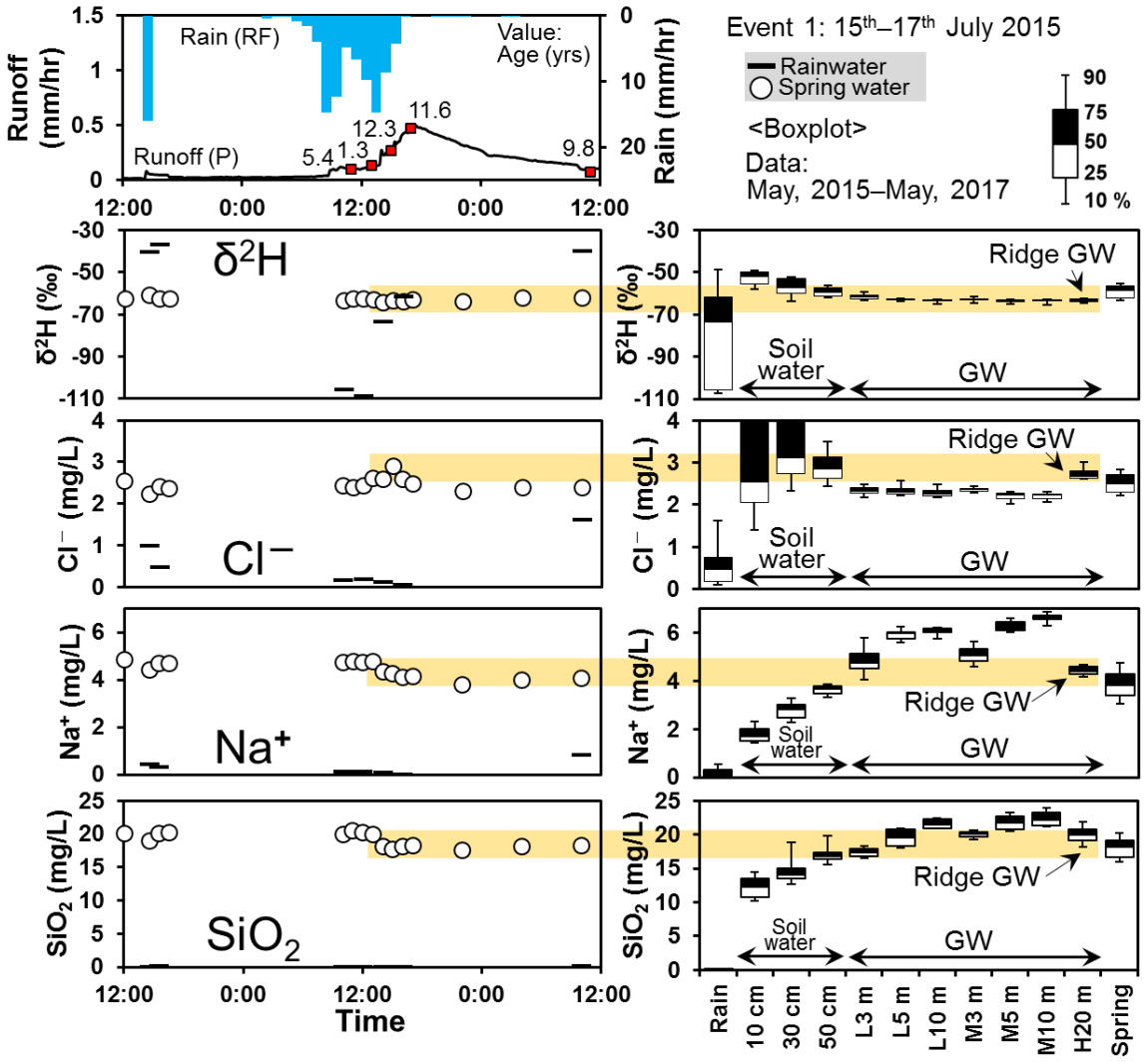

Figure 49. Temporal variations in SF_6 age of spring water with hydro-hyetograph and temporal variations in δ^2H, Cl^-, Na^+, and SiO_2 in spring water and rainwater during rainfall event 1 (July 15–17, 2015). The panels on the right show boxplots of relevant tracers for all water samples (rainwater, soil water, groundwater, and spring water) collected during the study period.

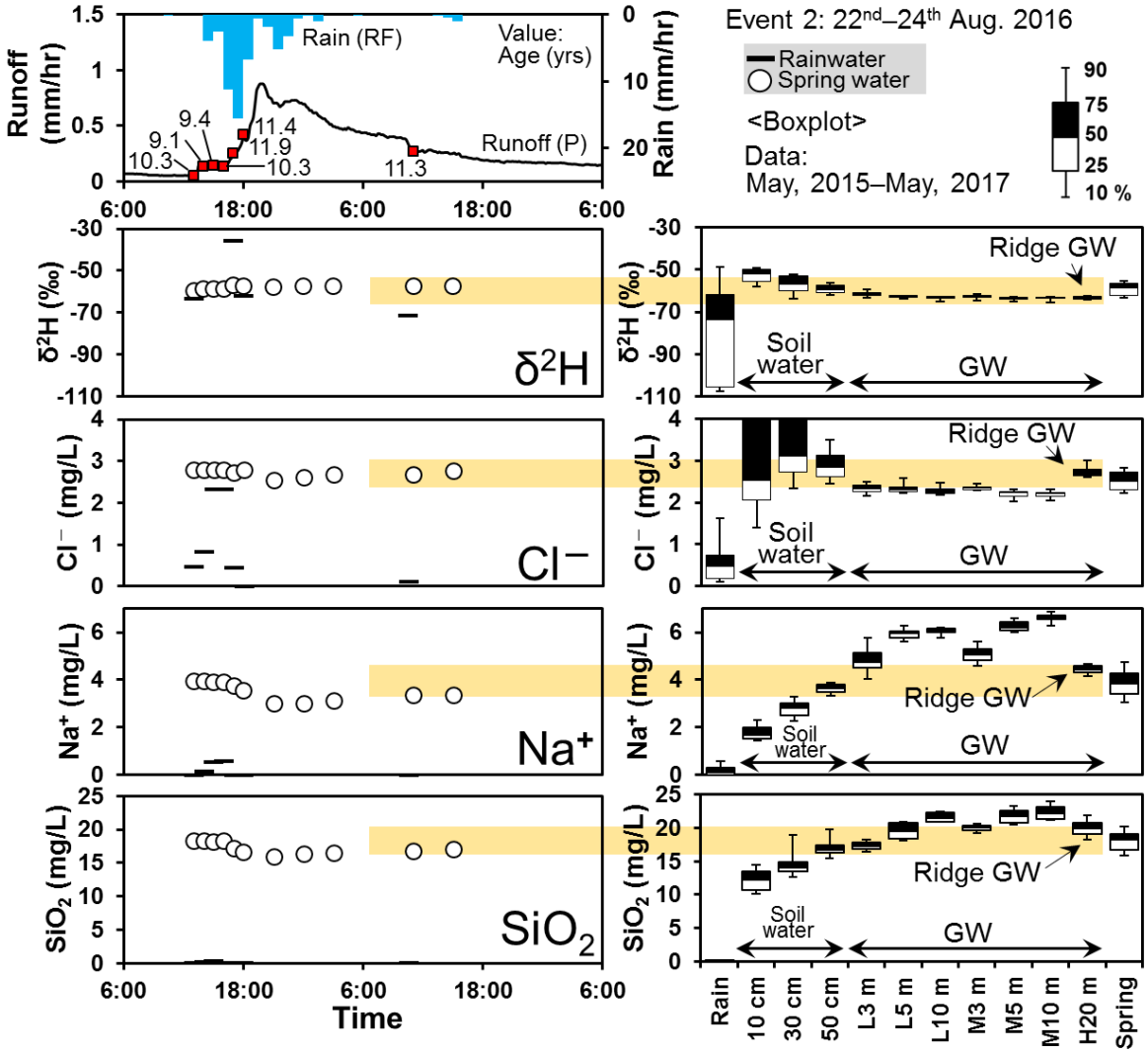

Figure 50. Temporal variations in SF_6 age of spring water with hydro-hyetograph and temporal variations in δ^2H, Cl^-, Na^+, and SiO_2 in spring water and rainwater during rainfall event 2 (August 22–24, 2016). The panels on the right show boxplots of relevant tracers for all water samples (rainwater, soil water, groundwater, and spring water) collected during the study period.

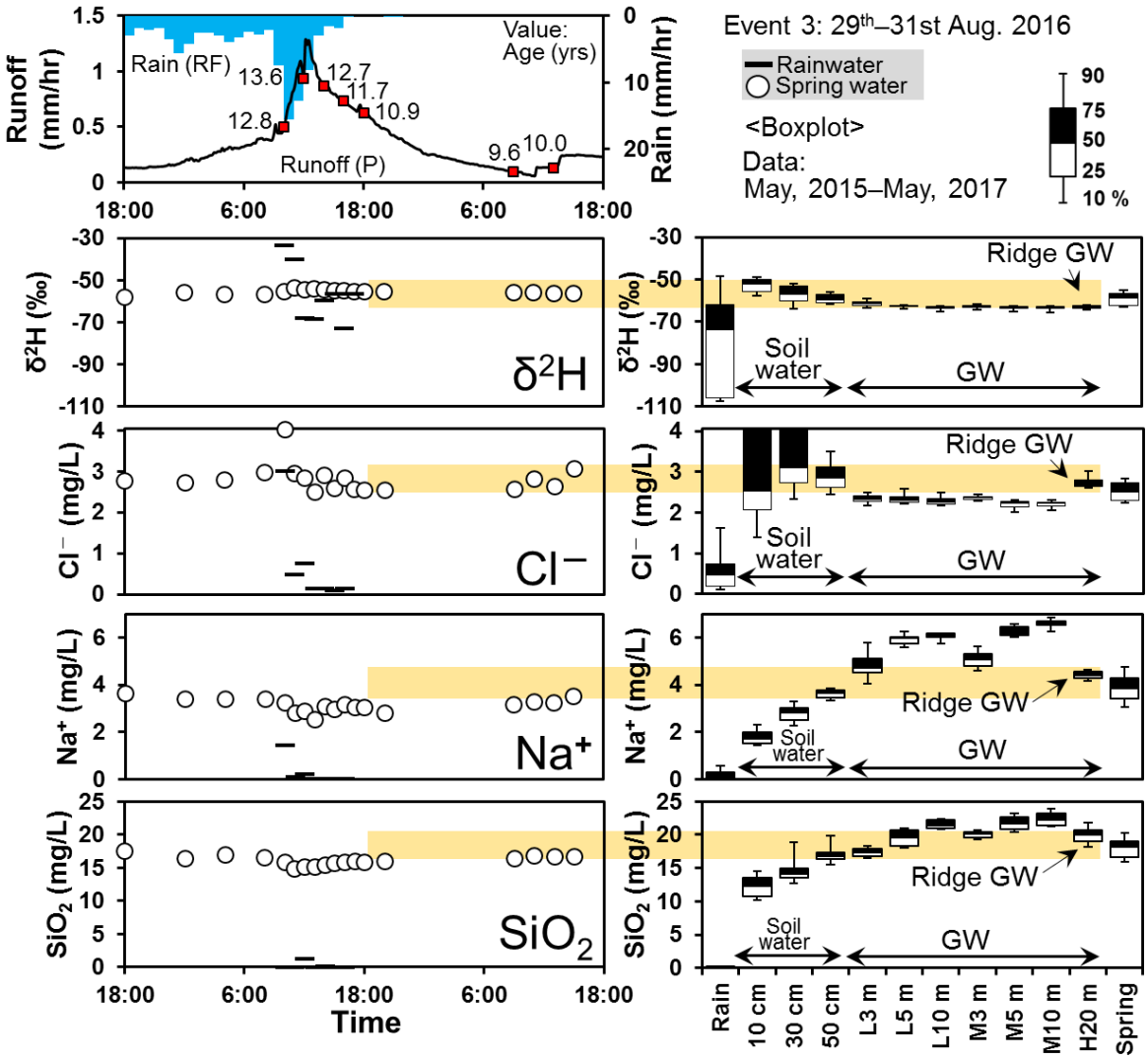

Figure 51. Temporal variations in SF_6 age of spring water with hydro-hyetograph and temporal variations in δ^2H, Cl^-, Na^+, and SiO_2 in spring water and rainwater during rainfall event 3 (August 29–31, 2016). The panels on the right show boxplots of relevant tracers for all water samples (rainwater, soil water, groundwater, and spring water) collected during the study period.

CHAPTER 5 DISCUSSION

5.1 Discharge process during rainless periods

Figure 52 shows the relation between the age and discharge volume of spring water. Each plot represents the collected spring water samples in the rainless periods and during the three rainfall events. The trends between the spring water in the rainless periods and during the rainfall events appear to be opposite. The spring age might decrease as the discharge volume increases in the rainless periods, whereas the spring age clearly increases with the discharge volume during rainstorms. This indicates different hydrological processes under the rainless condition and during rainfall events.

The dotted line in Figure 52 indicates the regression line of spring water in the rainless periods. The correlation coefficient of this regression line has a slightly high negative value; however, the spring water in October 2016 appears to be plotted off from this regression line. This may be because of a large antecedent precipitation with a volume of 660 mm in August and September 2016 before the sampling date (October 2016). The negative correlation between spring age and discharge volume over the long term has been reported in previous studies (e.g., Busenberg and Plummer, 2014). Busenberg and Plummer (2014) analyzed the relations among the amount of seasonal rainfall, discharge volume, and age of spring water, and inferred that the age of spring water decreases as the discharge volume increases after a rainy season. In other words, new water (rainwater) largely recharges the shallow groundwater contributing to spring water, which results in a larger discharge volume and decreased age of spring water. The rainy season in the study area is not clear; however, larger amounts of rainfall generally occur after the summer due to typhoons. In this context, the November and February cases of the spatial distribution of the water age in Figure 42 correspond to the post-heavy rainfall season cases in the previous studies. The ages of both spring water and shallow

groundwater (WL-3 m) in the valley area are similar or younger than their corresponding ages in May 2016. This result indicates that the age of spring water decreases owing to the large amount of groundwater recharge by rainfall in the typhoon season; this is supported by previous studies (Busenberg and Plummer, 2014). This is why spring water age and discharge volume are negatively correlated, as shown in Figure 52. From this interpretation, water discharge processes during rainless periods appear to be controlled by shallow subsurface water and amount of rainfall.

Figure 53 shows the relations between spring water age both in rainless periods and during rainfall events and groundwater table levels in each observation borehole. Focusing on the rainless condition, the groundwater table levels of valley groundwater (WL-3 m, 5 m, 10 m and WM-3 m, 5 m, 10 m) are not clearly related to water age; regardless of the spring water age under the rainless condition, groundwater table levels of valley groundwater remain nearly stable. In contrast, in the case of ridge groundwater, there appears to be a clear correlation between spring water age and ridge groundwater table level; as the age of spring water increases, ridge groundwater table level increases. In other words, when the spring water under the rainless conditions is older, the hydraulic potential gradient between the ridge and valley areas is high compared to that during the period of discharge of spring water under the rainless condition. Considering the older groundwater age of ridge groundwater (Figure 42) and the hydraulic gradient between the ridge and valley areas, a part of the older ridge groundwater seems to contribute to spring discharge, resulting in an increase in the age of spring water.

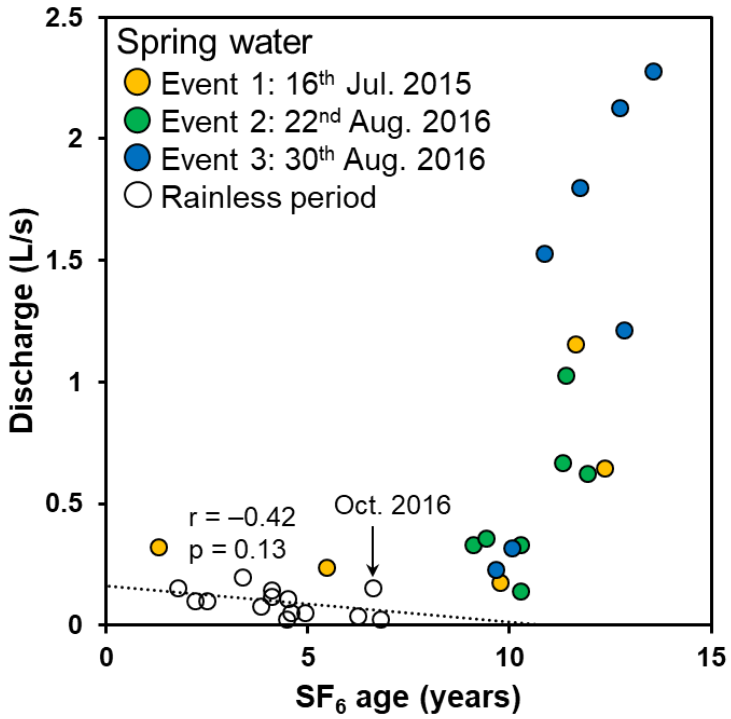

Figure 52. Relation between spring water age and spring discharge volume. Each plot represents the spring water sample collected during rainless periods and during the three rainfall events.

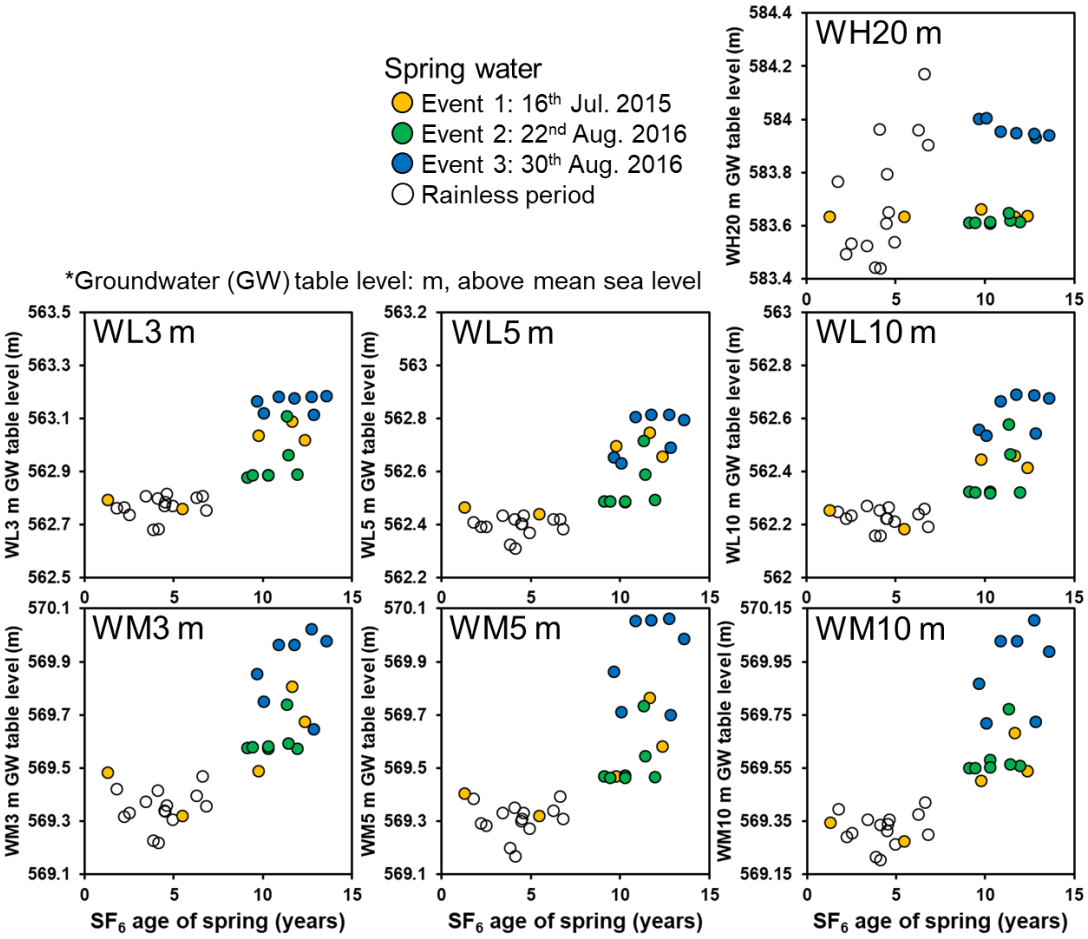

Figure 53. Relations between spring water age both in rainless periods and during rainfall events and groundwater table levels in each observation borehole.

5.2 Factors controlling the age of discharge water during rainstorms

Large variations in spring age are observed during rainstorms (e.g., event 1, 1.3–12.3 years; event 2, 9.1–11.9; event 3, 9.6–13.6 years; Figures 39 and 52). Especially, very young spring water (1.3 years) is only observed shortly before the rainfall peak during event 1 (not observed for events 2 and 3). The young spring water of event 1 immediately becomes older (12.3 years) at the rainfall peak; hence, most SF_6 ages of the spring during rainstorms (events 1, 2, and 3) are much older than those during the rainless periods; the spring maintains older SF_6 ages, even after the rainfall and in the hydrograph recession phase. Two major points are discussed in this study: "why does the age of spring water change within a short period" and "why are the ages of most spring waters during rainstorm clearly older than their ages during the rainless period"?

First, focusing on the effect of rainwater on spring water, the δ^2H of spring water does not change much throughout each rainfall event, despite the large differences in δ^2H of rainwater (Figures 49–51). Especially, the maximum differences between δ^2H of the spring water and rainwater during events 1, 2, and 3 are 47‰, 38‰, and 23‰, respectively, observed around the rainfall peak. These results indicate that rainwater does not largely or promptly affect spring water (rainfall–runoff water) in the study area; the contribution of rainwater to spring water is therefore not a factor controlling the age of spring water.

Considering the discharge of very young spring water during event 1, this timing corresponds to the phases of Cl^- increase and Na^+ and SiO_2 decrease in the spring water (Figure 49). The Cl^- concentration in the spring water increases from 2.4 to 2.9 mg/L during discharge of the youngest spring water. This Cl^- concentration (2.9 mg/L) is similar to that of the soil water sampled shortly before rainfall. In addition, the Na^+ and SiO_2 contents of spring water decrease toward those of precipitation and soil water. Considering that the stable isotopic composition (δ^2H) shows a small precipitation effect on spring discharge, these tracer signals (Cl^-, Na^+, and SiO_2) indicate that soil water components contribute to spring discharge, leading

to a decrease in the SF_6 age of spring water. The soil water is stored in an unsaturated subsurface area, where water coexists with the modern atmosphere (Busenberg and Plummer, 2000). If the soil water in SF_6 equilibrium with the atmosphere is discharged as a spring, the SF_6 age of the spring should be very young. In the case of event 3, the Cl^- concentration in the spring water sample on the rising limb of the hydrograph is high (4.0 mg/L) compared to that in other spring water samples (Figure 51). This high value is plotted within the boxplot of Cl^- in soil water; there is no other water (rainwater and groundwater) with high Cl^- content in the study area (Figure 51). Therefore, the soil water component should also contribute to spring discharge in event 3. In rainfall event 2, a higher Cl^- concentration indicating soil water contribution is not detected. This may have resulted from the large variety of Cl^- concentrations in soil water, as shown in the boxplot in Figure 37.

During the rainless period, the ridge groundwater (WH-20 m) whose screen is located in the bedrock shows the oldest SF_6 age compared to the other types of groundwater (WL-3 m, 5 m, and 10 m; WM-3 m, 5 m, and 10 m; Figure 42). Additionally, it has slightly different tracer characteristics than the other types of groundwater: the ridge groundwater has higher Cl^- and lower Na^+ and SiO_2 concentrations than the valley groundwater (Figure 37). Therefore, the ridge groundwater data can be assumed to reflect an older groundwater component stored in the bedrock in the study area.

The Cl^- concentration in the spring water decreases from 2.9 to 2.5 mg/L (event 1) and from 4.0 to 3.0 mg/L (event 3) at the older spring water discharge time on the rising limb of the hydrograph. The Na^+ and SiO_2 concentrations in the spring water seem to be lower than those before rainfall, even for hydrograph recession. These three tracer concentrations are similar to those of the ridge groundwater (median value of Cl^-, 2.7 mg/L; Na^+, 4.4 mg/L; SiO_2, 19.9 mg/L), especially during events 1 and 2 (Figures 49 and 50). In the case of event 3, the Na^+ and SiO_2 concentrations in the spring water are slightly lower than those during events 1 and 2 (Figure

51) due to the geology. The minimum Na^+ and SiO_2 concentrations in spring water during event 3 are 2.5 and 14.9 mg/L, respectively, and are considerably lower than the median values of the ridge groundwater (boxplots in Figure 51). Based on the boxplots, soil water and rainwater components are possible sources of the lower levels of Na^+ and SiO_2 in spring water during event 3. However, these possible sources can be ruled out based on the discharge of older spring water. Figure 54 presents key diagrams of three rainfall events. The spring water in the rising limb of the hydrograph and that in the falling limb of the hydrograph are plotted in Figure 54 with rainwater, soil water, and groundwater samples. The spring water in the rising limb, which is older, is plotted near the groundwater component (especially ridge groundwater). This suggests that the dilution effects of rainwater and soil water are limited in the rising limb of the hydrograph. Therefore, the older groundwater component (WH-20 m) with a higher level of Cl^- and lower levels of Na^+ and SiO_2 than the younger groundwater components (WL-3 m, 5 m, and 10 m; WM-3 m, 5 m, and 10 m) contributes to spring discharge during the rising limb of the hydrograph, causing the discharge of older spring water.

This possibility is supported by the spatial distribution of groundwater age shortly after heavy rainfall, as shown in Figure 42; the groundwater near the spring discharge point (WL-3, 5, and 10 m) is clearly older (9.2–12.8 years) shortly after the heavy rainfall event compared to that in the rainless period (<1–8.5 years). Older groundwater with age similar to that of the water in deeper subsurface areas (e.g., WM-10 m: 8.4–13.1 years) is replaced with shallow groundwater near the spring due to heavy rainfall, which then contributes to spring discharge. This phenomenon results in older spring water during rainfall events compared to those in rainless periods. The assumption of replacement is supported by the nitrate concentration in groundwater in the rainless period and shortly after heavy rainfall. The nitrate concentration in shallow groundwater decreases toward the deeper-groundwater-dominant value (WH-20 m) only shortly after a heavy rainstorm (Figure 34). This indicates the contribution of deeper

groundwater to the shallow groundwater during heavy rainstorms. Nitrate concentration is usually treated as a non-conservative tracer in the environment; however, nitrate ions can be treated as conservative tracers by focusing only on rainfall events (rapid hydrological processes) (Iwagami et al., 2010).

The hydraulic potential of groundwater in each borehole in the valley (WL-3, 5, and 10 m and WM-3, 5, and 10 m) increases rapidly during rainfall events (Figure 45); however, the hydraulic potential relation between the groundwater at WL and WM does not change even during rainfall events (the groundwater table level relations are always WL-3 m > WL-5 m > WL-10 m, and WM-3 m ≈ WM-5 m ≈ WM-10 m). This suggests that the groundwater flow path does not change within the depth of 10 m below the ground surface during rainfall events. Alternatively, it is reasonable to imply that the replacement of younger water with older groundwater in the valley occurs owing to the contribution of deeper groundwater (>10 m below the ground surface).

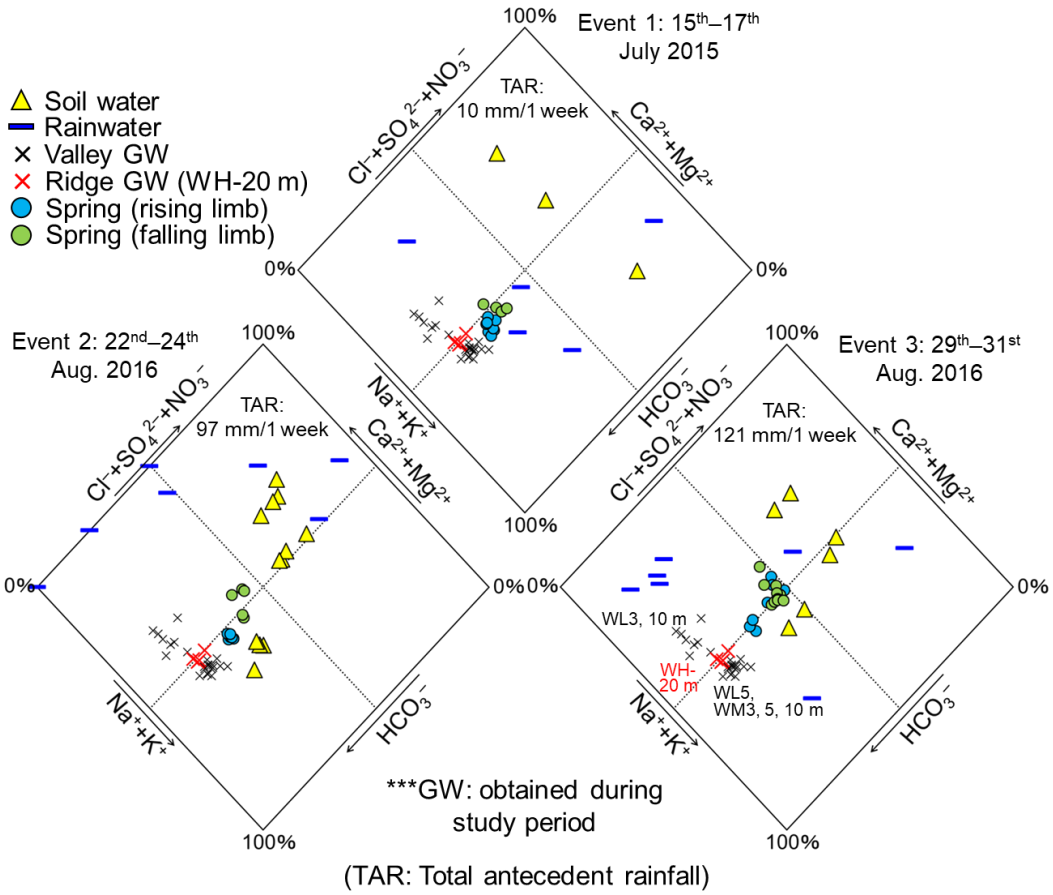

Figure 54. Key diagrams of three rainfall events. These highlight that spring water on the rising limb of the hydrograph has similar water quality composition to that of groundwater, whereas that on the falling limb of the hydrograph seems to be affected by rainwater or soil water.

5.3 Discharge process during rainstorms

In terms of water age variance and spatial distribution, the rainfall–runoff processes on the rising limb of hydrograph, peak rainfall, and hydrograph recession are discussed in this section, with a focus on event 1, July 15–17, 2015.

During the rising limb of the hydrograph, the spring water is very young (1.3 years) in event 1. At this stage, groundwater tables along the valley (WL-3, 5, and 10 m; WM-3, 5, and 10 m; Figure 45) increase rapidly by around several tens of centimeters. Therefore, the soil water should have positive hydraulic potential and start contributing to spring discharge (McGlynn and McDonnell, 2003).

In the stage around the peak rainfall, spring water older than that under the rainless condition is dominant. The contribution of soil water (modern water components) to spring water is smaller at this stage, considering the older spring water age. Unfortunately, there are no data on the spatial distribution of groundwater age around the peak discharge; however, considering the older spring water age, the groundwater age distribution seems to be similar to the conditions after heavy rainfall (9.2–12.9 years; Figure 42). Therefore, the older groundwater with age similar to that of the ridge and deeper subsurface areas replaces the shallow groundwater near the spring due to heavy rainfall, and then contributes to spring discharge, resulting in an older spring water (>10 years) around the rainfall peak on the rising limb of the hydrograph. The tracer data of the spring water (Cl^-, Na^+, and SiO_2) around the peak discharge stage are similar to those of the ridge groundwater as a representative of an older water component (Figure 49), supporting that interpretation.

The hydraulic potential of the groundwater in each borehole in the valley (WL-3, 5, and 10 m and WM-3, 5, and 10 m) increases slightly with the rising limb of the hydrograph (Figure 45). This results in a higher hydraulic gradient between each borehole and spring discharge point compared to that under the rainless condition. If the replacement of younger water with

older groundwater (9.2–12.9 years) in the valley occurs due to groundwater flow from the deeper subsurface area in the headwater region, as described by Gooddy et al. (2006) and Kamtchueng et al. (2015), the higher hydraulic gradient from the deeper subsurface area to shallow subsurface area is necessary. Unfortunately, the observed original hydraulic head data in this study cannot certify this; however, the observed tracer data such as Cl^-, NO_3^-, Na^+, SiO_2, and SF_6 surely support the assumption that older groundwater stored in deeper subsurface areas contributes to spring water during rainstorms.

Iwagami et al. (2010) concluded that bedrock groundwater, which is deeper groundwater, passes through weathered and fractured bedrock and contributes to discharge water during heavy rainstorms. The fractured bedrock (granite) lies several meters below the ground surface in the study area. It is therefore reasonable to assume that the older water stored in the bedrock flows to the shallower layer and pushes the younger water during heavy rainfall events. The younger water seems to have been discharged as spring or saturated surface water (Menichino and Hester, 2015) near the spring before the spring water apparently becomes older. Therefore, the discharge processes during rainfall events are controlled not only by the rainfall and shallow subsurface water but also by deeper groundwater with ages older than those of the spring water during rainless periods. However, the data available for determining where the younger water stored in the shallow subsurface area flows due to a heavy rainfall event are inadequate. In future studies, SF_6 data of the spring water with high time resolution (e.g., 30-min intervals) during rainstorms should be obtained to identify rapid changes in hydrological processes during rainstorms.

During hydrograph recession, the spring maintains an older age (~10 years) than that under the rainless condition (Figure 49). Based on the water age and tracer data of the spring water (Figure 49; discussed in the previous section), the older water component (ridge groundwater) should continuously contribute to the spring discharge, even during hydrograph recession. The

spatial distribution of groundwater age after heavy rainfall, which ranges from 9.2 to 12.9 years (Figure 42), strongly supports this interpretation. Additionally, the groundwater table level of the ridge groundwater (WH-20 m: older groundwater component) continuously increases during hydrograph recession, whereas the groundwater table levels of groundwater along the valley start to decrease (Figure 45), suggesting a higher hydraulic gradient between the older groundwater and the groundwater in the valley compared to that at peak rainfall. This condition is maintained throughout the hydrograph recession, leading to a prolonged existence of older groundwater in the valley; even modern water should recharge groundwater.

McGlynn and McDonnell (2003) performed component separation of the discharge water into riparian and hillslope runoff to determine the sources of rainfall–runoff water. They concluded that riparian runoff controls the new water component on the rising limb, whereas hillslope groundwater significantly contributes to the discharge at peak discharge and recession, causing hysteresis of the hydrograph (prolonged high flow of the recession). The observed results and interpretation that water aged above ~10 years discharges dominantly at and around peak rainfall (close timing to the peak discharge), as well as during hydrograph recession, are consistent with the conclusion of McGlynn and McDonnell (2003). However, sources of the older water might not be only hillslope groundwater but also deeper groundwater in the valley area based on the spatial distribution of the groundwater age, which indicates an older age (9.2–12.9 years) shortly after rainfall.

5.4 Hydrograph separation and quantitative consideration

Cl^- and SF_6 values are used as tracers to implement EMMA in this study. Various studies using EMMA have employed Cl^- as a tracer for calculations (e.g., Leaney et al., 1993; Jenkins et al., 1994; Liu and Yamanaka, 2012), whereas no studies have used SF_6 as a tracer. However, it is known that both Cl^- and SF_6 are highly conservative tracers that only change by mixing with other water sources in the groundwater flow system (Busenberg and Plummer, 2000; Dogramaci et al., 2015). Hence SF_6 is a potential tracer for applying EMMA. In this study, Cl^- concentration in soil water is relatively high and that in rainwater is considerably lower than its concentration in other water types (Figure 37). In addition, the SF_6 concentration in groundwater is lower than that in soil water and rainwater; especially, ridge groundwater has significantly lower SF_6 concentration than valley groundwater. Therefore, Cl^- and SF_6 values can be used to characterize rainwater, soil water, valley groundwater, and ridge groundwater.

Stable isotopic compositions and silica concentrations have also been recognized as useful tracers for applying EMMA, especially when focusing on rainfall–runoff processes (e.g., Iwagami et al., 2010; Klaus et al., 2013). This is because stable isotopic compositions can characterize the behavior of rainwater and silica concentration can characterize bedrock groundwater with high silica concentration. The relation between δ^2H and SiO_2 in water in this study is shown in Figure 55. Each plot of rainwater, soil water, valley groundwater, and ridge groundwater is an average value with standard deviation of the analyzed results. There are two problems if δ^2H and SiO_2 are used as tracers for EMMA. First, the δ^2H of rainwater varies significantly throughout the year, as represented by a large error bar. It seems to be difficult to characterize the behavior of the rainfall by using stable isotopic compositions when water-mixing processes are assumed in EMMA. Second, the silica and stable isotopic compositions in valley groundwater and ridge groundwater are similar; therefore, it is difficult to separate spring water into valley groundwater and ridge groundwater components. Consequently, the

present study does not use silica and stable isotopic compositions as tracers; alternatively, Cl^- and SF_6 are used for applying EMMA.

Figure 56 shows the relation between Cl^- and SF_6 concentrations in water. Each plot of rainwater, soil water, valley groundwater, and ridge groundwater shows average values with standard deviation of the analyzed results. SF_6 concentrations in soil water and rainwater are assumed as the equilibrium concentration with the modern atmospheric SF_6 mixing ratio because of the difficulties associated with direct measurement. Excess air (1.4 cm^3/L) was also considered for SF_6 concentrations in soil water and rainwater. More than 80% of the spring water collected in rainless periods is plotted inside of the triangle among rainwater, soil water, and valley groundwater, suggesting that under rainless conditions, the spring water mainly consists of these three components. In the spring water collected during the rainfall events, each marker is located outside of the triangle of rainwater, soil water, and valley groundwater and is plotted close to ridge groundwater component (older water component). This result indicates the contribution of older groundwater to spring discharge during rainfall. This interpretation is consistent with the results of other tracers such as NO_3^-, Na^+, SiO_2, and δ^2H.

Considering the overall hydrological processes both in rainless periods and during rainfall, all spring water samples fall inside of the triangle of rainwater, soil water, and ridge groundwater (older water). Therefore, it can be assumed that all spring water is a mixture of these three components (Figures 56 and 57). Based on this assumption, EMMA is implemented and the contributions of each end-member to spring water are determined. In addition, the ages of the three components are calculated based on SF_6 concentration (Rainwater: 0 year, Soil water: 0 year, and Older water: 21.7 years, Figure56).

Temporal variations in the calculated contributions of rainwater, soil water, and older groundwater on spring water discharge are shown in Figure 58. These contributions during rainfall events with hydro-hyetograph and spring water age are presented in Figures 59–61 as

well. The contribution of rainwater to spring water is around 40% throughout the year, whereas the contribution of rainwater is significantly low during rainfall events. In contrast, the older groundwater component is the main component of spring water during rainfall events, with the highest value of 67%.

During rainfall event 1, the soil water component and rainwater component make larger contributions to spring discharge than the older groundwater at the beginning of the rainfall event. However, the contribution of older groundwater increases to 67% and that of rainwater decreases to 6% during the peak rainfall. After the peak rainfall, the high contribution of older groundwater to spring water is maintained (56%–67%). In the case of rainfall events 2 and 3, the older groundwater component contributes continuously to spring discharge and its value ranges from 48% to 67% throughout the events. Rainfall events 2 and 3 show large contributions of older groundwater from the beginning of the rainfall event, possibly because of a large amount of antecedent rainfall. Therefore, the replacement of younger water with older groundwater in the valley area can be thought to have started before each observed rainfall event 2 and 3. In contrast, in the case of event 1, these phenomena seem to have started in the beginning of the rainfall event because of the small contribution of the older groundwater component to spring discharge at the beginning of rainfall. Therefore, rainfall event 1 is the best case for discussing water balance and evaluating the replacement of younger water with older groundwater in the valley area.

In terms of the contribution of spring discharge during rainstorms, especially events 1 and 3, some spring water samples have little rainwater contribution (5%–6%) even at rainfall peak (event 1) (Figures 59 and 61). Sayama et al. (2009) and Iwagami et al. (2010) applied the distributed model and EMMA by using $\delta^{18}O$, SiO_2, and NO_3^- to separate hydrographs and found that rainwater (event water) does indeed contribute, at least during rainfall. In this study, the contribution of rainwater to spring discharge seems to be absent because of large variations

in the concentration of Cl^- (a selected tracer for applying EMMA) in soil water (an end-member) (Figure 56).

Figure 62 shows the calculated discharge volume of rainwater, soil water, and older water components based on the observed discharge data and EMMA results. The total discharge volumes of rainwater, soil water, and older groundwater components during rainfall event 1 are 12700, 12600, and 35300 L, respectively. With a focus on the discharged volume of soil water during the rainfall event, discharged soil water with the volume of 12600 L is stored in the shallow subsurface area before rainfall (Figure 63). The effects of each parameter on spring discharge, including porosity of the subsurface layer and source area, are listed in Table 6. The source area of spring water discharge is directly measured in the study area with a focus on the saturated area during the rainfall event (Figure 64). The porosity of the subsurface area below the ground surface is obtained by direct measurement (Figure 9) and the porosity of the granitic geology is taken from Watanabe and Seki (1982) (Figure 65). The calculated depth below the ground surface in which discharged soil water is stored is 0.5 m (Table 6). This indicates soil water stored in subsurface areas at a depth of 0.5 m below the ground surface is discharged as spring water during rainfall. This results in the replacement of younger water with older groundwater in shallow subsurface areas near the spring discharge point. In other words, older groundwater (>10 years) contributes to the spring water during heavy rainfall in a headwater catchment owing to the discharge of soil water stored in shallow subsurface areas.

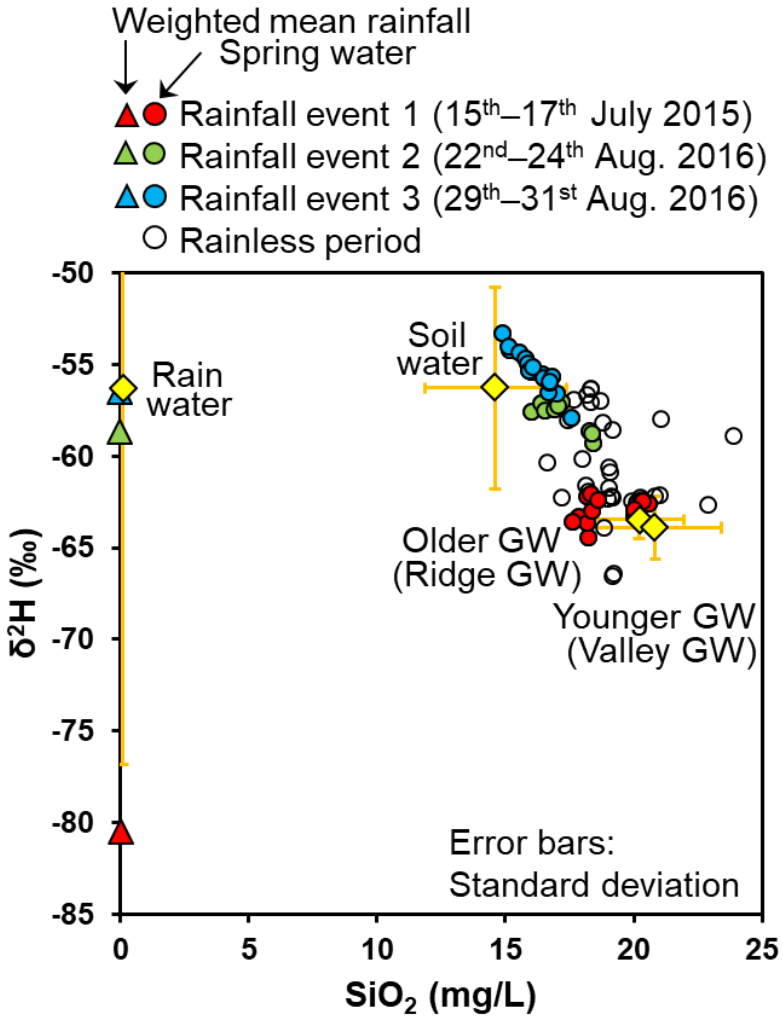

Figure 55. Mixing diagram between δ^2H and SiO_2 in water.

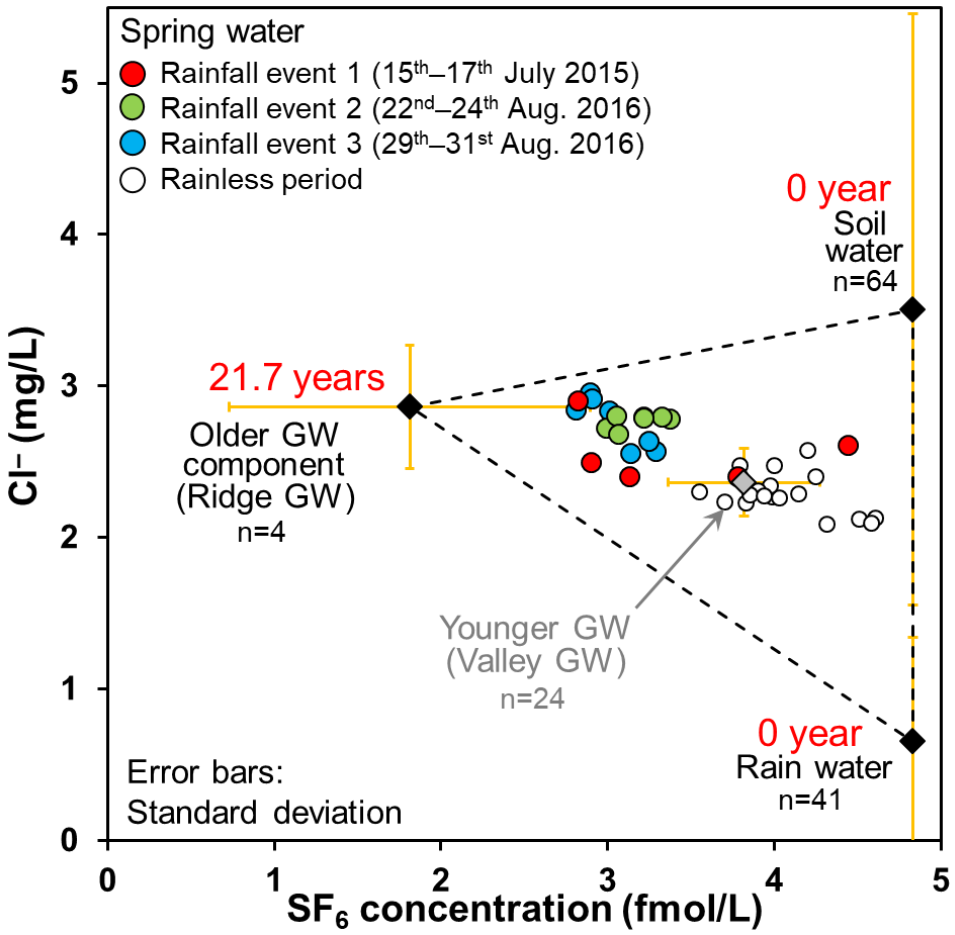

Figure 56. Mixing diagram between Cl^- and SF_6 in water with SF_6 age of end-member components.

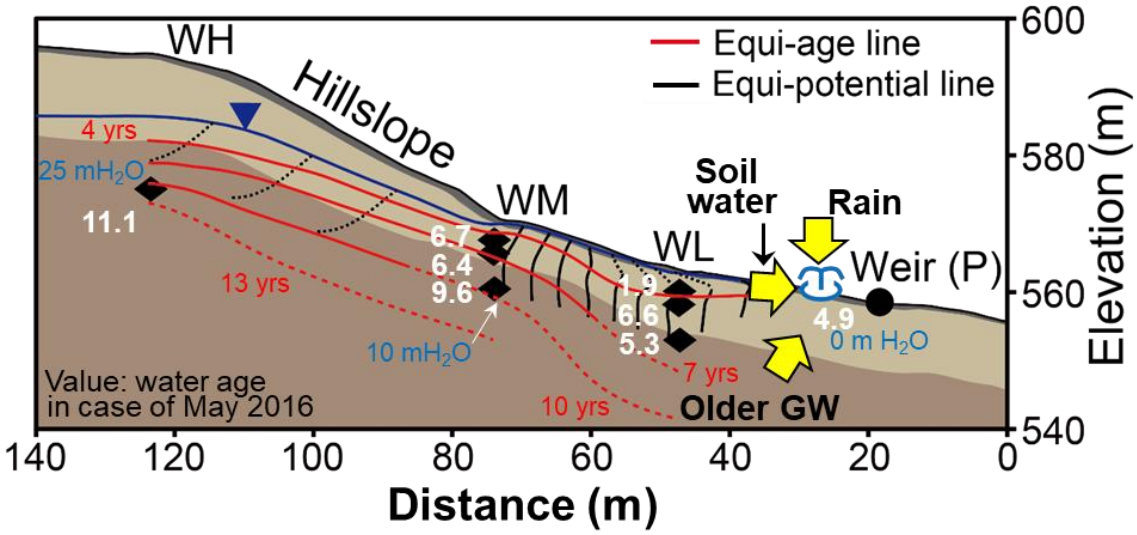

Figure 57. Conceptual model of EMMA setting for spring water.

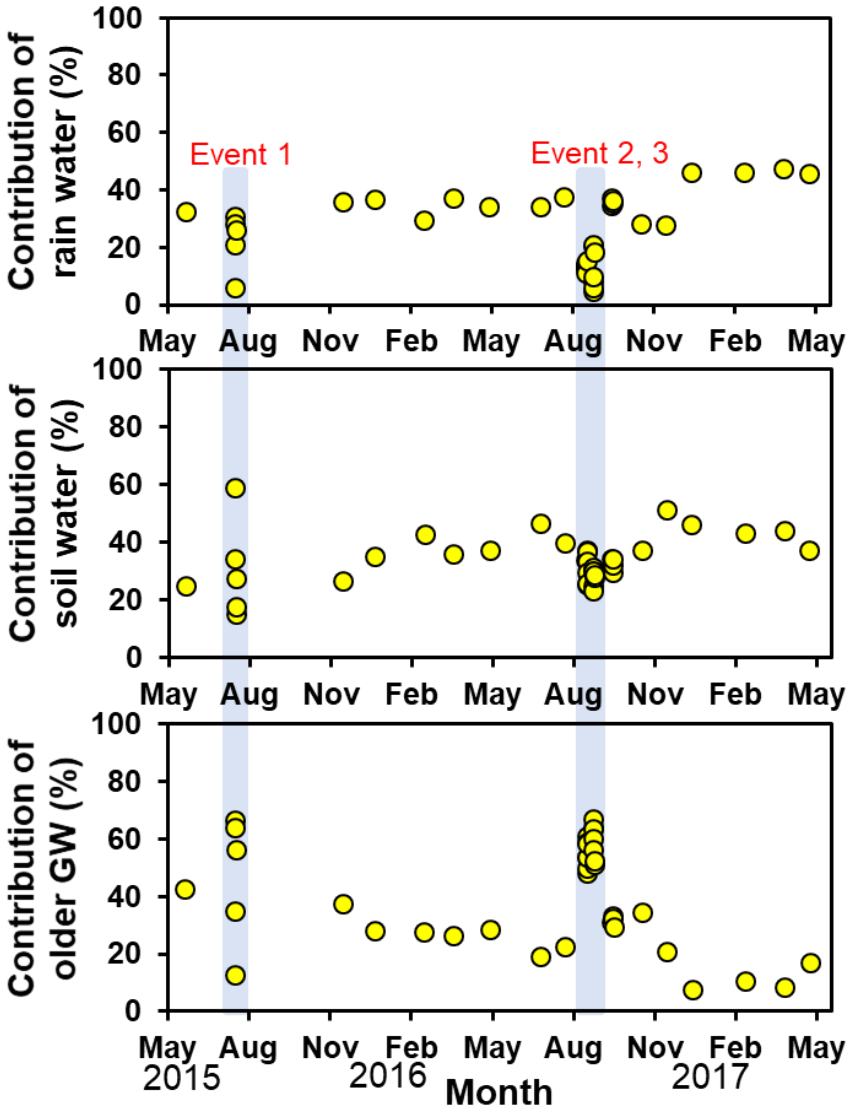

Figure 58. Temporal variations in calculated contributions of rainwater, soil water, and older groundwater to spring discharge.

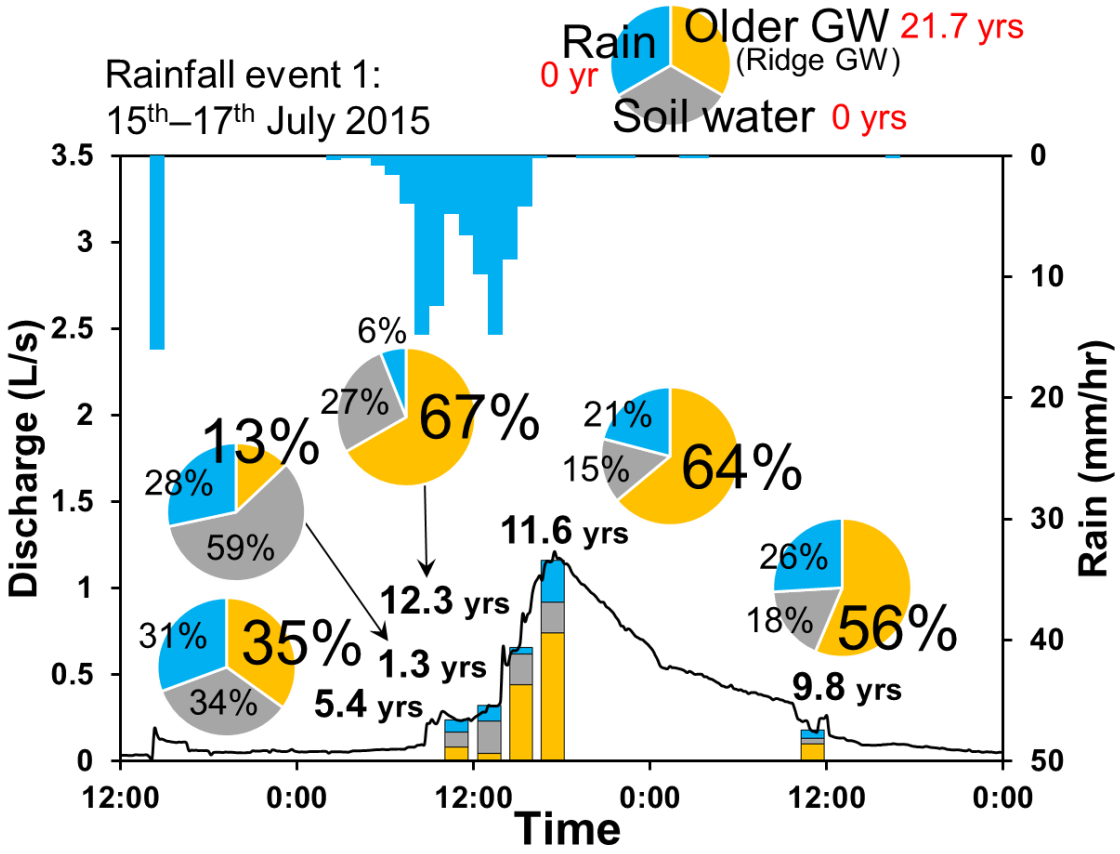

Figure 59. Contributions of rainwater, soil water, and older groundwater to spring discharge during rainfall event 1 (July 15–17, 2015) with hydro-hyetograph and spring water age.

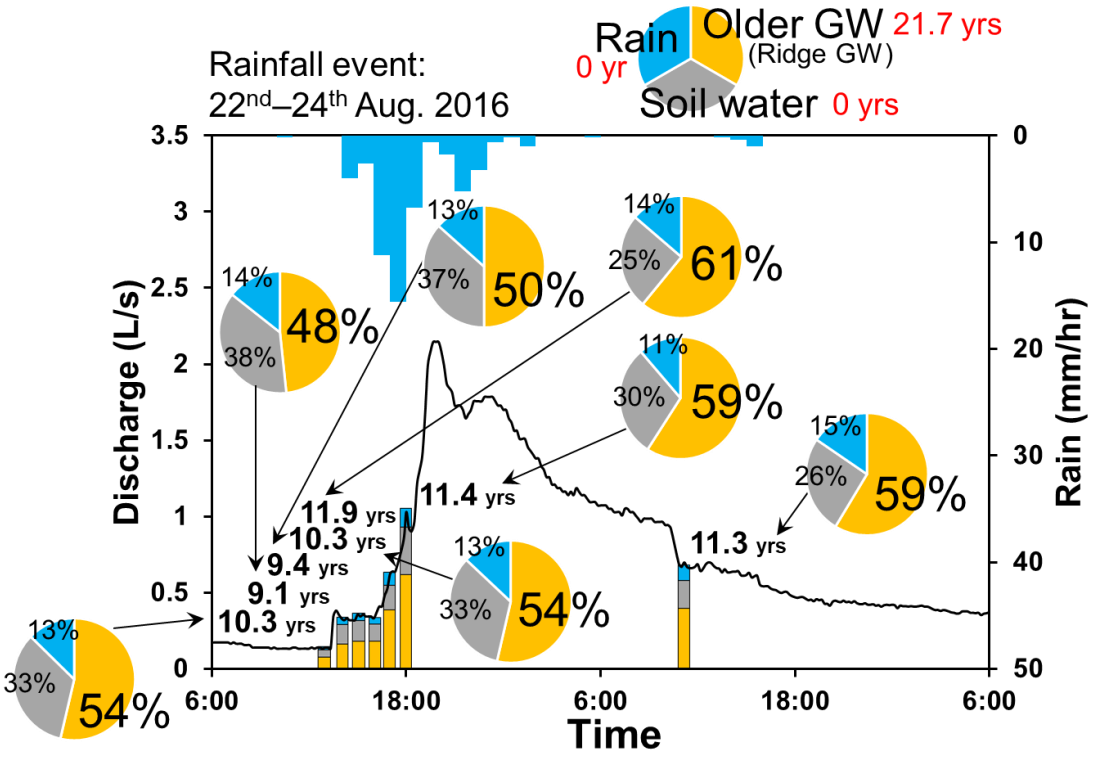

Figure 60. Contributions of rainwater, soil water, and older groundwater to spring discharge during rainfall event 2 (August 22–24, 2016) with hydro-hyetograph and spring water age.

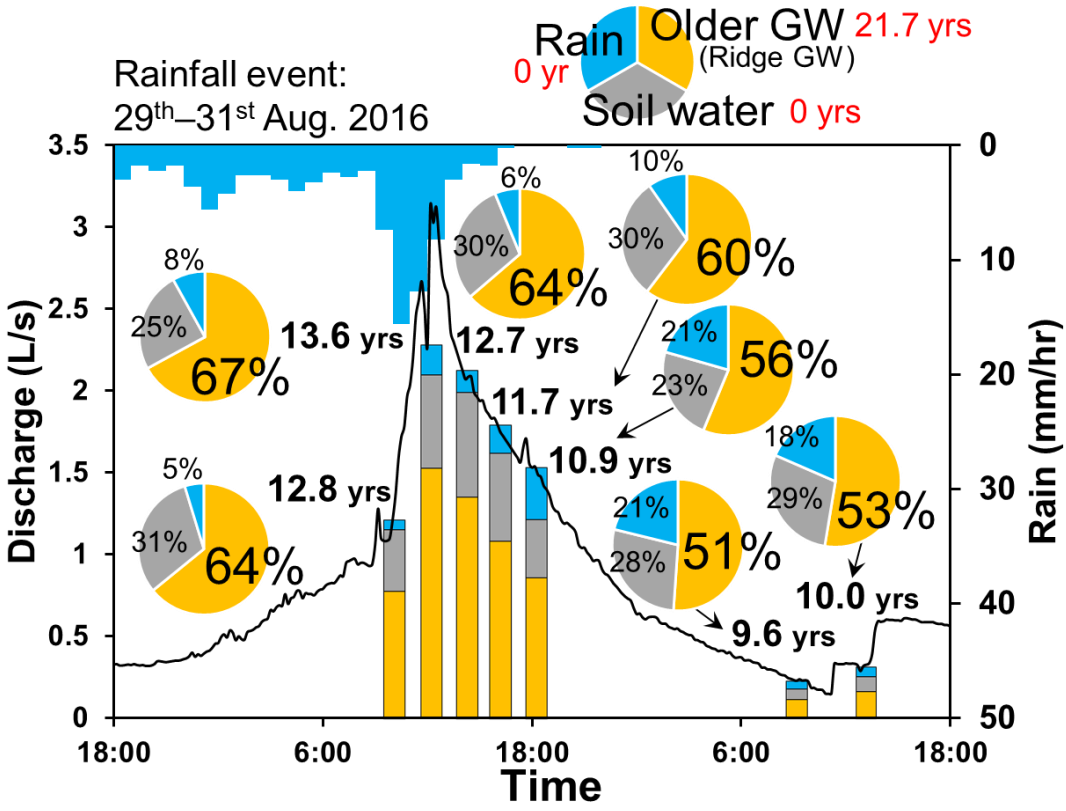

Figure 61. Contributions of rainwater, soil water, and older groundwater to spring discharge during rainfall event 3 (August 29–31, 2016) with hydro-hyetograph and spring water age.

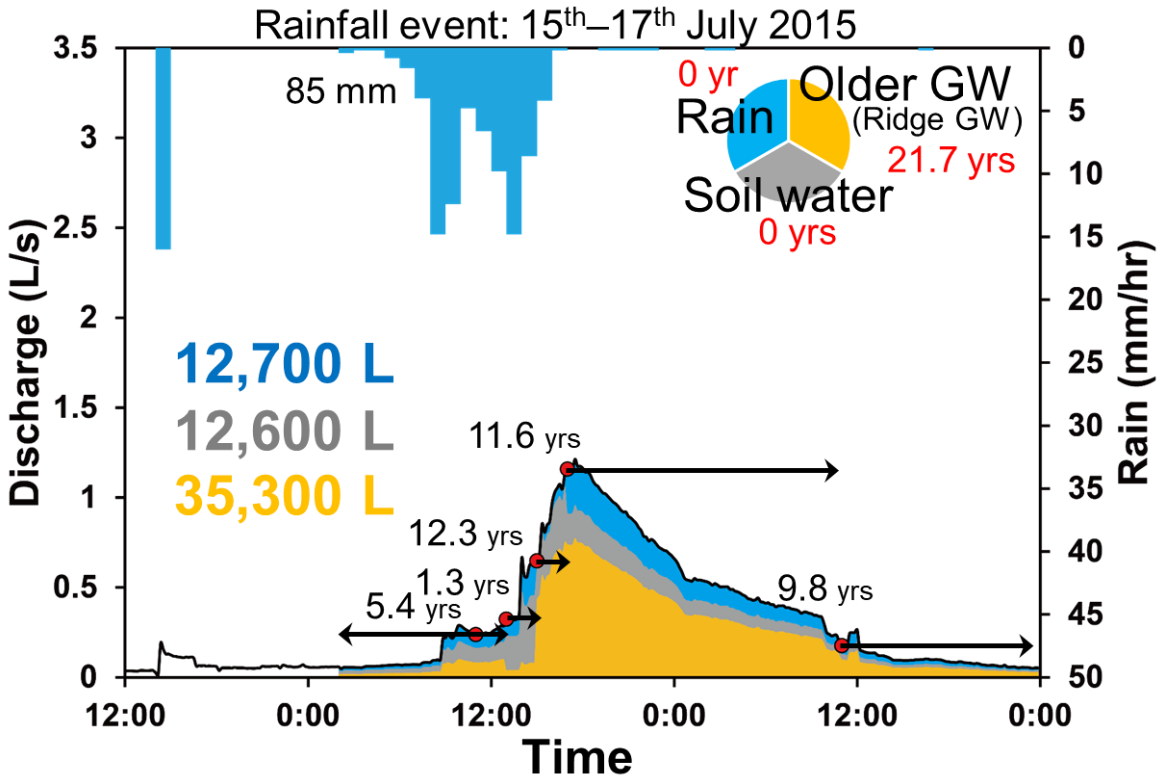

Figure 62. Discharge volume of rainwater, soil water, and older groundwater components calculated using EMMA results.

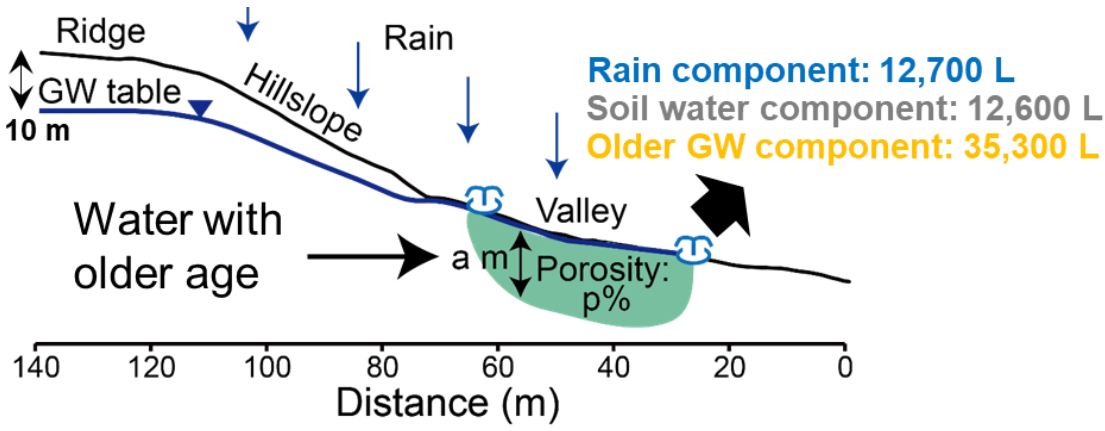

Figure 63. Conceptual model for water balance calculation with focus on discharge of shallow subsurface water during rainfall event 1.

Table 6. Porosity of subsurface layer, area contributing to spring discharge, and estimated depth of contribution below ground surface.

Porosity (p)	65%	Observed value
Source area (S)	40 m^2	Measured at the study area
Depth (a)	0.5 m	Calculated

Figure 64. Apparent saturated area in valley area during rainfall.

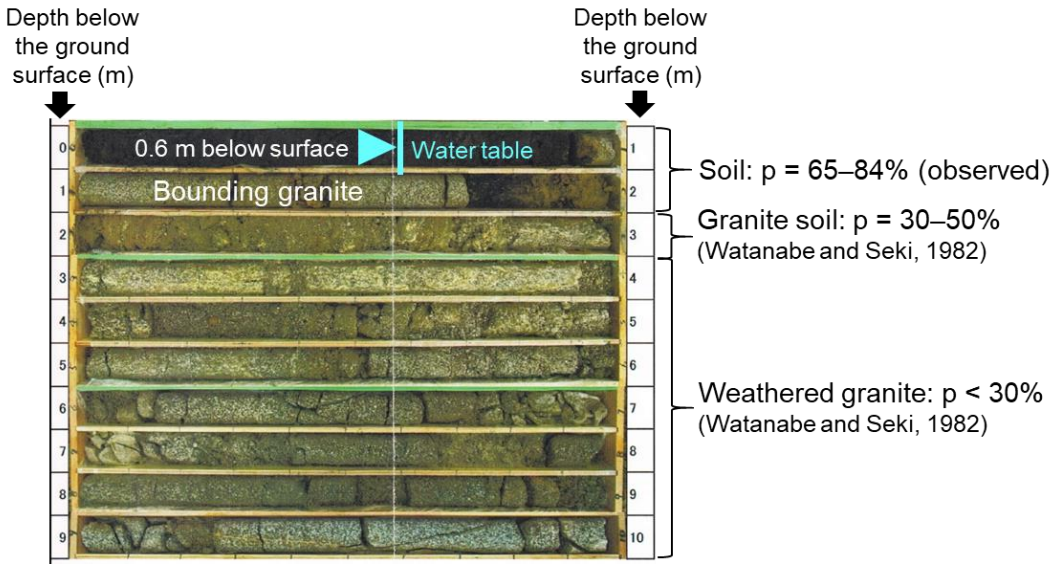

Figure 65. Boring core at WL with constant groundwater table, measured porosity (p) of soil layer, and porosity of granite soil and weathered granite referred from Watanabe and Seki (1982).

CHAPTER 6 GENERAL DISCUSSION

Numerous studies on rainfall–runoff processes have focused on stream water. Studies using the observed tracer data, such as stable isotopic compositions and solute concentrations in water, have found that the pre-event water more dominantly contributes to rainfall–runoff water (stream) than new water (rainwater) (Sklash and Farvolden, 1979; Sklash et al., 1986; Klaus and McDonnell, 2013). This has been explained by phenomena such as saturated overland flow (riparian groundwater flow; Menichino and Hester, 2015), pipe (preferential) flow (Meerveld and McDonnell, 2006), and hillslope groundwater contribution (McGlynn et al., 2002). Other studies (Kosugi et al., 2006; Kosugi et al., 2008; Iwagami et al., 2010; Gabrielli et al., 2012) have concluded that not only shallow subsurface water but also bedrock groundwater contributes to rainfall–runoff water through fractures in the bedrock due to intense rainfall input on catchments. However, bedrock groundwater might show older water, and previous studies using stable isotopes have always indicated younger rainfall–runoff water (<5 years) (Tetzlaff et al., 2014; Klaus et al., 2015; Soulsby et al., 2015). In contrast, previous studies using dating tracers (e.g., CFCs and SF_6) have often presented older discharge water (>20 years) (Koh et al., 2007; Gourcy et al., 2009; Ako et al., 2013; Hiyama et al., 2013; Kamtchueng et al., 2015). These results are clearly inconsistent in terms of water age (Stewart et al., 2010; Frisbee et al., 2013), possibly due to problems regarding catchment scale and analysis time resolution. Therefore, it is very important to clarify the research focus before discussing rainfall–runoff processes in detail.

The present study mainly aimed to determine the responses of groundwater components to rainfall input during rainstorm events. Spring water at the discharge point was selected as the research target to avoid considerations of other complex hydrological processes such as pipe flow, saturated surface flow, and direct rainfall mixing with discharge water. In addition, the

determined SF_6 age of groundwater and spring water reflected the apparent water age (residence time) from the time when the water recharged groundwater. For this reason, both rainwater and soil water components were treated as new (or modern) water components in this study. All settings were selected to simplify the hydrological processes during the rainfall events.

The observed SF_6 concentration data for rainless conditions indicated seasonal changes in the spring water age ranging from 1.8 to 6.8 years (Figure 39), which are similar to the results of previous studies (Busenberg and Plummer, 2014). However, the age of spring water clearly increased during rainstorms (>10 years), with tracer signals as older groundwater components (Figures 49–51). Note that this phenomenon occurred even in a very small headwater catchment with an area of only 0.045 km^2.

The detailed rainfall–runoff processes are explained by using the summarized figure based on the observed data (Figure 66) and conceptual model (Figure 67). Figure 66 shows the observed hydro-hyetograph, temporal variation in spring water age, results of component separation of the hydrograph, spatial distribution of groundwater age, hydraulic potential distribution, and nitrate concentration in water. At the beginning of the rainfall, groundwater in the shallow subsurface area near the spring discharge point was still young (<10 years). Hydraulic potential distribution indicated that this groundwater contributed to spring discharge, and as a result, spring water continued to appear young in the results (1.3–5.4 years). In this period, the contribution of the rainwater and soil water components to spring discharge (65–87%) was the largest. At peak rainfall and in the rising phase of the hydrograph, the age of spring water changed to 12.3 years from 1.3–5.4 years, and the contribution of the older groundwater component aged 21.7 years on the spring clearly increased to 67% from 13–35%. In this phase, although no clear change in the groundwater flow system was observed based on the hydraulic potential distribution, the solute concentrations (especially, Cl^-, Na^+, and SiO_2) in spring water became similar to those of the older groundwater component. In addition, the

hydraulic gradient between the groundwater around WL and the spring discharge point increased by 10% compared to that at the beginning of the rainfall. Therefore, this 10% increase in the hydraulic gradient led to the replacement of younger water with older groundwater stored in the subsurface area near the spring discharge point. Then, the replaced older groundwater started contributing to the spring discharge according to the hydraulic potential distribution. This is suggested as the principal mechanism of older spring water discharge in the peak rainfall phase on the rising limb of the hydrograph. This phenomenon was prolonged even in the hydrograph recession after rainfall. As a result, there was a continuous large contribution of the older groundwater component (56–64%) to the spring water discharge, although the contribution of the new water (21–26%) increased slightly. This finding suggests that rainstorm events play important roles as triggers in discharging older water stored in the catchment.

However, it is somewhat difficult to consider that only a 10% increase in the hydraulic gradient causes replacement of younger water with older groundwater because older groundwater might be stored in deeper subsurface areas. Considering the tracer signature in spring water during rainstorms (Figures 49–51) and groundwater age distribution shortly after heavy rainfall (Figure 42), we cannot help but think that the hydraulic gradient from the deeper subsurface area to the shallow subsurface area is larger than that from the groundwater around WM (boundary location between hillslope and valley) to the valley groundwater (WL). In other words, groundwater flow from deeper subsurface areas to shallow subsurface areas should occur during heavy rainfall and such flow seems to be facilitated by abundant fractures in the bedrock. The nitrate concentration in groundwater can certify this (Figure 66); the nitrate concentration in groundwater shortly after heavy rainfall (after peak rainfall) clearly decreased toward the older groundwater dominant value compared to that in the rainless period (beginning of rainfall). The groundwater quality compositions (Figure 54) remained almost stable even shortly after heavy rainfall; therefore, rainwater or soil water with lower nitrate concentration

does not contribute largely to groundwater. Thus, the decrease in nitrate concentration in groundwater shortly after heavy rainfall must be due to the contribution of older groundwater with lower nitrate concentration. This assumption is supported by Iwagami et al. (2010) and Gabrielli et al. (2012); nevertheless, there are no data on the hydraulic gradient observed from deeper subsurface areas to shallow subsurface areas owing to the lack of observation boreholes with screens in deeper subsurface areas. Obtaining the hydraulic potential data of deeper subsurface areas and certifying this hypothesis are avenues for future work.

This section discusses the uncertainties of this study and the scope for future research. The first topic is the observed stable isotopic signature in the water, which has previously been used by multiple studies on rainfall–runoff processes (e.g., Klaus and McDonnell, 2013). In the three observed rainfall events, the δ^2H of spring water (rainfall–runoff water) did not change significantly (Figures 49–51). The δ^2H of groundwater, too, did not change significantly in space and time (Figure 30). Moreover, the δ^2H values of spring water (from −64‰ to −53‰) observed during rainfall events and the groundwater (from −64‰ to −60‰) collected at four different times were similar, compared to the large δ^2H variations in rainwater during the rainfall events (Figures 49–51). Therefore, the stable isotopic data can separate the rainfall–runoff water into the new water component (rainwater) and the water stored in the catchment before the rainfall event, as shown in previous studies (Sklash and Farvolden, 1979; Sklash et al., 1986; Klaus and McDonnell, 2013). However, the similar isotopic signatures of the subsurface waters make it difficult to examine and quantify the contribution of each subsurface water source (e.g., ridge groundwater, valley groundwater, or bedrock groundwater) to the rainfall–runoff water.

This study applied the SF_6 tracer to examine the role of groundwater in the rainfall–runoff processes to overcome the above-described problem of stable isotopic tracers. This newly applied method can provide the time scale (age information) of rainfall–runoff processes; the

most important result is that the age of spring water obviously increased (>10 years) during rainstorm events compared to rainless periods, which indicates the discharge of older and deeper groundwater. However, this result clearly disagrees with the general knowledge, which decrees that discharge water becomes younger during rainstorm events due to the contribution of new water (rainwater) (Klaus et al., 2015). This may result from tracer-oriented limitations such as stable isotopes or different research targets (in this study, spring water as a groundwater component is the target versus stream water in previous studies). Nevertheless, to verify that the results of the present study are general, it is necessary to accumulate SF_6 data on dated rainfall–runoff water during rainstorms not only in the same catchment as in this study but also at other locations worldwide.

The second topic concerns uncertainties in the SF_6 method. The SF_6 tracer method was used in this study to determine the age of water. Recent studies have indicated the spatiotemporal variant transit time distribution, corresponding to the mixing process, of water in catchments (e.g., Hrachowitz et al., 2009; Soulsby et al., 2015). Especially, Tetzlaff et al. (2014) clearly indicated different transit time distribution shapes of stream water, soil water, and groundwater. In addition, Birkel et al. (2012) pointed out seasonal differences in the transit time distribution according to stable isotopic data with high time resolution during rainfall events. However, the present study employed constant transit time distributions (the groundwater mixing model) to calculate the age of water by using the SF_6 tracer. Although a few studies have indicated that the flow of groundwater in the upstream area can be illustrated with a piston flow model (Kamtchueng et al., 2015), it cannot be denied that time-variant mixing processes occur during rainfall events. Therefore, it is important to consider mixing of waters of different origins to obtain the real transit time distribution (mixing model) of rainfall–runoff water by using, for example, the multiple tracer method (IAEA, 2006; Kashiwaya et al., 2014).

In addition, the EA and natural sources of SF_6 in the sampled water were not discussed

sufficiently in this study because the SF_6 concentration did not exceed the current atmospheric mixing ratio. Moreover, intense rainfall might cause EA, resulting in underestimation of the age of water (Gooddy et al., 2006; Darling et al., 2012; Hall et al., 2012); however, our observations indicate an older water than that in the rainless periods. This indicates that EA does not significantly affect the main findings in the study area. Nevertheless, the strong and weak points of each tracer method need to be fully understood to support our interpretation.

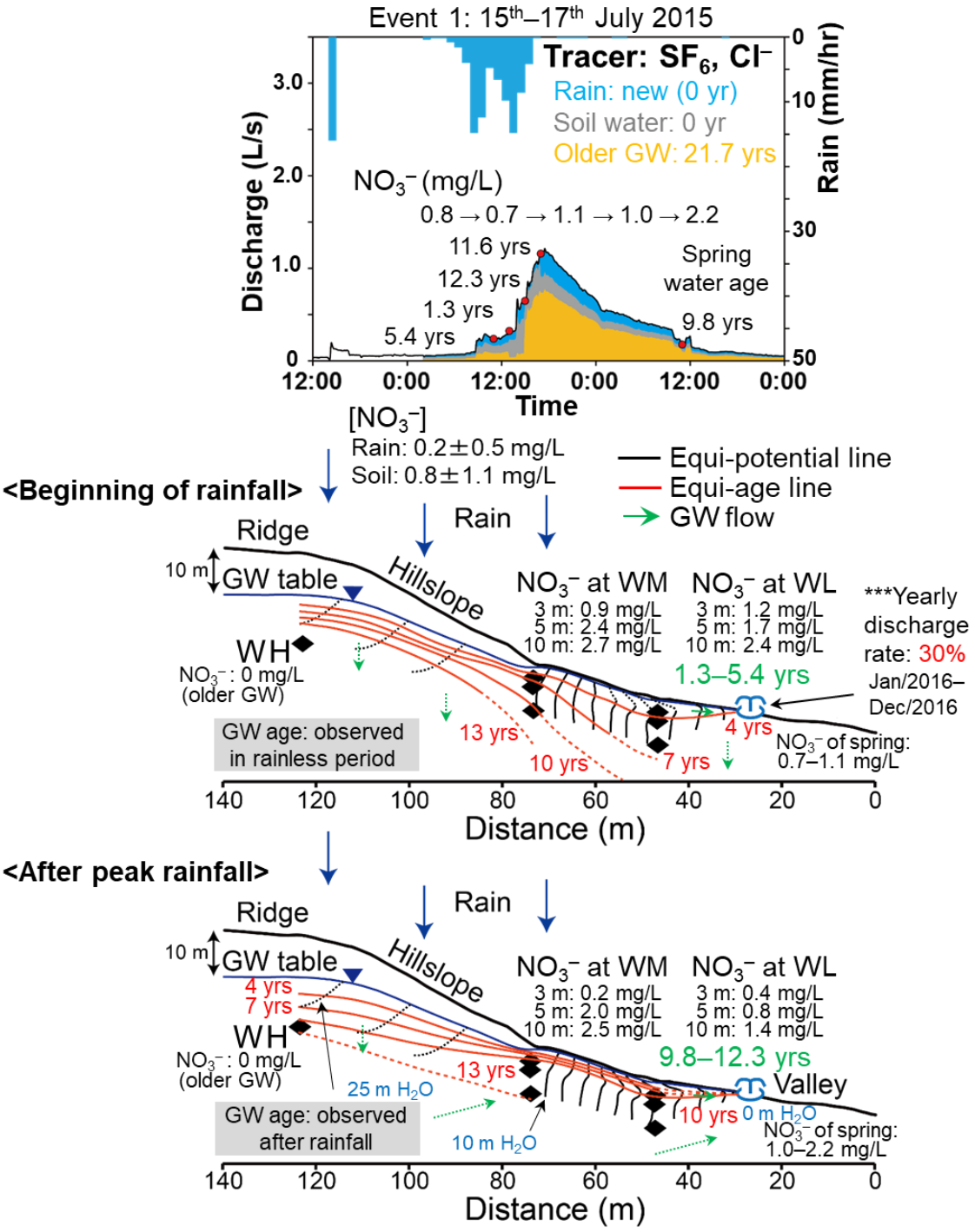

Figure 66. Schematic of rainfall–runoff processes based on observed data (water age, hydraulic potential, and nitrate concentration) and hydrograph separation result in terms of water age. Groundwater age and nitrate concentration in groundwater at the beginning of rainfall and after peak rainfall are observed values in rainless periods and shortly after rainfall, respectively. Nitrate concentration in rainwater and soil water is average value ± standard deviation of all collected samples throughout the observation period.

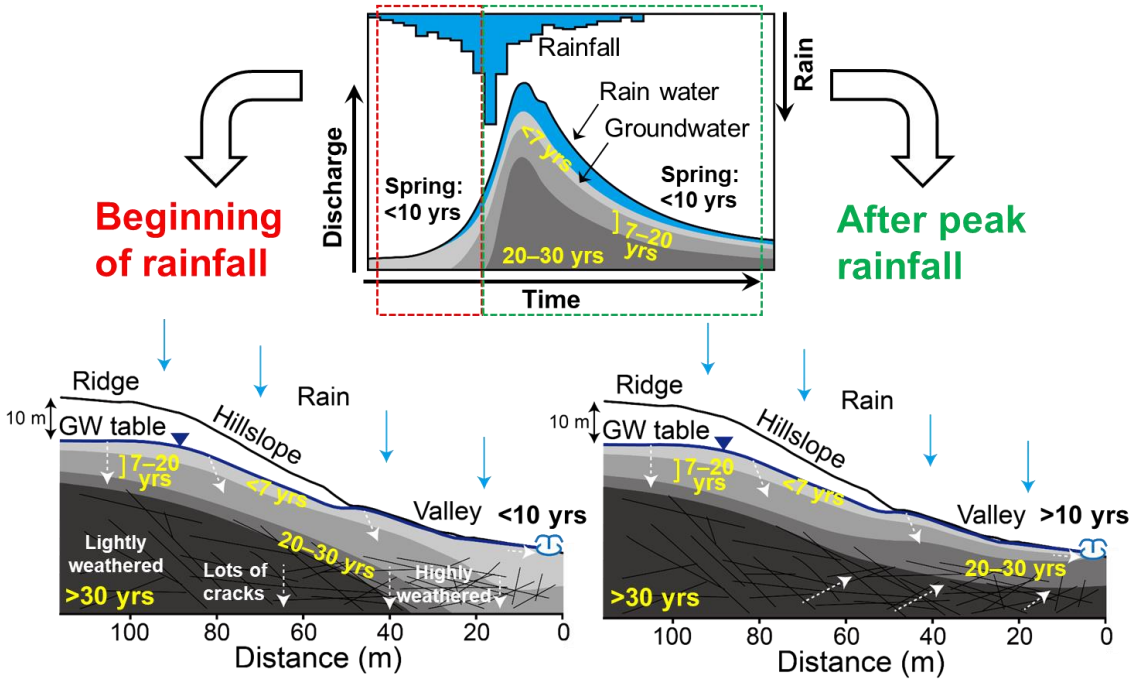

Figure 67. Conceptual model of rainfall-runoff processes. The figure highlights how the older groundwater (>10 years) stored in deeper subsurface areas in the bedrock flows toward shallow subsurface areas through fractures in the bedrock due to heavy rainfall input on headwater catchment, and subsequently, contributes to spring water.

CHAPTER 7 CONCLUSIONS

We examined the temporal variation in rainfall–runoff water age and the related discharge processes by using unique SF_6 data of spring water/groundwater during rainfall and rainless periods and hydrometric, stable isotopic, and chemical data in a headwater catchment in Japan. An apparatus for measuring dissolved SF_6 in water was developed by the author; its novelty lies in its ease of use and suitability for analyzing dissolved SF_6 in water. Therefore, the developed system was used to determine dissolved SF_6 in water samples in this study. The conclusions of this study are summarized as follows:

[About apparatus installation and development]

- The trap-and-purge procedure using the bubbling system, an ultra-pure N_2 carrier gas, and −80°C ethanol was applied to determine the concentration of SF_6 in water, resulting in sharp and clear SF_6 peaks on each analysis chromatogram.
- Analytical accuracies were determined by repeated analyses; analytical accuracies of standard gasses were ±0.02 fmol and that of dissolved SF_6 concentration in water was ±0.07 fmol/L. The detection limit of the analytical system was 0.1 fmol. However, if SF_6 standard gas with lower concentration or smaller constant-volume tube are installed in the system, a SF_6 detection limit lower than 0.1 fmol can be achieved.
- Three future works were identified: determination of exact SF_6 detection limit, improvement of the back-flush system, and improvement of the purge housing system.

[About rainfall–runoff processes]

- The spring age varied from 1.8 to 6.8 years during the rainless period based on SF_6 concentration in spring water, and increased as the discharge volume decreased. The

hydraulic potential distribution and groundwater age near the discharge point indicated the contribution of shallow subsurface groundwater to the spring during the rainless period. This suggested that the water discharge processes during rainless periods are controlled by the shallow subsurface water and the amount of rainfall.

- Spring age clearly increased (>10 years) as the discharge volume increased during rainstorms, indicating different hydrological processes from those in the rainless period. The oldest age of spring water (at most 13.6 years) was found during peak rainfall on the rising limb of the hydrograph in the three observed intense rainfall events.
- The stable isotopic composition of rainwater changed largely during the rainfall events, whereas that of spring water did not change significantly. This implies that the rainfall component did not contribute significantly to the spring water during the rainstorm.
- In each rainfall event, the concentrations of chloride ions, sodium ions, and silica in spring water changed toward the dominant values of the older groundwater component (ridge groundwater) stored in the catchment. The timing of this change is thought to correspond to that of the discharge of older spring water during rainstorms, indicating the contribution of the older groundwater component (ridge groundwater) to spring discharge.
- After heavy rainfall, the age of valley groundwater near the spring discharge point increased (9.2–12.8 years) compared to that under the rainless condition (<1–8.5 years). This indicated replacement of the younger subsurface water component with the older groundwater component in the valley due to intense rainfall.
- During rainfall, although no clear change in the groundwater flow system was observed, the hydraulic gradient between the groundwater near the spring and the discharge point increased by 10% as compared to that before rainfall. This 10% increase in the hydraulic gradient caused the replacement of younger water with older groundwater. Then, the

replaced older groundwater started contributing to the spring discharge according to the hydraulic potential distribution. This is suggested as the principal mechanism of the discharge of older spring water in the peak rainfall phase on the rising limb of the hydrograph.

- This study provided new insights into the dynamics of older water and responses to rainfall in terms of water age variance in headwater regions, which are important source regions of discharge water. Future studies should discuss how rainfall (directly or indirectly) affects the older groundwater to further interpret rainfall–runoff processes based on water age information with high time resolution during rainstorms.

Acknowledgements

First, the author would like to express his sincere gratitude to his supervisor, Prof. Dr. Maki TSUJIMURA, for his warm encouragement and expert guidance throughout the author's graduate work. The author is also grateful to Prof. Dr. Maki TSUJIMURA for providing ample opportunities to attend international conferences, join field surveys, and discuss research contents with experts. Every opportunity surely led to improvement of not only the author's graduate work but also the author's attitude toward research. Without this kind and insightful help, the present work would not have been achieved.

The author would also like to express his deepest appreciation to the members of the evaluation committee for his PhD thesis— Prof. Dr. Kuniaki MIYAMOTO, Prof. Dr. Yuichi ONDA, Prof. Dr. Jun ASANUMA, Prof. Dr. Zhenya ZHANG, and Associate Prof. Dr. Norifumi HOTTA—for their careful review of and insightful questions and comments about his graduate work.

The author is also grateful to the watershed/hydrological research members of University of Tsukuba—Prof. Dr. Michiaki SUGITA, Prof. Dr. Jun ASANUMA, Associate Prof. Dr. Tsutomu YAMANAKA, and Assistant Prof. Dr. Marino HIRAOKA—for their advice and encouragement. Joint seminars between the watershed and hydrological groups were undoubtedly fruitful for improving the author's graduate work.

The author's deep appreciation goes to Dr. Sho IWAGAMI, Mr. Ryohei KONUMA, Mr. Yutaro SATO, and Mr. Kosuke NAGANO. Without their support on field surveys and analysis processes, this work would not have been achieved. In addition, discussions with them were surely fruitful and have improved this work significantly.

Special thanks to all members of the Tsujimura Laboratory. Their suggestions and comments were helpful for improving this research. The author cannot forget the days he spent with them during his PhD course.

The author wishes to thank the research fellowship for young scientists (DC1) of the Japan Society for the Promotion of Science (JSPS) [KAKENHI grant number 15J00384] for financially supporting his PhD work. This research was also supported by JSPS [KAKENHI grant numbers 16H03111 and 24110006].

Finally, the author would like to extend his gratitude to his parents for understanding, supporting, and encouraging him throughout the PhD work.

Koichi SAKAKIBARA

References

Ako, A. A., Shimada, J., Hosono, T., Kagabu, M., Richard, A., Nkeng, G. E., Tongwa, A. F., Ono, M., Eyong, G. E. T., Tandia, B. K., and Mouncherou, O. F. (2013). Flow dynamics and age of groundwater within a humid equatorial active volcano (Mount Cameroon) deduced by δD, $\delta^{18}O$, ^{3}H and chlorofluorocarbons (CFCs). *Journal of Hydrology*, **502**, 156–176.

Anderson, S. P., Dietrich, W. E., Montgomery, D., Torres, R., Conrad, M., and Loague, K. (1997). Subsurface flow paths in a steep unchanneled catchment. *Water Resources Research*, **33**, 2637–2653.

Asai, K., Tsujimura, M., Fantong, W. Y., and Satake, H. (2011). Impact of natural and local anthropogenic SF_6 sources on dating springs and groundwater using SF_6 in central Japan. *Hydrological Research Letters*, **5**, 42–46.

Asai, K., Tsujimura, M., and Mogi, K. (2017). Distribution of atmospheric SF_6 around urban area in Japan – Impact for groundwater dating using SF_6. *Journal of Groundwater Hydrology*, **59**, 345–354 (in Japanese).

Asano, Y., Uchida, T., and McDonnell, J. J. (2005). Searching for "post" variable source area concept of rainfall-runoff response in headwater. Where does water go when it rains? Journal of Japan Society of Hydrology and Water Resources, **18**, 459–468 (in Japanese).

Barnes, C. J., and Allison, G. B. (1988). Tracing of water movement in the unsaturated zone using stable isotopes of hydrogen and oxygen. *Journal of Hydrology*, **100**, 143–176.

Barthold, F. K., Tyralla, C., Schneider, K., Vache, K. B., Frede, H., and Breuer, L. (2011). How many tracers do we need for end member mixing analysis (EMMA)? A sensitivity analysis. *Water Resources Research*, **47**, W08519, doi: 10. 1029/2011WR010604.

Beyer, M., Raaij, R., Morgenstern, U., and Jackson, B. (2014). Potential groundwater age tracer found: Halon-1301 (CF_3Br), as previously identified as CFC-13 (CF_3Cl). *Water Resources Research*, **50**, 7318–7331.

Birkel, C., Soulsby, C., Tetzlaff, D., Dunn, S., and Spezia, L. (2012). High-frequency storm event isotope sampling reveals time-variant transit time distributions and influence of diurnal cycles. *Hydrological Processes*, **26**, 308–316.

Bohlke, J. K., Verstraeten, I. M., and Kraemer, T. F. (2007). Effects of surface-water irrigation on sources,

fluxes, and residence times of water, nitrate, and uranium in an alluvial aquifer. Applied *Geochemistry*, **22**, 152–174.

Botter, G., Bertuzzo, E., and Rinaldo, A. (2010). Transport in the hydrologic response: Travel time distributions, soil moisture dynamics, and the old water paradox. *Water Resources Research*, **46**, W03514, doi:10.1029/2009WR008371.

Burguete, J., Garcia-Navarro, P., and Aliod, R. (2002). Numerical simulation of runoff from extreme rainfall events in a mountain water catchment. *Natural Hazards and Earth System Sciences*, **2**, 109–117.

Burns, D. A., McDonnell, J. J., Hooper, R. P., Peters, N. E., Freer, J. E., Kendall, C., and Beven, K. (2001). Quantifying contributions to storm runoff through end-member mixing analysis and hydrologic measurements at the Panola Mountain Research Watershed (Georgia, USA). *Hydrological Processes*, **15**, 1903–1924.

Busenberg, E., and Plummer, L. N. (1992). Use of chlorofluorocarbons ($CC1_3F$ and $CC1_2F_2$) as hydrologic tracers and age-dating tools: The alluvium and terrace system of central Oklahoma. *Water Resources Research*, **28**, 2257–2283.

Busenberg, E., and Plummer, L. N. (2000). Dating young groundwater with sulfur hexafluoride: Natural and anthropogenic sources of sulfur hexafluoride. *Water Resources Research*, **36**, 3011–3030.

Busenberg, E., and Plummer, L. N. (2014). A 17-year record of environmental tracers in spring discharge, Shenandoah national park, Virginia, USA: Use of climatic data and environmental conditions to interpret discharge, dissolved solutes, and tracer concentrations. *Aquatic Geochemistry*, **20**, 267–290.

Chou, C. (2007). Efficient nonlinear modeling of rainfall-runoff process using wavelet compression. *Journal of Hydrology*, **332**, 442–455.

Christophersen, N., and Hooper, R. P. (1992). Multivariate analysis of stream water chemical data: The use of principal components analysis for the end-member mixing problem. *Water Resources Research*, **28**, 99–107.

Cloke, H. L., Anderson, M. G., McDonnell, J. J., and Renaud, J. P. (2006). Using numerical modelling to evaluate the capillary fringe groundwater ridging hypothesis of streamflow generation. *Journal of Hydrology*, **316**, 141–162.

Danesh-Yazdi, M., Foufoula-Georgiou, E., Karwan, D. L., and Botter, G. (2016). Inferring changes in water cycle dynamics of intensively managed landscapes via the theory of time-variant travel time distributions. *Water Resources Research*, **52**, 7593–7614.

Darling, W. G., Gooddy, D. C., MacDonald, A. M., and Morris, B. L. (2012). The practicalities of using CFCs and SF_6 for groundwater dating and tracing. *Applied Geochemistry*, **27**, 1688–1697.

Dogramaci, S., Firmani, G., Hedley, P., Skrzypek, G., and Grierson, P. F. (2015). Evaluating recharge to an ephemeral dryland stream using a hydraulic model and water, chloride and isotope mass balance. *Journal of Hydrology*, **521**, 520–532.

Friedrich, R., Vero, G., Rohden, C., Lessmann, B., Kipfer, R., and Aeschbach-Hertig, W. (2013). Factors controlling terrigenic SF_6 in young groundwater of the Odenwald region (Germany). *Applied Geochemistry*, **33**, 318–329.

Frisbee, M. D., Phillips, F. M., Campbell, A. R., Liu, F., and Sanchez, S. A. (2011). Streamflow generation in a large, alpine watershed in the southern Rocky Mountains of Colorado: Is streamflow generation simply the aggregation of hillslope runoff responses?. *Water Resources Research*, **47**, W06512, doi:10.1029/2010WR009391.

Frisbee, M. D., Wilson, J. L., Gomez-Velez, J. D., Phillips, F. M., and Campbell, A. R. (2013). Are we missing the tail (and the tale) of residence time distributions in watersheds?. *Geophysical Research Letters*, **40**, 4633–4637.

Gabrielli, C. P., McDonnell, J. J., Jarvis, W. T. (2012). The role of bedrock groundwater in rainfall-runoff response at hillslope and catchment scales. *Journal of Hydrology*, **450–451**, 117–133.

Gardner, W. P., Harrington, G. A., Solomon, D. K., and Cook, P. G. (2011). Using terrigenic ^4He to identify and quantify regional groundwater discharge to streams. *Water Resources Research*, **47**, W06523, doi:10.1029/2010WR010276.

Gooddy, D. C., Darling, W. G., Abesser, C., and Lapworth, D. J. (2006). Using chlorofluorocarbons (CFCs) and sulphur hexafluoride (SF_6) to characterise groundwater movement and residence time in a lowland Chalk catchment. *Journal of Hydrology*, **330**, 44–52.

Gourcy, L., Baran, N., and Vittecoq, B. (2009). Improving the knowledge of pesticide and nitrate transfer processes using age-dating tools (CFC, SF_6, ^3H) in a volcanic island (Martinique, French West

Indies). *Journal of Contaminant Hydrology*, **108**, 107–117.

Gracz, M. B., Moffett, M. F., Siegel, D. I., and Glaser, P. H. (2015). Analyzing peatland discharge to streams in an Alaskan watershed: An integration of end-member mixing analysis and a water balance approach. *Journal of Hydrology*, **530**, 667–676.

Gusyev, M. A., Toews, M., Morgenstern, U., Stewart, M., White, P., Daughney, C., and Hadfield, J. (2013). Calibration of a transient transport model to tritium data in streams and simulation of groundwater ages in the western Lake Taupo catchment, New Zealand. *Hydrology and Earth System Sciences*, **17**, 1217–1227.

Haase, K. B., Busenberg, E., Plummer, L. N., Casile, G., and Sanford, W. E. (2014). Measurements of HFC-134a and HCFC-22 in groundwater and unsaturated-zone air: Implications for HFCs and HCFCs as dating tracers. *Chemical Geology*, **385**, 117–128.

Hall, C. M., Castro, M. C., Lohmann, K. C., and Sun, T. (2012). Testing the noble gas paleothermometer with a yearlong study of groundwater noble gases in an instrumented monitoring well. *Water Resources Research*, **48**, W04517, doi: 10.1029/2011WR010951.

Hewlett, J. D., and Hibbert, A. R. (1967). Factors affecting the response of small watersheds to precipitation in humid areas. In International Symposium on Forest Hydrology. Sopper, W.E., Lull, H.W. (eds). Pergamon, Oxford, 275–290.

Hiyama, T., Asai, K., Kolesnikov, A. B., Gagarin, L. A., and Shepelev, V. V. (2013). Estimation of the residence time of permafrost groundwater in the middle of the Lena River basin, eastern Siberia. *Environmental Research Letters*, **8**, doi:10.1088/1748-9326/8/3/035040.

Hooper, R. P., and Christophersen, N., Peters, N. E. (1990). Modelling streamwater chemistry as a mixture of soilwater end-members: An application to the Panola Mountain catchment, Georgia, U.S.A. *Journal of Hydrology*, **116**, 321–343.

Hrachowitz, M., Soulsby, C., Tetzlaff, D., Dawson, J. J. C., and Malcolm, I. A. (2009). Regionalization of transit time estimates in montane catchments by integrating landscape controls. W*ater Resources Research*, **45**, W05421, doi:10.1029/2008WR007496.

IAEA (2006). Use of chlorofluorocarbons in hydrology: A guidebook, STI/PUB/1238.

Iwagami, S., Tsujimura, M., Onda, Y., Nishino, M., Konuma, R., Abe, Y., Hada, M., Pun, I., Sakaguchi,

A., Kondo, H., Yamamoto, M., Miyata, Y., and Igarashi, Y. (2017). Temporal changes in dissolved ^{137}Cs concentrations in groundwater and stream water in Fukushima after the Fukushima Dai-ichi Nuclear Power Plant accident. *Journal of Environmental Radioactivity*, **166**, 458–465.

Iwagami, S., Tsujimura, M., Onda, Y., Shimada, J., and Tanaka, T. (2010). Role of bedrock groundwater in the rainfall–runoff process in a small headwater catchment underlain by volcanic rock. *Hydrological Processes*, **24**, 2771–2783.

Jaunat, J., Huneau, F., Dupuy, A., Celle-Jeanton, H., Vergnaud-Ayraud, V., Aquilina, L., Labasque, T., and Coustumer, P. (2012). Hydrochemical data and groundwater dating to infer differential flowpaths through weathered profiles of a fractured aquifer. *Applied Geochemistry*, **27**, 2053–2067.

Jenkins, A., Ferrier, R. C., Harriman, R., and Ogunkoya, Y. O. (1994). A case study in catchment hydrochemistry: Conflicting interpretations from hydrological and chemical observations. *Hydrological Processes*, **8**, 335–349.

Jothityangkoon, C., and Sivapalan, M. (2001). Temporal scales of rainfall–runoff processes and spatial scaling of flood peaks: space–time connection through catchment water balance. *Advances in Water Resources*, **24**, 1015–1036.

Kabeya, N., Katsuyama, M., Kawasaki, M., Ohte, N., and Sugimoto, A. (2007). Estimation of mean residence times of subsurface waters using seasonal variation in deuterium excess in a small headwater catchment in Japan. *Hydrological Processes*, **21**, 308–322.

Kamtchueng, B. T., Fantong, W. Y., Wirmvem, M. J., Tiodjio, R. E., Takounjou, A. F., Asai, K., Djomou, S. L. B., Kusakabe, M., Ohba, T., Tanyileke, G., Hell, J. V., and Ueda, A. (2015). A multi-tracer approach for assessing the origin, apparent age and recharge mechanism of shallow groundwater in the Lake Nyos catchment, Northwest, Cameroon. *Journal of Hydrology*, **523**, 790–803.

Kashiwaya, K., Hasegawa, T., Nakata, K., Tomioka, Y., and Mizuno, T. (2014). Multiple tracer study in Horonobe, northern Hokkaido, Japan: 1. Residence time estimation based on multiple environmental tracers and lumped parameter models. *Journal of Hydrology*, **519**, 532–548.

Kato, H., Onda, Y., Hisadome, K., Loffredo, N., and Kawamori, A. (2017). Temporal changes in radiocesium deposition in various forest stands following the Fukushima Dai-ichi Nuclear Power Plant accident. *Journal of Environmental Radioactivity*, **166**, 449–457.

Katsuyama, M., Tani, M., and Nishimoto, S. (2010). Connection between streamwater mean residence

time and bedrock groundwater recharge/discharge dynamics in weathered granite catchments. *Hydrological Processes*, **24**, 2287–2299.

Kawaraya, H., Matsuda, H., and Matsubaya, O. (2000). Origin and mixing of groundwater estimated by oxygen and hydrogen isotope tracers technique in Yachi landslide area, Akita, Japan. *Journal of Japan Landslide Society*, **36**, 48–55 (in Japanese).

Kelly, J. L., and Glenn, C. R. (2015). Chlorofluorocarbon apparent ages of groundwaters from west Hawaii, USA. *Journal of Hydrology*, **527**, 355–366.

Kirchner, J. W. (2003). A double paradox in catchment hydrology and geochemistry. *Hydrological Processes*, **17**, 871–874.

Klaus, J., Chun, K. P., McGuire, K. J., and McDonnell, J. J. (2015). Temporal dynamics of catchment transit times from stable isotope data. *Water Resources Research*, **51**, 4208–4223.

Klaus, J., and McDonnell, J. J. (2013). Hydrograph separation using stable isotopes: Review and evaluation. *Journal of Hydrology*, **505**, 47–64.

Koh, D., Plummer, L. N., Busenberg, E., and Kim, Y. (2007). Evidence for terrigenic SF_6 in groundwater from basaltic aquifers, Jeju Island, Korea: Implications for groundwater dating. *Journal of Hydrology*, **339**, 93–104.

Kosugi, K., Katsura, S., Katsuyama, M., and Mizuyama, T. (2006). Water flow processes in weathered granitic bedrock and their effects on runoff generation in a small headwater catchment. *Water Resources Research*, **42**, W02414, doi:10.1029/2005WR004275.

Kosugi, K., Katsura, S., Mizuyama, T., Okunaka, S., and Mizutani, T. (2008). Anomalous behavior of soil mantle groundwater demonstrates the major effects of bedrock groundwater on surface hydrological processes. *Water Resources Research*, **44**, W01407, doi:10.1029/2006WR005859.

Labasque, T., Aquilina, L., Vergnaud, V., Barbecot, F., and Contributors from participating laboratories (2014). Inter-laboratory comparison of the analyses of sulphur hexafluoride (SF_6) and three chlorofluorocarbons (CFC-11, -12 and -113) in groundwater and an air standard. *Applied Geochemistry*, **50**, 118–129.

Lamb, R., Faulkner, D., Wass, P., and Cameron, D. (2016). Have applications of continuous rainfall–runoff simulation realized the vision for process-based flood frequency analysis? *Hydrological*

Processes, **30**, 2463–2481.

Lapworth, D. J., MacDonald, A. M., Tijani, M. N., Darling, W. G., Gooddy, D. C., Bonsor, H. C., and Araguás-Araguás, L. J. (2013). Residence times of shallow groundwater in West Africa: implications for hydrogeology and resilience to future changes in climate. *Hydrogeology Journal*, **21**, 673–686.

Leaney, F. W., Smettem, K. R. J., and Chittleborough, D. J. (1993). Estimating the contribution of preferential flow to subsurface runoff from a hillslope using deuterium and chloride. *Journal of Hydrology*, **147**, 83–103.

Leibundgut, C., Maloszewski, P., and Kulls, C. (2009). Environmental tracers, In *Tracers in Hydrology* (pp. 13–50). John Wiley and Sons, Ltd, Chichester, UK.

Liu, Y., and Yamanaka, T. (2012). Tracing groundwater recharge sources in a mountain-plain transitional area using stable isotopes and hydrochemistry. *Journal of Hydrology*, **464–465**, 116–126.

Long, A. J., and Putnam, L. D. (2006). Translating CFC-based piston ages into probability density functions of ground-water age in karst. *Journal of Hydrology*, **330**, 735–747.

MEXT (2011). Ministry of education, culture, sports, science and technology. Housha-senryo tou Bumpu mappu. http://ramap.jaea.go.jp/map/map.html (in Japanese).

Ma, W., and Yamanaka, T. (2016). Factors controlling inter-catchment variation of mean transit time with consideration of temporal variability. *Journal of Hydrology*, **534**, 193–204.

Magi, M., and Shitashima, K. (2002). Estimation of the CO_2 exchange process at the Air–Sea interface using SF_6. *Abiko Research Laboratory Report*, **U01029**, pp 24 (in Japanese).

Mahara, Y. (2009). Groundwater dating. *Journal of Groundwater Hydrology*, **51**, 55–59 (in Japanese).

Maiss, M., and Brenninkmeijer, C. A. M. (1998). Atmospheric SF_6: Trends, sources, and prospects. *Environmental Science and Technology*, **32**, 3077–3086.

Maiss, M., and Levin, I. (1994). Global increase of SF_6 observed in the atmosphere. *Geophysical Research Letters*, **21**, 569–572.

Maloszewski, P., and Zuber, A. (1982). Determining the turnover time of groundwater systems with the aid of environmental tracers, 1. Models and their applicability. *Journal of Hydrology*, **57**, 207–231.

Manning, A. H., Clark, J. F., Diaz, S. H., Rademacher, L. K., Earman, S., and Plummer, L. N. (2012). Evolution of groundwater age in a mountain watershed over a period of thirteen years. *Journal of Hydrology*, **460–461**, 13–28.

Marui, A. (1991). Rainfall–runoff process and function of subsurface water storage in a layered hillslope. *Geographical Review of Japan*, **64**, 145–166 (in Japanese).

McDonnell, J. J. (1990). A rationale for old water discharge through macropores in a steep, humid catchment. *Water Resources Research*, **26**, 2821–2932.

McDonnell, J. J. (2003). Where does water go when it rains? Moving beyond the variable source area concept of rainfall-runoff response. *Hydrological Processes*, **17**, 1869–1875.

McDonnell, J. J., et al. (2010). How old is streamwater? Open questions in catchment transit time conceptualization, modelling and analysis. *Hydrological Processes*, **24**, 1745–1754.

McGlynn, B. L., McDonnell, J. J., and Brammer, D. D. (2002). A review of the evolving perceptual model of hillslope flowpaths at the Maimai catchments, New Zealand. *Journal of Hydrology*, **257**, 1–26.

McGlynn, B., and McDonnell, J. J. (2003). Quantifying the relative contributions of riparian and hillslope zones to catchment runoff. *Water Resources Research*, **39**, W01310, doi:10.1029/2003WR002091.

McGuire, K. J., and McDonnell, J. J. (2006). A review and evaluation of catchment transit time modeling. *Journal of Hydrology*, **330**, 543–563.

Meerveld, H. J. T., and McDonnell, J. J. (2006). Threshold relations in subsurface stormflow: 1. A 147-storm analysis of the Panola hillslope. *Water Resources Research*, **42**, W02410, doi:10.1029/2004WR003778.

Menichino, G. T., and Hester, E. T. (2015). The effect of macropores on bi-directional hydrologic exchange between a stream channel and riparian groundwater. *Journal of Hydrology*, **529**, 830–842.

Montgomery, D. R., Dietrich, W. E., Torres, R., Anderson, S. P., Heffner, J. T., and Loague, K. (1997). Hydrologic response of a steep, unchanneled valley to natural and applied rainfall. *Water Resources Research*, **33**, 91–109.

Morgenstern, U., Stewart, M. K., and Stenger, R. (2010). Dating of streamwater using tritium in a post nuclear bomb pulse world: Continuous variation of mean transit time with streamflow. *Hydrology and Earth System Sciences*, **14**, 2289–2301.

Morikawa, N. (2004). Dissolved helium distribution in deep groundwaters from the Tono area, central Japan: a tool for tracing groundwater flow in fractured granite. *Limnology*, **5**, 61–69.

Nakaya, S., Uesugi, K., Motodate, Y., Ohmiya, I., Komiya, H., Masuda, H., and Kusakabe, M. (2007). Spatial separation of groundwater flow paths from a multi-flow system by a simple mixing model using stable isotopes of oxygen and hydrogen as natural tracers. *Water Resources Research*, **43**, W09404, doi: 10.1029/2006WR005059.

Onda, Y., Komatsu, Y., Tsujimura, M., and Fujihara, I. (2001). The role of subsurface runoff through bedrock on storm flow generation. *Hydrological Processes*, **15**, 1693–1706.

Onda, Y., Tsujimura, M., Fujihara, J., and Ito, J. (2006). Runoff generation mechanisms in high-relief mountainous watersheds with different underlying geology. *Journal of Hydrology*, **331**, 659–673.

Onodera, S. (1991). Subsurface water flow in the multi-layered hillslope. *Geographical Review of Japan*, **64**, 549–568 (in Japanese).

Pearce, A. J., Stewart, M. K., and Sklash, M. G. (1986). Storm runoff generation in humid headwater catchments 1. Where does the water come from? *Water Resources Research*, **22**, 1263–1272.

Plummer, L. N., Busenberg, E., Bohlke, J. K., Nelms, D. L., Michel, R. L., and Schlosser, P. (2001). Groundwater residence times in Shenandoah National Park, Blue Ridge Mountains, Virginia, USA: a multi-tracer approach. *Chemical Geology*, **179**, 93–111.

Reilly, T. E., Plummer, L. N., Phillips, P. J., and Busenberg, E. (1994). The use of simulation and multiple environmental tracers to quantify groundwater flow in a shallow aquifer. *Water Resources Research*, **30**, 421–433.

Rigby, M., et al. (2010). History of atmospheric SF_6 from 1973 to 2008. *Atmospheric Chemistry and Physics*, **10**, 10305–10320.

Salle, C. G., Aquilina, L., Fourre, E., Jean-Baptiste, P., Michelot, J. L., Roux, C., Bugai, D., Labasque, T., Simonucci, C., Meir, N., Noret, A., Bassot, S., Dapoigny, A., Baumier, D., Verdoux, P., Stammose,

D., and Lancelot, J. (2012). Groundwater residence time downgradient of Trench No. 22 at the Chernobyl Pilot Site: Constraints on hydrogeological aquifer functioning. *Applied Geochemistry*, **27**, 1304–1319.

Sklash, M. G., Stewart, M. K., and Pearce, A. J. (1986). Storm runoff generation in humid headwater Catchments 2. A case study of hillslope and low-order stream response. *Water Resources Research*, **22**, 1273–1282.

Sklash, M. G., and Farvolden, R. N. (1979). The role of groundwater in storm runoff. *Journal of Hydrology*, **43**, 45–65.

Solomon, D. K., Gilmore, T. E., Solder, J. E., Kimball, B., and Genereux, D. P. (2015). Evaluating an unconfined aquifer by analysis of age-dating tracers in stream water. *Water Resources Research*, **51**, 8883–8899.

Soulsby, C., Birkel, C., Geris, J., Dick, J., Tunaley, C., and Tetzlaff, D. (2015). Stream water age distributions controlled by storage dynamics and nonlinear hydrologic connectivity: Modeling with high-resolution isotope data. *Water Resources Research*, **51**, 7759–7776.

Stewart, M. K., Morgenstern, U., and McDonnell, J. J. (2010). Truncation of stream residence time: How the use of stable isotopes has skewed our concept of streamwater age and origin. *Hydrological Processes*, **24**, 1646–1659.

Suarez, V. V. C., Okello, A. M. L. S., Wenninger, J. W., and Uhlenbrook, S. (2015). Understanding runoff processes in a semi-arid environment through isotope and hydrochemical hydrograph separations. *Hydrology and Earth System Sciences*, **19**, 4183–4199.

Suckow, A. (2014). The age of groundwater –Definitions, models and why we do not need this term–. *Applied Geochemistry*, **50**, 222–230.

Takahashi, J., Tamura, K., Suda, T., Matsumura, R., and Onda, Y. (2015). Vertical distribution and temporal changes of ^{137}Cs in soil profiles under various land uses after Fukushima Dai-ichi Nuclear Power Plant Accident. *Journal of Environmental Radioactivity*, **139**, 351–361.

Tanaka, T., Yasuhara, M., and Marui, A. (1984). Runoff mechanism during a storm event in the headwaters of the Tama hills. *Geographical Review of Japan*, **57**, 1–19 (in Japanese).

Tetzlaff, D., Birkel, C., Dick, J., Geris, J., and Soulsby, C. (2014). Storage dynamics in hydropedological

units control hillslope connectivity, runoff generation, and the evolution of catchment transit time distributions. *Water Resources Research*, **50**, 969–985.

Tokieda, T., Ishii, M., Saito, S., and Midorikawa, T. (2007). Highly developed precise analysis of atmospheric and oceanic sulfur hexafluoride (SF_6) and evaluation of SF_6 standard gas stability. *Technical Reports of the Meteorological Research Institute*, **51**, pp 43 (in Japanese).

Tsuchihara, T., Okuyama, T., Yoshimoto, S., Shirahata, K., and Ishida, S. (2014). Sulfur hexafluoride-based age dating of groundwater in the Shimekake landslide in Yamagata, Japan. *Irrigation, Drainage, and Rural Engineering Journal*, **294**, 65–74 (in Japanese).

Tubau, I., Vazquez-Sune, E., Jurado, A., and Carrera, J. (2014). Using EMMA and MIX analysis to assess mixing ratios and to identify hydrochemical reactions in groundwater. *Science of the Total Environment*, **470–471**, 1120–1131.

Uhlenbrook, S., Frey, M., Leibundgut, C., and Maloszewski, P. (2002). Hydrograph separations in a mesoscale mountainous basin at event and seasonal timescales. *Water Resources Research*, **38**, W01096, doi:10.1029/2001WR000938.

Watanabe, K., and Seki, Y. (1982). Natures of under ground water flow in granite acting as an agent in weathering. *Journal of the Japanese Association of Mineralogists, Petrologists and Economic Geologists*, **77**, 37–46 (in Japanese).

Whipkey, R. Z. (1965). Subsurface stormflow from forested slopes. *Bulletin of IASH*, **10**, 74–85.

Wilson, G. B., and McNeill, G. W. (1997). Noble gas recharge temperatures and the excess air component. *Applied Geochemistry*, **12**, 747–762.

Xing, B., Liu, Z., Liu, G., and Zhang, J. (2015). Determination of runoff components using path analysis and isotopic measurements in a glacier-covered alpine catchment (upper Hailuogou Valley) in southwest China. *Hydrological Processes*, **29**, 3065–3073.

Yager, R. M., Plummer, L. N., Kauffman, L. J., Doctor, D. H., Nelms, D. L., and Schlosser, P. (2013). Comparison of age distributions estimated from environmental tracers by using binary-dilution and numerical models of fractured and folded karst: Shenandoah Valley of Virginia and West Virginia, USA. *Hydrogeology Journal*, **21**, 1193–1217.

Yang, L., Chang, S., Shin, H., and Hur, J. (2015). Tracking the evolution of stream DOM source during

storm events using end member mixing analysis based on DOM quality. *Journal of Hydrology*, **523**, 333–341.

Young, C., Kroeger, K. D., and Hanson, G. (2013). Limited denitrification in glacial deposit aquifers having thick unsaturated zones (Long Island, USA). *Hydrogeology Journal*, **21**, 1773–1786.

Zuber, A., Witczak, S., Rozanski, K., Sliwka, I., Opoka, M., Mochalski, P., Kuc, T., Karlikowska, J., Kania, J., Jackowicz-Korczynski, M., and Dulinski, M. (2005). Groundwater dating with ^{3}H and SF_6 in relation to mixing patterns, transport modelling and hydrochemistry. *Hydrological Processes*, **19**, 2247–2275.